(2)

AFWAL-TR-86-3058

AN INVESTIGATION OF CLASSICAL DYNAMIC SCALING TECHNIQUES APPLIED TO AN OLEO-PNEUMATIC LANDING GEAR STRUT

Archie B. Clark III, Captain, USAF
Mechanical Branch
Vehicle Equipment Division

February 1987

Final Report for Period October 1983 - July 1985

FLIGHT DYNAMICS
AIR FORCE WRIGHT AERONAUTICAL LABORATORIES
AIR FORCE SYSTEMS COMMAND
WRIGHT-PATTERSON AIR FORCE BASE, OHIO 45433-6553

NOTICE

When Government drawings, specifications, or other data are used for any purpose other than in connection with a definitely related Government procurement operation, the United States Government thereby incurs no responsibility nor any obligation whatsoever; and the fact that the government may have formulated, furnished, or in any way supplied the said drawings, specifications, or other data, is not to be regarded by implication or otherwise as in any manner licensing the holder or any other person or corporation, or conveying any rights or permission to manufacture use, or sell any patented invention that may in any way be related thereto.

This report has been reviewed by the Office of Public Affairs (ASD/PA) and is releasable to the National Technical Information Service (NTIS). At NTIS, it will be available to the general public, including foreign nations.

This technical report has been reviewed and is approved for publication.

ARCHIE B. CLARK, III, Capt, USAF
Project Engineer
Special Projects Group
Mechanical Branch

AIVARS V. PETERSONS
Chief, Mechanical Branch
Vehicle Equipment Division

FOR THE COMMANDER

RICHARD E. COLCLOUGH, JR.
Chief
Vehicle Equipment Division

If your address has changed, if you wish to be removed from our mailing list, or if the addressee is no longer employed by your organization please notify AFWAL/FIEMB *W-PAFB, OH 45433 to help us maintain a current mailing list.*

Copies of this report should not be returned unless return is required by security considerations, contractual obligations, or notice on a specific document.

UNCLASSIFIED
SECURITY CLASSIFICATION OF THIS PAGE

AD-A187 664

REPORT DOCUMENTATION PAGE

1a. REPORT SECURITY CLASSIFICATION: UNCLASSIFIED	1b. RESTRICTIVE MARKINGS
2a. SECURITY CLASSIFICATION AUTHORITY	3. DISTRIBUTION/AVAILABILITY OF REPORT: Approved for public release; Distribution is unlimited.
2b. DECLASSIFICATION/DOWNGRADING SCHEDULE	
4. PERFORMING ORGANIZATION REPORT NUMBER(S): AFWAL-TR-86-3058	5. MONITORING ORGANIZATION REPORT NUMBER(S)
6a. NAME OF PERFORMING ORGANIZATION: Air Force Wright Aeronautical Laboratories; 6b. OFFICE SYMBOL (If applicable): AFWAL/FIEMB	7a. NAME OF MONITORING ORGANIZATION
6c. ADDRESS (City, State and ZIP Code): AFWAL/FIEMB Wright-Patterson AFB OH 45433	7b. ADDRESS (City, State and ZIP Code)
8a. NAME OF FUNDING/SPONSORING ORGANIZATION; 8b. OFFICE SYMBOL (If applicable)	9. PROCUREMENT INSTRUMENT IDENTIFICATION NUMBER
8c. ADDRESS (City, State and ZIP Code)	10. SOURCE OF FUNDING NOS.

PROGRAM ELEMENT NO.	PROJECT NO.	TASK NO.	WORK UNIT NO.
62201F	2402	240201	24020146

11. TITLE (Include Security Classification): An Investigation of Classical Dynamic Scaling Techniques Applied to an Oleopneumatic Landing Gear Strut

12. PERSONAL AUTHOR(S): CLARK ARCHIE BERNARD, III

13a. TYPE OF REPORT	13b. TIME COVERED	14. DATE OF REPORT (Yr., Mo., Day)	15. PAGE COUNT
Final	FROM Oct 83 TO Jul 85	1987 February	160

16. SUPPLEMENTARY NOTATION

17. COSATI CODES		
FIELD	GROUP	SUB. GR.
01	03	
14	02	

18. SUBJECT TERMS (Continue on reverse if necessary and identify by block number): Landing Gear; Scale Models; Dynamically Scaled Models

19. ABSTRACT (Continue on reverse if necessary and identify by block number)

A program was conducted to investigate the technical feasibility and practicality of using dynamic scale modeling techniques to design, fabricate, and test a scale model of an aircraft landing gear strut and tire. Dynamic scaling laws were developed and used to design a one-third model of an A-37 Nose Landing Gear strut and tire. The A-37 NLG strut and the model gear were tested under dynamically similar conditions of weight, speed, and forcing function on a circular track, Dynamic Test Machine at the Mobility Development Laboratory, Wright-Patterson AFB OH. Comparison of time history data, recorded during each phase of testing, indicated good correlation of the dynamic response of the model gear, in relation to the scaling laws and the A-37 NLG dynamic response. Presented in the report is the development and analytical verification of the scaling laws, test data and comparisons, conclusions, and recommendations.

20. DISTRIBUTION/AVAILABILITY OF ABSTRACT	21. ABSTRACT SECURITY CLASSIFICATION
UNCLASSIFIED/UNLIMITED ☒ SAME AS RPT. ☐ DTIC USERS ☐	UNCLASSIFIED

22a. NAME OF RESPONSIBLE INDIVIDUAL	22b. TELEPHONE NUMBER (Include Area Code)	22c. OFFICE SYMBOL
ARCHIE B. CLARK, Capt, USAF	(513) 257-2129	AFWAL/FIEMB

DD FORM 1473, 83 APR — EDITION OF 1 JAN 73 IS OBSOLETE.

UNCLASSIFIED
SECURITY CLASSIFICATION OF THIS PAGE

SUMMARY

The objective of this program was to assess the feasibility and practicality of applying dynamic scale modeling techniques and principles to design, fabricate, and test scale models of landing gear struts and tires.

This report describes the requirements which led to the conception of this program; the development, and analytical verification of a model law; and the application of the model law to design a functional scale model of an A-37 Nose Landing Gear (NLG) strut and tire. The fabrication of the model landing gear strut and subsequent testing of the model gear, and an A-37 NLG at the Mobility Development Laboratory (MDL) is also documented in this report. Also presented are the results of test data analysis, conclusions, and recommendations.

The dynamically scaled model landing gear strut was designed and fabricated by the Cleveland Pneumatic Company (CPC), on a cost sharing basis with AFWAL/FIEMB. A dynamically scaled model A-37 NLG tire was designed and fabricated by Precision Measurement Company, Ann Arbor MI, under contract to AFWAL/FIEMB. An analytical model of a single oleo-pneumatic landing gear strut, tire, and ground surface features, was developed with the assistance of the Mechanical Subsystems Group (AFWAL/FIEMA). This computerized model was very useful in the analytical verification of the model law, and aided in the development of a test plan for the model gear and A-37 NLG struts. All testing was conducted In-House in the MDL, with technical support provided by the Systems Research Laboratories (SRL), Dayton OH. Data reduction and analysis was accomplished within the Special Projects Group.

FOREWORD

This report documents an in-house effort conducted by personnel of the Mechanical Branch (FIEM), Vehicle Equipment Division, Flight Dynamics Laboratory, Air Force Wright Aeronautical Laboratories, Wright-Patterson AFB Ohio, under Project 2402, "Mechanical Systems for Advanced Military Vehicles," Task Number 24020146, "Aircraft Mobillity Systems Models." This report covers work performed from October 1983 to July 1985, by Capt Archie B. Clark, III (AFWAL/FIEMB), the Project Engineer. This report was released by the author in June 1986.

The author wishes to express appreciation to Dr Arnold Mayer for his assistance and support during the program, Greer McClain of the Mechanical Branch for his technical support, Peter C. Vorum and William K. Smith, also of the Mechanical Branch, and Diane O'Connell, for her clerical support in preparing this Technical Report.

TABLE OF CONTENTS

LIST OF ILLLUSTRATIONS

LIST OF ILLUSTRATIONS
(continued)

LIST OF ILLUSTRATIONS
(continued)

LIST OF ILLUSTRATIONS
(continued)

LIST OF TABLES

LIST OF ACRONYMS AND SYMBOLS

A	Area
a	Acceleration
AFWAL	Air Force Wright Aeronautical Laboratories
AGILE	Aircraft Ground Induced Loads Excitation
BDR	Bomb Damage Repair
c	Viscous Damping Coefficient
$\bar{c}$	Dimensionless Viscous Damping Coefficient
C_d	Orifice Discharge Coefficient
C_1	Empirical O-Ring Seal Constant
d	Orifice Throat Diameter
D_m	O-Ring Seal Mean Diameter
DTM	Dynamic Test Machine
F	Force
G	Uninstalled Gap Width of a Split Ring Seal
g_c	A Constant that Relates Force, Mass, Length and Time
k	Stiffness Coefficient
K_1	Empirical O-Ring Seal Constant
K_2	Empirical Seal Constant
L_a	Moment Arm from Top Bearing Centerline to Axle Centerline
L_s	Moment Arm from Bottom Strut Seal/Bearing Centerline to Axle Centerline (Fully Extended Strut)
LGDF	Landing Gear Development Facility
m	Mass
MDL	Mobility Development Laboratory
N	Polytropic Exponent
NLG	Nose Landing Gear

LIST OF ACRONYMS AND SYMBOLS
(continued)

P	Pressure
R_e	Reynolds Number
s	Stroke
$\dot{s}$	Stroke Rate
S	Cross-sectional Squeeze of an O-Ring Seal (Percent)
t	Time
$\bar{t}$	Dimensionless Time
V	Volume
V_0	Reference Pneumatic Volume
v	Horizontal Velocity
w	Orifice Seal Width
x	Vertical Displacement
$\dot{x}$	First Time Derivative of x
$\ddot{x}$	Second Time Derivative of x
$\bar{x}$	Dimensionless Vertical Displacement
β	Ratio of Orifice Throat Diameter to the Approach Diameter
λ	Scaling Factor
μ	Absolute Viscosity of a Fluid
ν	Friction Coefficient
ρ	Mass Density
ω	Frequency

SUBSCRIPTS

A	Area
a	Ambient

LIST OF ACRONYMS AND SYMBOLS
(continued)

F	Force
g	Gauge
m	Mass
o	Original (Full-Scale) System
P	Pressure
p	Pneumatic
s	Scaled System
t	Time
V	Volume
v	Velocity
x	Displacement or Some Linear Dimension

SECTION I

BACKGROUND

Current emphasis in the development of advanced landing gear technology is focused on improving the capabilities of tactical and transport aircraft to operate from bomb damaged runways and contingency launch surfaces. The requirement for increased flexibility in aircraft ground operations is based on concern over the critical dependency of present aircraft on smooth, paved runways and taxiways.

A successful enemy airstrike against a forward NATO airbase would result in extensive damage to paved launch surfaces. An example of bomb inflicted damage is shown in Fig. 1. Such damage would clearly eliminate the possibility of launching an immediate counter strike; thus, airpower would be effectively neutralized, until time consuming runway repairs could be completed.

Techniques have been developed to temporarily restore a section of runway for resumption of aircraft launch operations, following an attack. Craters are repaired by backfilling them with debris and other stockpiled aggregate, and then covering the damaged area with Bomb Damage Repair (BDR) mats (Ref. 5). This matting is designed to support the weight of an aircraft as it traverses the damaged area during takeoff or recovery. However, the mats are not flush with the rest of the runway surface, and can induce severe dynamic loads into an airframe and landing gear strut. The capability of a particular aircraft to operate over a rough runway surface generally depends on the gross weight and weapons configuration of the aircraft, and mat spacing on the runway, if there are multiple repairs. The type of operation being conducted (i.e. landing, takeoff, or rejected takeoff) is also a critical factor that must be considered. Currently, there are several full-scale test methods used to establish

FIGURE 1. Bomb Damaged Runway

the limits of various existing aircraft to operate in a rough field environment. HAVE BOUNCE is a test program initiated to measure dynamic loads induced in fighter and transport aircraft, during taxi and takeoff operations over BDR mats. Fig. 2 is a photograph of an F-16 HAVE BOUNCE test run. This test method involves substantial expense and support, since an operational aircraft must be instrumented and tested.

Aircraft Ground Induced Loads Excitation (AGILE) is another full-scale test method which also involves instrumentation and testing of an actual aircraft. In this technique, a mechanical shaker platform is placed beneath each landing gear tire. A digital controller is used to induce a pre-programmed forcing function into each tire (via the shakers) to simulate a particular type of surface roughness e.g., a BDR mat. Fig. 3 shows an F-16 in place on the AGILE test fixture.

A similar technique is used in development and evaluation of improved landing gear struts and tires capable of dissipating the high loads associated with rough field operations. At the Landing Gear Development Facility (LGDF), Wright-Patterson AFB, Ohio, single struts are mounted to a large test fixture which, like AGILE testing, simulates a particular ground loading condition via a digitally controlled shaker platform placed beneath the tire. Aircraft weight is simulated with a dead load, which is constrained to move in the vertical direction only. Fig. 4 shows an F-15 main gear strut and tire in the test fixture.

AGILE testing of an aircraft, and single strut tests at the LGDF, offer the advantages of obtaining valuable dynamic performance data more economically than HAVE BOUNCE tests, since engine and pilot time are not required. Also, data acquisition and reduction is facilitated in a fully equipped laboratory

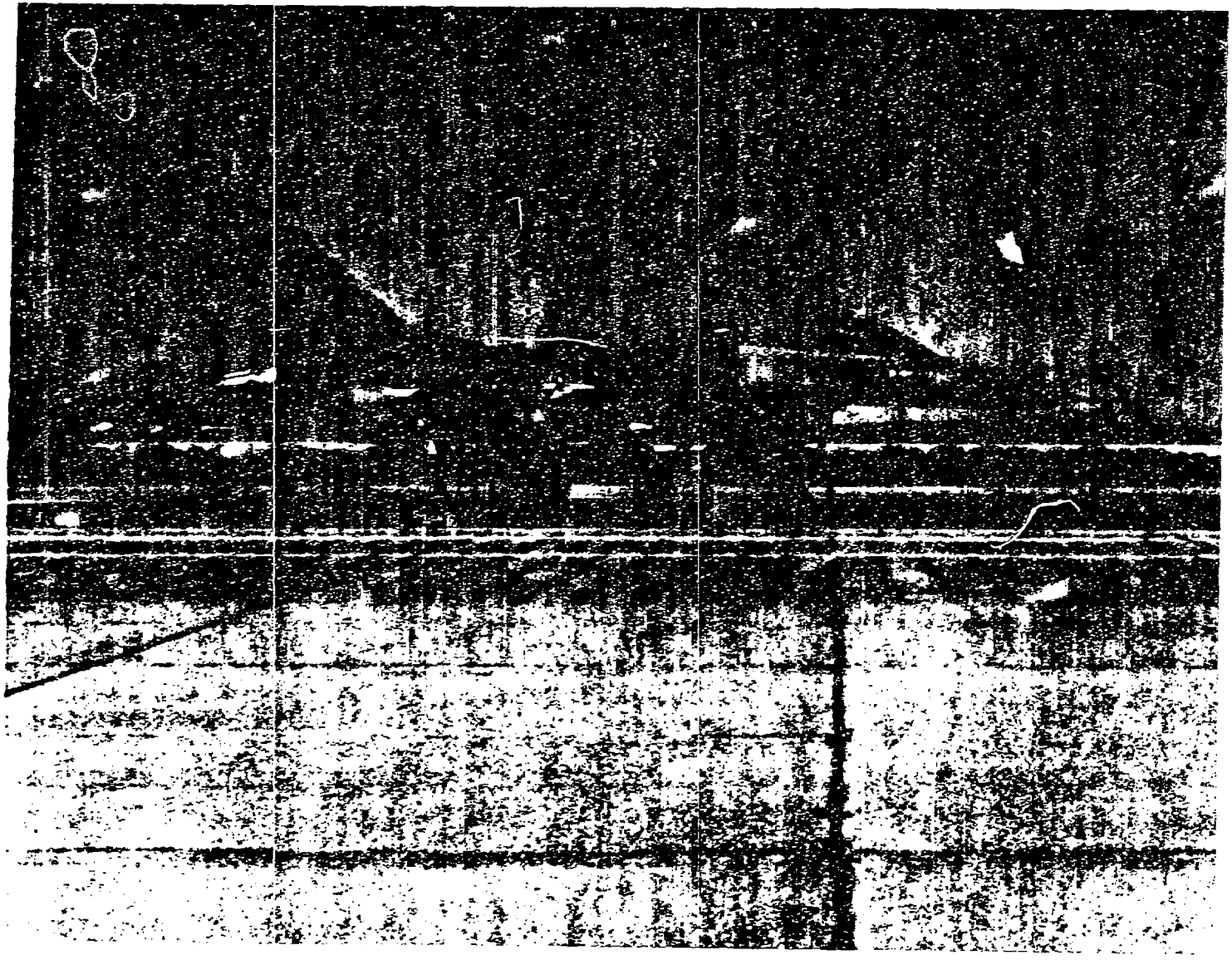

FIGURE 2. F-16 HAVE BOUNCE Test

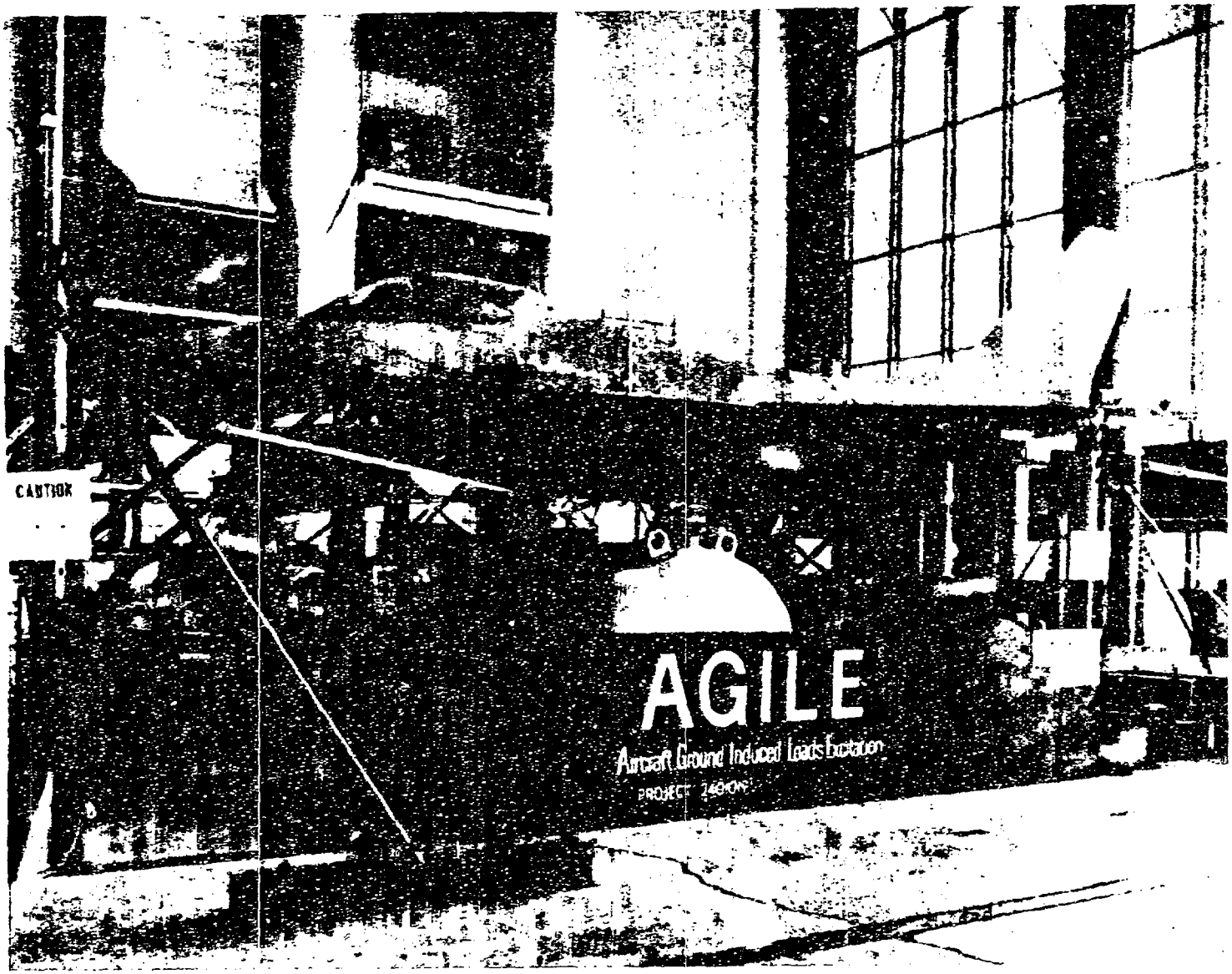

FIGURE 3. F-16 AGILE Test Arrangement

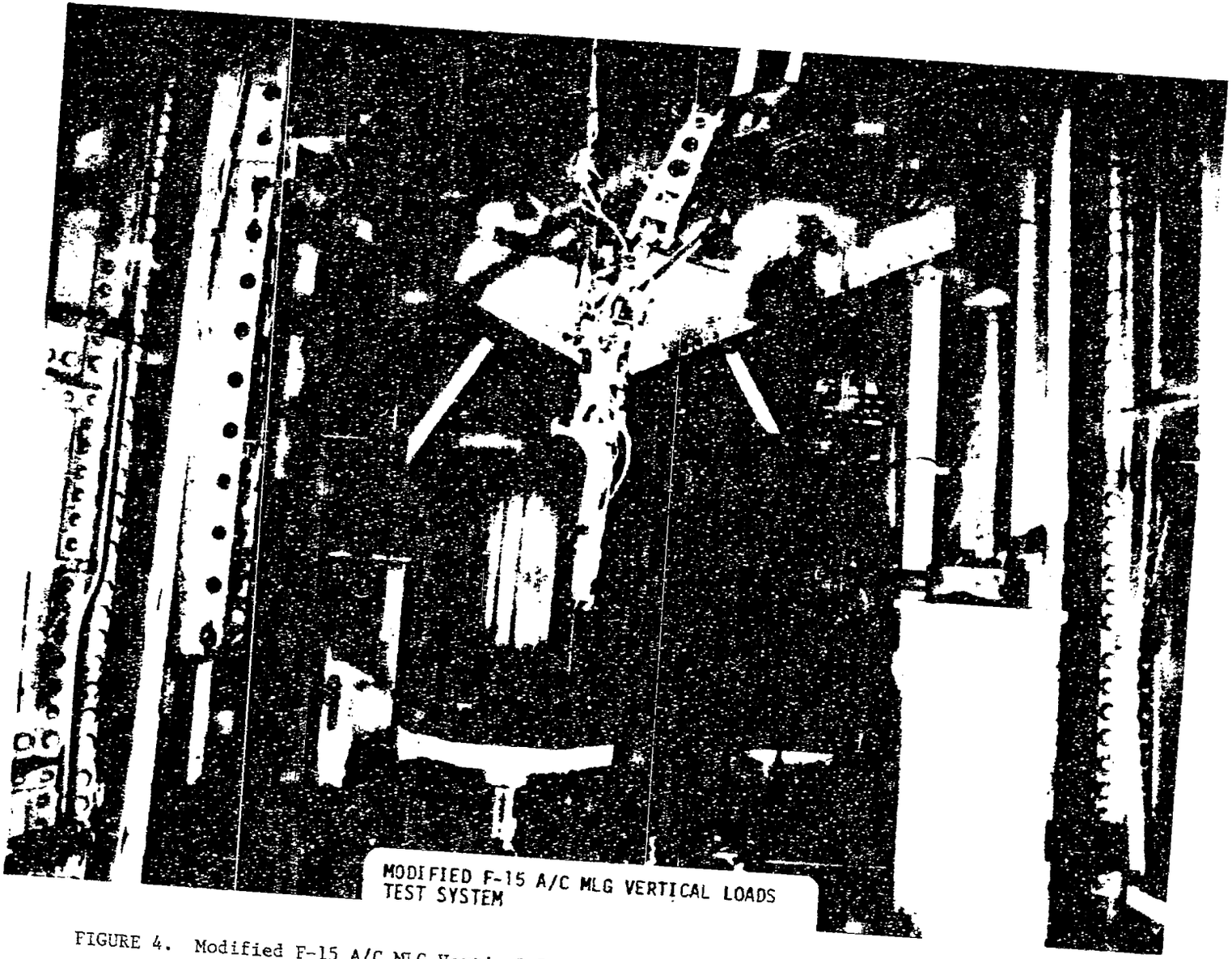

FIGURE 4. Modified F-15 A/C MLG Vertical Loads Test System

where test conditions can be easily and quickly varied with a minimum of down time between tests. However, there are also disadvantages with these test methods. It is difficult or too costly to properly simulate rolling, braking, tire envelopment, strut drag loads, and aerodynamic damping effects. Also, with each of the test methods discussed, extreme test conditions must be avoided to prevent possible over-stressing of test hardware, even though such conditions may be realistically expected in an actual post attack scenario. Another problem with these full-scale test methods is the difficulty and cost associated with obtaining production hardware for test purposes.

Analytical models are also used to predict landing gear and aircraft structural dynamic response; however, they must be validated with experimental data whenever possible. The required data is presently obtained from full-scale prototype tests, provided that resources are available to conduct such test programs.

Testing dynamically scaled models of aircraft landing gear struts and tires is an attractive alternative to full-scale prototype testing. The use of scale models in engineering practice is well documented as an efficient and cost effective method of satisfying many data requirements. The most common example is the use of scale wind tunnel models to obtain aereodynamic data for a new aircraft or missle design. This is clearly a more economical and practical approach than a full-scale prototype test program. Also, data can be acquired more safely, and for a much broader range of conditions than full-scale testing. It may be possible to realize the same benefits by applying a similar approach in the area of landing gear development and evaluation.

The objective of a scale model test program is usually to predict the characteristics of a full-scale design; however, there is no known precedent for the use of scale landing gear models to satisfy performance data requirements. Therefore, this program was initiated to assess the technical and practical feasibilities of designing and fabricating a dynamically scaled model of an existing landing gear strut and tire. Successful development of this test approach could potentially result in significant reductions in the costs of developing advanced landing gear hardware.

The scope of this initial program was limited to the most rudimentary type of aircraft shock strut available. The development and verification of dynamic scaling techniques for a simple strut configuration was considered as prerequisite to scaling of a more complex landing gear strut. An A-37 NLG strut and tire was selected as the "full-scale" representative for this program. This particular strut was chosen primarily because it was available at no cost, and its size and weight were within the capabilities of the test fixture at the MDL. Also, it met program requirements for simplicity of design. A photograph of the A-37 NLG strut, and a one-third scale model of this strut, is shown in Fig. 5.

In general, the A-37 NLG strut is a typical example of oleo-pneumatic landing gear struts used on practically every aircraft in the USAF inventory, although it is not as complex as most struts. However, despite the simple design and function of the A-37 NLG, the physical laws and processes which govern its dynamic behavior are the same for any other oleo-pneumatic strut, regardless of complexity. Thus, the analysis which follows in the next section can be perceived in context of any landing gear strut.

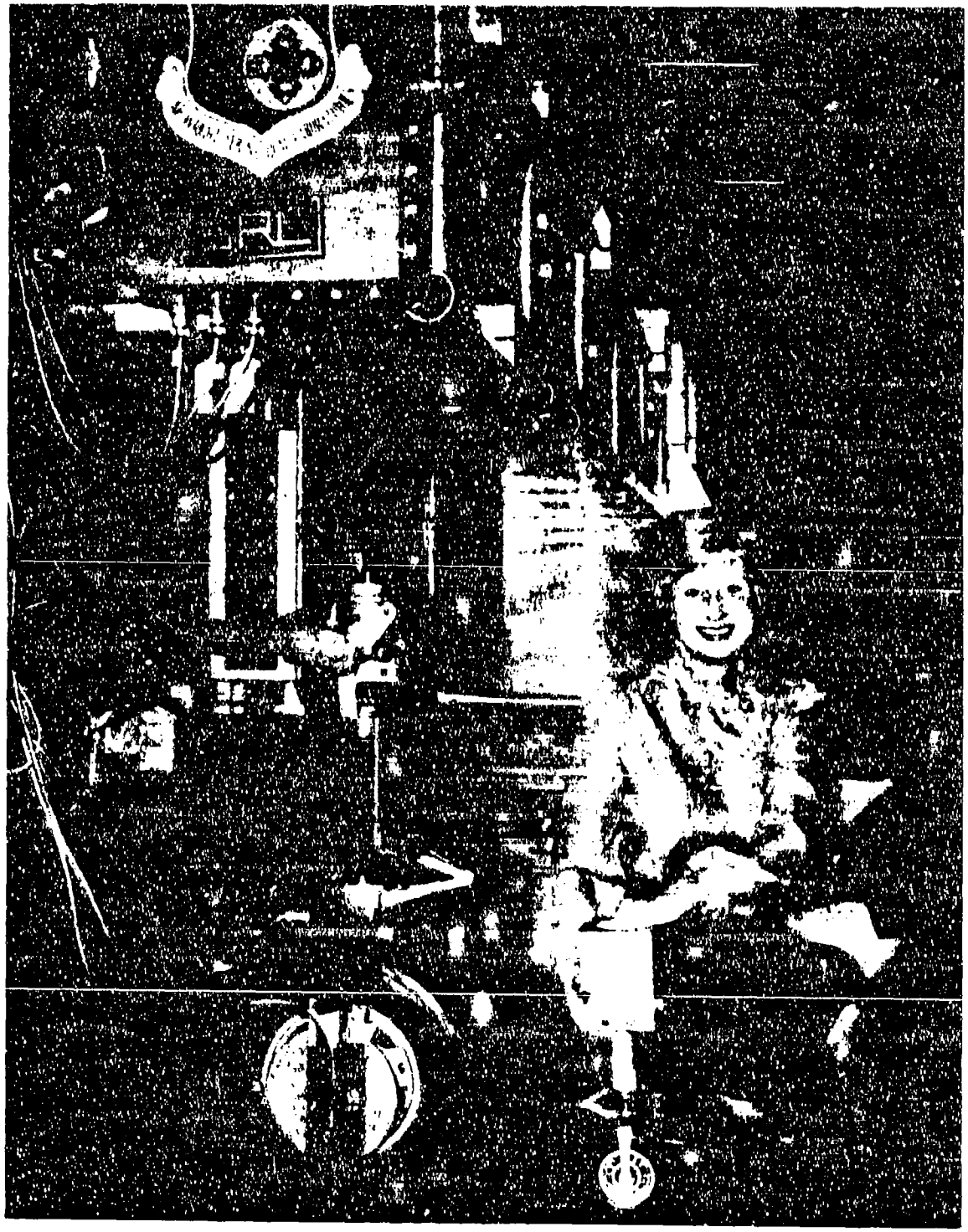

FIGURE 5. A-37 NLG and One-Third Scale Model Gear

SECTION II

DYNAMIC SCALING PRINCIPLES

1. FORMULATION OF THE MODEL LAW

The design of a dynamically scaled model of any physical system is based on a corresponding full-scale system design, and a model law. Proper formulation of an appropriate model law requires careful analysis of the physical laws and processes which govern the dynamic behavior of the system. An accurately scaled model requires that all dominant factors in the original system be identified, scaled according to the model law, and incorporated into the model system design. If this is successfully accomplished, then the two physical systems are dynamically similar, and it is possible to predict the full-scale behavior by observing the model behavior to a similar set of conditions, and applying the model law to scale the results. Mathematically, dynamic similarity requires two conditions: 1) The governing equations and boundary conditions that describe each physical system must have the same form, and 2) the coefficients in the normalized equations must be identical.

The model law consists of a set of scaling factors which dictate the relationships that must exist between scaled and full-scale system parameters, for dynamic similarity. A scaling factor, represented by λ, is specifically defined as the ratio of a model parameter to the same parameter in the original system e.g.,

$$\lambda_m = \frac{m_s}{m_o}$$

Here, λ_m is the scaling factor for mass where the subscript "s" denotes a

parameter in the scaled system, and the subscript "o" denotes a corresponding parameter in the original full-scale system. Scaling factors are similarly defined for all other pertinent quantities.

The scaling factors which make up a model law are best expressed in terms of a single common scaling factor. This scaling factor is the "independent variable" which is selected at the discretion of the model designer. All other scaling factors are determined according to this one raised to some power, i.e.:

$$\lambda_F = \lambda^a \qquad \text{(Force)}$$

$$\lambda_m = \lambda^b \qquad \text{(Mass)}$$

$$\lambda_v = \lambda^c \qquad \text{(Velocity)}$$

etc. Thus, the model designer is free to choose the desired relationship for one physical parameter, represented by λ, and all other scaling factors are based on that selection. Commonly accepted practice is to define the model law in terms of the scaling factor, λ_x. This allows the designer to select the desired goemetric relationship between the scaled and original systems.

The exponents a, b, c,...etc. are determined by combining system parameters into nondimensional groups called Pi numbers. The power relationships are then determined by equating the Pi numbers, and applying the above definition of a scaling factor. There are several approaches which are commonly used to develop the required Pi numbers, including the Buckingham Pi Theorem (also called dimensional analysis), the Equation Method, and the Law Method. Selection of an approach that is best suited for a particular scaling problem depends on the scope and objectives of a scale model test program. The Buckingham Pi Theorem is most appropriate for problems in which little is known about the relative effects of certain parameters on the dynamic behavior of a system. The objectives of model testing in this case would be to quantify

these effects, rather than attempting to predict the performance of another dynamically similar system.

Successful application of the theorem requires identification of all system parameters which may have some possible physical significance in the behavior of the system. Writing governing equations is not a part of this technique. The theorem is applied, which results in the generation of several nondimensional groups (the Pi numbers). Model tests are then conducted to establish an empirical relationship between the various Pi numbers. Analysis of test results yields information concerning which parameters are dominant, and which are insignificant, for the conditions of the tests. With this information, it may be possible to either create an analytical model, which includes all of the observed effects, or to design a scale model, which can accurately duplicate full-scale system performance. The latter approach would be pursued if the analytical situation was too complex, or to obtain more detailed empirical data to "fine tune" an analytical model.

The Buckingham Pi Theorem is a valid approach to obtaining valuable empirical data, provided that all dominant system parameters are identified before it is applied. If some important parameter is not included, then the test results will be incomplete, or possibly, even meaningless. Thus, care, combined with some experience, is required to optimize the benefits gained from this method. A complete explanation of how to use the Buckingham Pi Theorem is provided in Ref. 4.

The Equation Method and the Law Method are more appropriate for the development of a model law. The governing laws and physical processes must already be well defined in order to write equations which account for all of the dominant effects in the system. An advantage of this approach is that any

model law developed, is easily verified by substituting scaled parameters into the governing equations.

A combination of the Equation Method and the Law Method was used to form the required model law for an oleo-pneumatic landing gear strut, since the equations of motion are straight forward, and the physical processes are well defined. The Pi numbers were extracted directly from the normalized equations and other applicable physical laws. The scaling factors were then obtained by equating Pi numbers, and applying the definition of a scaling factor.

Solution of the equations of motion is not necessary for development of the Pi numbers, therefore, they are not developed here in complete detail. Only the general form of the equations is used in the ensuing analysis. The terms in the equation represent the major effects which contribute to the dynamic response of a landing gear strut. Assumptions made in the analysis are as follows:

1. The components of the strut are rigid, i.e., material deformation caused by dynamic loading was not considered, nor was there any attempt at scaling this effect;

2. Only vertical dynamics of the strut are accounted for. Other possible modes of oscillation, such as fore-aft, torsional, wheel shimmy, etc., were not considered;

3. The components of the strut were lumped together into two representative weights. Scaling the weight of each individual component was not considered. All components which comprise the sprung weight (weight supported by the air spring) were lumped together, and unsprung weight components were similarly lumped together.

4. Aerodynamic damping terms were neglected.

Development of the governing equations of motion was based on an

analysis of the forces acting on a frictionless strut as it oscillates. These forces are depicted in Fig. 6. The pneumatic force, F_a, is generated by compression of an air spring, and hydraulic damping represented by F_h, results as fluid is forced through a small orifice. Since the component weights are lumped together into two representative weights, the motion of the strut can be described by two coupled differential equations of the general form:

$$m\ddot{x} + c\dot{x} + kx = F(\omega t) \tag{1}$$

Normalization of this equation can be accomplished by defining a nondimensional displacement $\bar{x}$, and a nondimensional time $\bar{t}$ as:

$$\bar{x} = \frac{xk}{F} \tag{2}$$

and

$$\bar{t} = t\left(\frac{k}{m}\right) \tag{3}$$

The ratio k/F can be interpreted as a displacement of a spring having a stiffness k, and subjected to a force F. Also, the ratio $(k/M)^{1/2}$ can be construed as a natural frequency of the system. Normalization of equation (1) is accomplished by substituting appropriate derivatives of $\bar{x}$ and $\bar{t}$, with the following results:

$$\ddot{\bar{x}} + \bar{c}\dot{\bar{x}} + \bar{x} = f(\bar{t}) \tag{4}$$

where

$$\bar{c} = \frac{c^2 g_c}{k\,m} \tag{5}$$

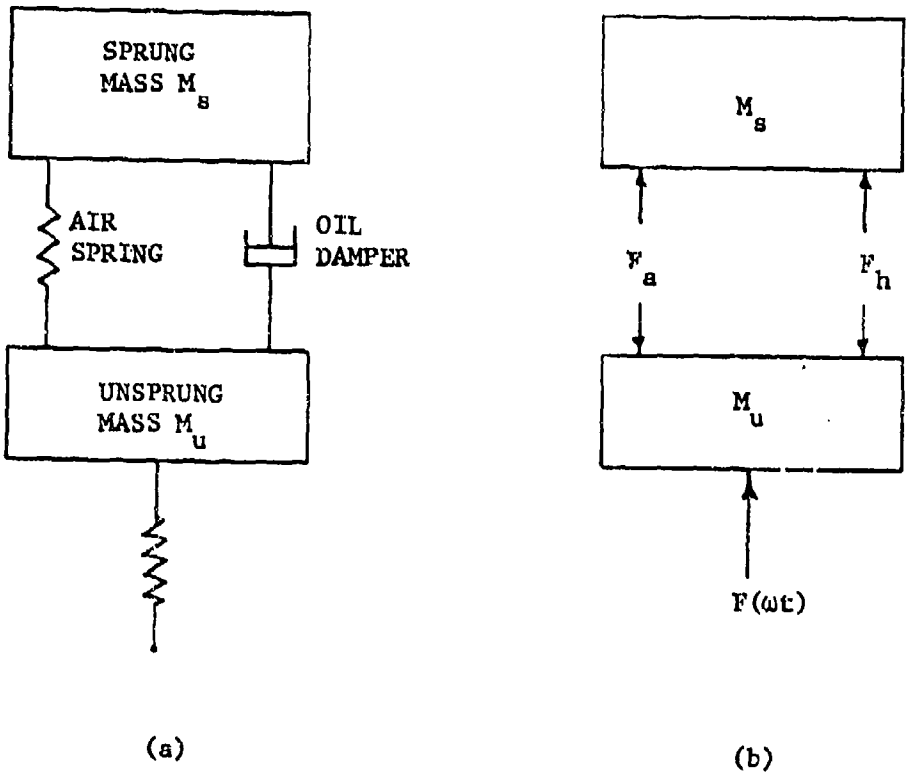

FIGURE 6. Oleo-Pneumatic Strut
Force Diagram

Thus, three Pi numbers: $\bar{x}$, $\bar{t}$, and $\bar{c}$ have resulted from this simple analysis of the forces acting on a landing gear strut.

The first condition required for dynamic similarity is similitude, i.e., the model and full-scale system are both governed by the same physical laws. The above analysis is considered valid for any system which is represented by Fig. 6, including the model and full-scale systems, thus, similitude is an inherent assumption. Recalling that dynamic similarity also requires an invariance of Pi numbers, then

$$\bar{x}_s = \bar{x}_o \tag{6}$$

$$\bar{t}_s = \bar{t}_o \tag{7}$$

$$\bar{c}_s = \bar{c}_o \tag{8}$$

Substituting in the respective expressions for $\bar{x}$, $\bar{t}$, and $\bar{c}$ yields

$$\left(\frac{x\,k}{F}\right)_s = \left(\frac{x\,k}{F}\right)_o \tag{9}$$

$$\left(\frac{t^2 k}{m}\right)_s = \left(\frac{t^2 k}{m}\right)_o \tag{10}$$

$$\left(\frac{c^2}{k\,m}\right)_s = \left(\frac{c^2}{k\,m}\right)_o \tag{11}$$

Applying the definition of a scaling factor to these expressions results in the following:

$$\lambda_x\,\lambda_k = \lambda_F \tag{12}$$

$$\lambda_t^2\,\lambda_k = \lambda_m \tag{13}$$

$$\lambda_k\,\lambda_m = \lambda_c^2 \tag{14}$$

These expressions are useful in that they describe the interrelationship that must be maintained between several of the important system scaling factors to satisfy the conditions for dynamic similarity, however, the key to completing the model law formulation is to establish the relationship between the primary scaling factors of the system.

Primary scaling factors represent the parameters of a system that are expressed in terms of a fundamental unit of measurement (length, mass, temperature, electric current, or luminous intensity). All other scaling factors are secondary i.e., they can be determined by multiplying or dividing two or more primary scaling factors. As an example, an area scaling factor can be obtained directly from the scaling factor λ_x, since geometric scaling has been indirectly specified as linear. Area is the product of two dimensions (e.g. length and width) thus,

$$\lambda_A = \frac{A_s}{A_o} = \frac{\lambda_x \cdot \ell \cdot \lambda_x \cdot w}{\ell \cdot w} = \lambda_x^2$$

In this case, the primary scaling factor, λ_x is used to determine the secondary scaling factor, λ_A.

The fundamental parameters for a dynamic system such as a landing gear strut are easily identified as mass, length, and time. A relationship between the primary scaling factors λ_x and λ_t can be determined from expressions (12) and (13) by first relating λ_m and λ_F. This relationship is established by considering the fundamental law of motion,

$$F = m\,a$$

A Pi number is formed by combining all parameters together on the right side, or,

$$\pi = \frac{m\ a}{F} \tag{15}$$

Dynamic similarity requires identical Pi numbers, therefore,

$$\left(\frac{m\ a}{F}\right)_s = \left(\frac{m\ a}{F}\right)_o \tag{16}$$

and, by applying the scaling factor definition,

$$\lambda_m\ \lambda_a = \lambda_F \tag{17}$$

The model law must provide for dynamic similarity in the same linear acceleration field (gravity), thus, an assumption is made that

$$\lambda_a = 1$$

which yields

$$\lambda_m = \lambda_F \tag{18}$$

combining (12), (13), and (18) gives the desired relationship between two primary scaling factors:

$$\lambda_x = \lambda_t^2 \tag{19}$$

An additional relationship is required to complete the basic model law formulation. λ_m or λ_F must be expressed in terms of either λ_x or λ_t.

Another Pi number can be formed by considering mass as a product of density and volume or,

$$m = \rho V$$

As usual, a Pi number is formed, and equated, to satisfy dynamic similarity. The results upon application of the scaling factor definition is

$$\lambda_\rho\ \lambda_V = \lambda_m \tag{20}$$

It is convenient here to set $\lambda_\rho = 1$, from which it follows that

$$\lambda_V = \lambda_m$$

But volume is expressed dimensionally as the product of three linear dimensions therefore,

$$\lambda_m = \lambda_x^3 \tag{21}$$

The required relationships between primary scaling factors have now been established, and are summarized in terms of λ_x as follows:

$$\lambda_m = \lambda_x^3 \tag{22}$$

$$\lambda_F = \lambda_x^3 \tag{23}$$

$$\lambda_t = \lambda_x^{\frac{1}{2}} \tag{24}$$

This represents one possible formulation of a model law. It can easily be verified by substituting scaled parameters into the original equations of motion, and simplifying. The resulting equation is identical to the original equation, which satisfies both conditions of dynamic similarity. (Theoretically, any power relationship of λ_m and λ_F with λ_x will satisfy the model law, provided that λ_m and λ_F both have identical power relationships with λ_x. This is true, since both conditions of dynamic similarity are satisfied under this criteria.)

All applicable secondary scaling factors can now be determined through appropriate combinations of the above primary scaling factors. As an example, the scaling factor for velocity is easily obtained by combining the dimension and time scaling factors, i.e.,

$$\lambda_v = \frac{v_s}{v_o}$$

$$= \frac{x_s}{t_s} \cdot \frac{t_o}{x_o}$$

$$= \frac{\lambda_x \cdot x_o \cdot t_o}{\lambda_x^{\frac{1}{2}} \cdot t_o \cdot x_o} = \lambda_x^{\frac{1}{2}}$$

The complete model law is summarized in Table (1). This particular formulation corresponds to the Froude Model Law, which has been proven as useful in scaling of other dynamic systems. (The Froude Law derives its name from the Froude Number, which is defined as the ratio of inertial and gravitational forces. This Pi number was originally formulated by a Naval architect, William Froude, who discovered the importance of this parameter in flows with free surface effects.)

2. GENERAL COMMENTS ON RELAXATIONS AND SIMPLIFICATIONS

In the last section, it was shown that two conditions must be satisfied for complete dynamic similarity. They are repeated here for emphasis:

1. Similitude is required i.e., both physical systems must be governed by the same laws and processes. In the case of a landing gear strut, the original and scale model system must each have an air spring, a hydraulic damper, frictional effects, and a tire. Each can be described with the same normalized equations of motion and initial conditions;

2. Also required is an equivalence of applicable Pi numbers, i.e., the nondimensional coefficients in the normalized equations of motion must be identical.

Any deviation in the value of an important Pi number between two dynamically similar systems, will cause a corresponding departure from similarity. It can generally be expected that the result will be some loss of accuracy in predicting the dynamic response of one system, based on observations of the other.

The model designer is often forced to compromise some quantitative accuracy, in favor of increasing the practicality of fabricating a functional

FULL-SCALE PARAMETERS	SCALE FACTOR	MODEL PARAMETERS
m (Mass)	λ^3	$\lambda^3 m$
F (Force)*	λ^3	$\lambda^3 F$
x (Length)*	λ	λ x
t (Time)*	$\lambda^{\frac{1}{2}}$	$\lambda^{\frac{1}{2}} t$
a (Acceleration)	1	a
v (Velocity)	$\lambda^{\frac{1}{2}}$	$\lambda^{\frac{1}{2}} v$
A (Area)	λ^2	$\lambda^2 A$
V (Volume)	λ^3	$\lambda^3 V$
P (Pressure)	λ	λ P

TABLE 1. The Model Law (Dynamic Scale Factors)

*Primary scaling factor

model, because, in most realistic cases, it is either not physically possible to scale some effect, or it is not practical to do so. Usually, a model law can be formulated in such a way that the necessity of scaling some non-scalable constant (i.e., gravity) is eliminated. Practicality considerations are best illustrated by example: Complete dynamic similarity of a landing gear strut would theoretically call for proper scaling of component structural deformations, however, this would require fabrication of the model using a material with physical properties that satisfy the model law. In all likelihood, such a material would not exist in nature, or would be too costly to manufacture. This apparent dilemma is circumvented by neglecting structural deformation as a small effect, when compared to the relatively large vertical displacements which occur during strut actuation. Thus, material strain is neglected as a "weak" effect, as compared to vertical displacement, which is the dominant effect. This involves some deviation from the model law however, the model design problem is greatly simplified.

The technique of identifying and separating the strong effects from the weak effects is called relaxation. This is considered as a very important factor in scale model design, since in most practical applications, it is not realistic to expect that all parameters can be scaled and incorporated into the model with complete fidelity. Relaxation techniques are commonly referred to in dynamic scaling literature as an art, since there are no well defined procedures which are universally applicable to any scaling problem. Relaxation must be ultimately based on engineering judgement, and experience in scaling of a particular type of dynamic system.

SECTION III

SUBSYSTEM SCALING

The physical processes that govern the dynamic response of a landing gear strut (the air spring, hydraulic damping orifice, friction and tire characteristics) must be scaled according to the model law developed in the preceding section, and incorporated as accurately as possible or practical, into the scale model design. This section is intended to provide an understanding of the approach used to scale the individual subsystems of the A-37 NLG strut for this particular program. The basic subsystems of an oleo-pneumatic strut are depicted in Fig. 7.

1. AIR SPRING SCALING AND ASSOCIATED SCALING EFFECTS

An air spring can be represented very simply as a piston-cylinder arrangement (Ref. Fig. 8). An external force F_e, acting on the piston, compresses the gas inside the cylinder from s_o, until an equal and opposite force is generated at s_1. The magnitude of the pressure force increases exponentially between the reference and end state, according to the relation

$$\frac{P_g(s) + P_a}{P_{g_0} + P_a} = \left(\frac{V_0}{V(s)}\right)^N \tag{25}$$

where $P_g(s)$: Pneumatic pressure at stroke s,

P_{g_0}: Reference pressure (gauge),

V_0: Reference volume,

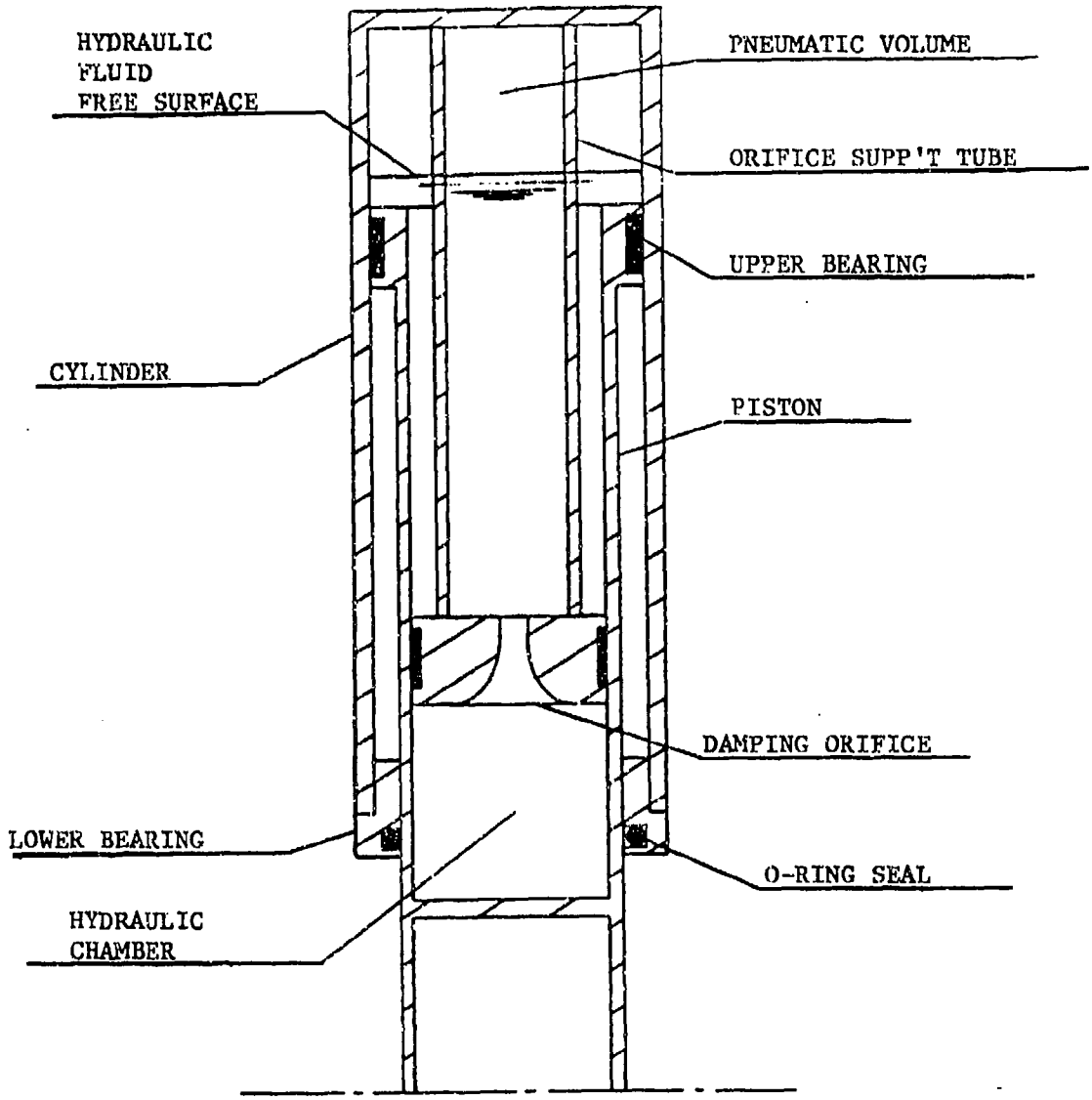

FIGURE 7. Shock Strut Components

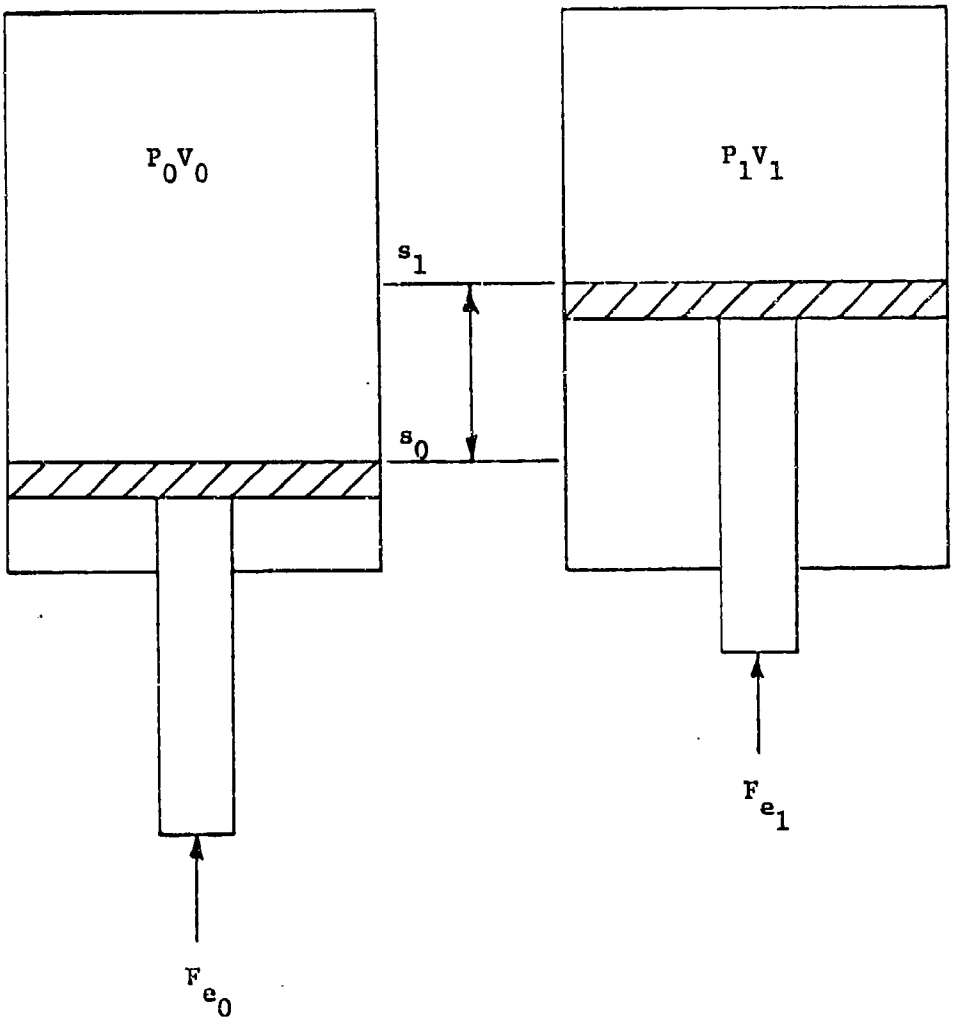

FIGURE 8. Pneumatic Air Spring

$V(s)$: Volume at stroke s,

s: Stroke position

N: Polytropic gas exponent

P_a: Ambient pressure

This relation is derived from the Second Law of Thermodynamics for an isentropic process. The value of the polytropic exponent, N, defines the actual process which occurs during compression or rarefaction of the enclosed gas, since there are no real processes that are isentropic. Its value generally ranges from 1.0 for an isothermal (constant temperature) process, to 1.4 for an adiabatic (zero net heat transfer) process. Thus, the polytropic exponent is used to define the heat transfer characteristics of the air spring, and its value generally depends on the rate of compression or rarefaction, and on the type of gas used.

The physical process governed by equation (25) must be properly incorporated into the model strut design to obtain dynamically similar pneumatic force characteristics. Mathematically, the task is easily accomplished by applying the appropriate scaling factors from the model law, to each of the parameters, which results in the following scaled parameters:

$$P_{g_s}(s) = \lambda_P P_{g_0}(s)$$

$$P_{g_{0_s}} = \lambda_P P_{g_{0_o}}$$

$$V_{0_s} = \lambda_V V_{0_o}$$

$$V_s(s) = \lambda_V V_o(s)$$

$$s_s = \lambda_x s_o$$

$$P_{a_s} = \lambda_P P_{a_o}$$

These values clearly satisfy the conditions for dynamic similarity, however, there is an apparent problem with ambient pressure scaling. Proper scaling of ambient pressure is required to satisfy the model law for dynamically similar pneumatic loads, however, this cannot realistically be accomplished for model tests. Only the gauge component of the total pressure can be scaled properly.

The nonsimilar effects of unscaled ambient pressure on the static pneumatic force vs. stroke characteristics of the model gear strut can be analyzed by reformulating equation (25) as follows:

$$\left(\frac{P_g(s)}{P_a'} + \frac{P_a}{P_a'}\right) \Bigg/ \left(\frac{P_{g_0}}{P_a'} + \frac{P_a}{P_a'}\right) = \left(\frac{V_0}{V(s)}\right)^N \qquad (26)$$

P_a: Actual ambient pressure,

P_a': Ambient pressure component required to satisfy conditions for dynamic similarity.

For scale model tests, the following condition is required to satisfy the model law:

$$P_a' = P_{a_s} = \lambda_P \; P_{a_o}$$

Hypothetically, if it is somehow possible to obtain this value (perhaps by conducting model tests inside a vacuum chamber), then equation (26) reduces to equation (25), which satisfies the conditions for dynamic similarity. However, it is not realistic or economically feasible to reduce ambient pressure to the required level. The model gear must be tested in nonsimilar ambient pressure conditions, which requires that

$$P_{a_s} = P_{a_o}$$

With these parameters, equation (26) reduces to

$$\left(\frac{P_g(s)}{P_a} + \frac{1}{\lambda_p}\right) \Big/ \left(\frac{P_{g_0}}{P_a} + \frac{1}{\lambda_p}\right) = \left(\frac{V_0}{V(s)}\right)^N \qquad (27)$$

This equation contains a "nonsimilar term," $1/\lambda_p$. Thus, the degree of nonsimilarity depends on the pressure scaling factor, λ_p. It is also apparent from equation (27), that the nonsimilar effects are reduced at higher strut pressures, for a given scaling factor. If the gauge component, P_{g_0}, is very large, then the contribution of P_a becomes insignificant i.e.,

$$\frac{P_g(s)}{P_a} \rightarrow P_g(s)$$

Also, if the scale factor λ_p is not excessively small, then

$$\frac{P_g(s)}{P_a} + \frac{1}{\lambda_p} \rightarrow P_g(s)$$

The nonsimilar effects on the static pressure-stroke characteristics of an air spring, caused by an unscaled ambient pressure, are shown graphically in Fig. 9, 10, and 11. Fig. 9 shows a large departure from similarity for small scaling factors and small gauge pressures. Fig. 10 shows the same trends, but the nonsimilar effects are smaller, since the gauge component is much larger than the ambient pressure. Fig. 11 shows the nonsimilar effects that occur if the reference state is taken at the static equilibrium condition.

Another approach to the air spring scaling problem is to insure that the natural frequency of the full-scale air spring-mass system is scaled properly, rather than applying the model law directly to scale V_0 and P_{g_0}, as was done in the preceding analysis of the static case.

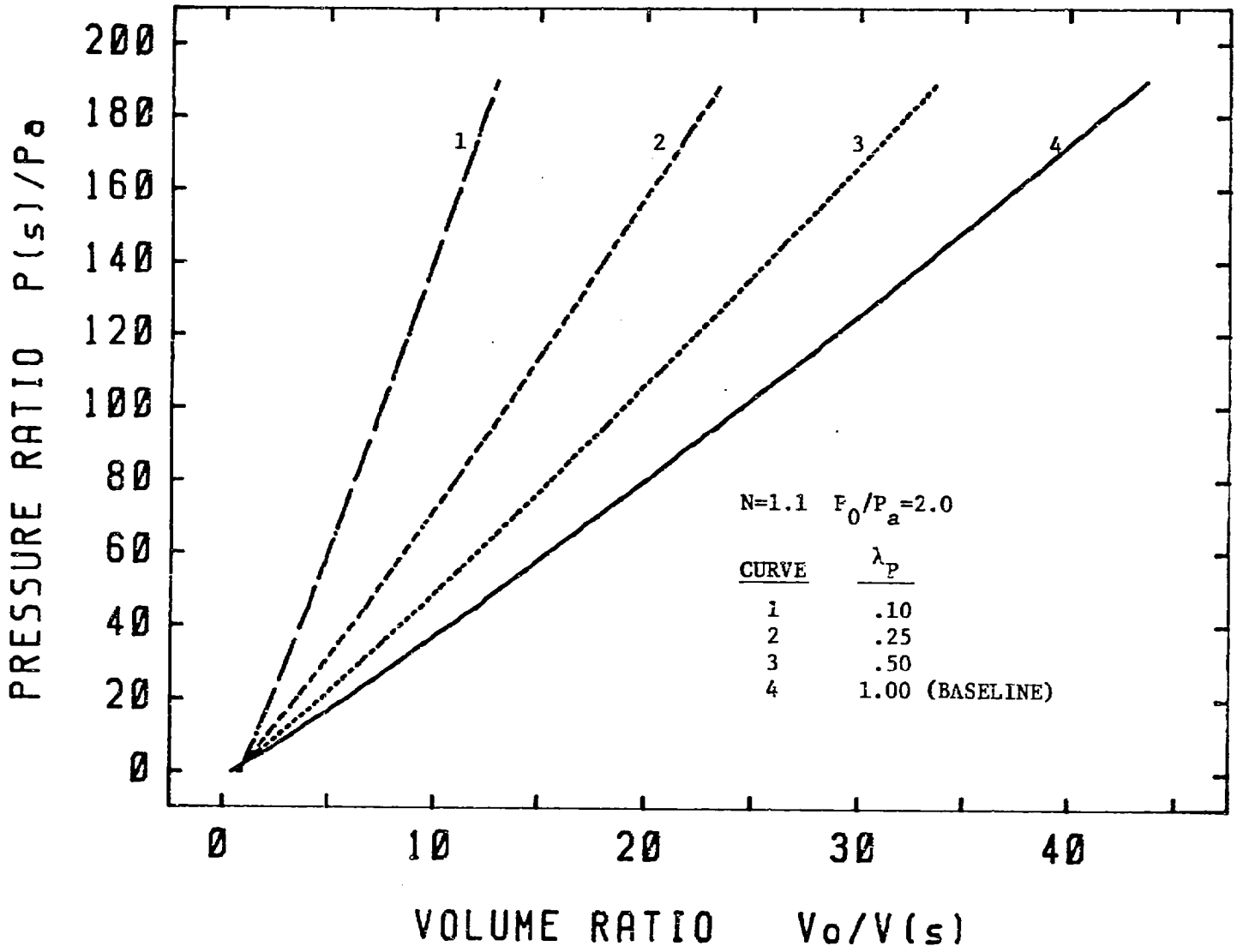

FIGURE 9. Polytropic Curves - Effect on Dynamic Similarity of Decreasing Scale Factor at Small Guage Pressure

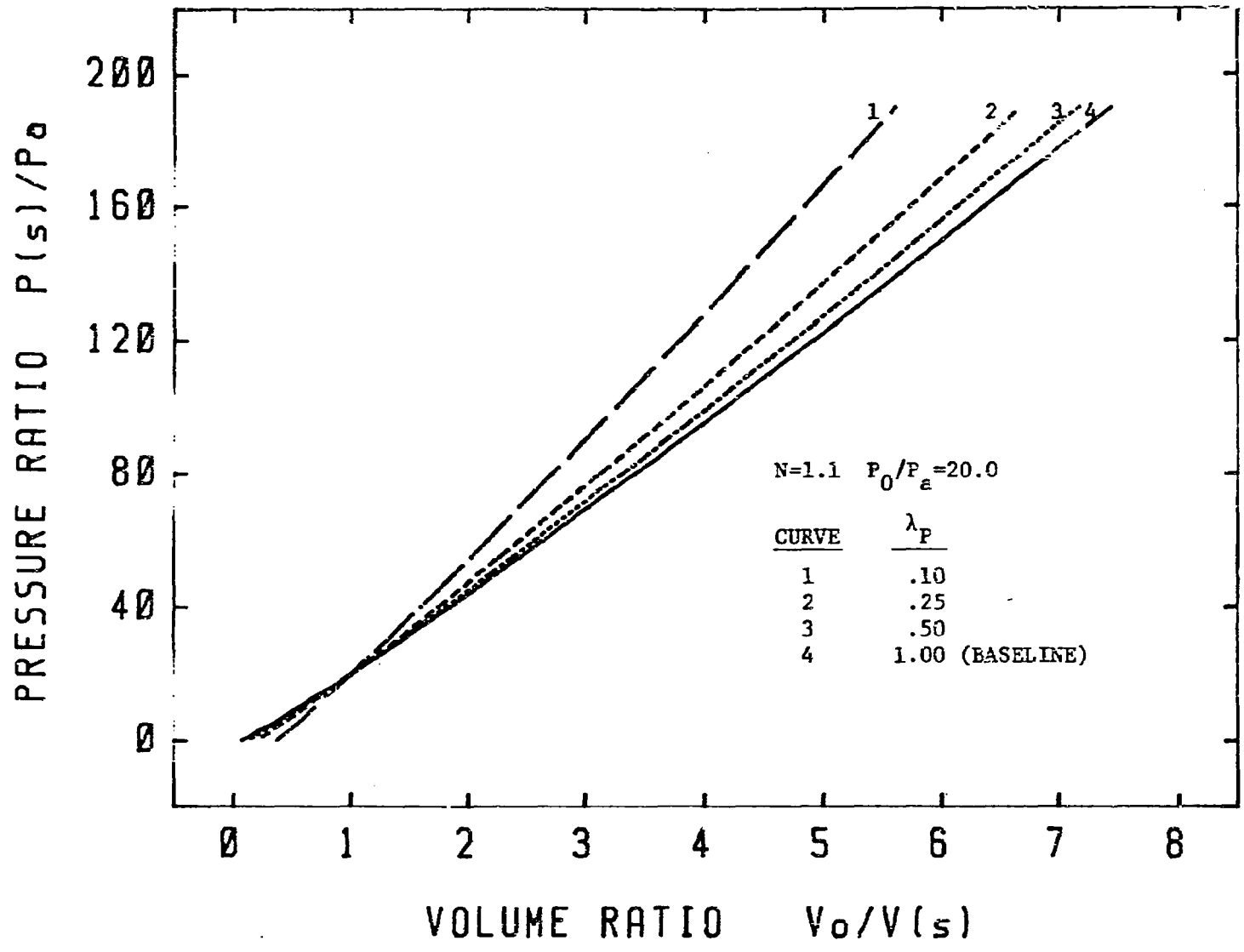

FIGURE 10. Polytropic Curves - Effect on Dynamic Similarity of Decreasing Scale Factor at Larger Guage Pressure

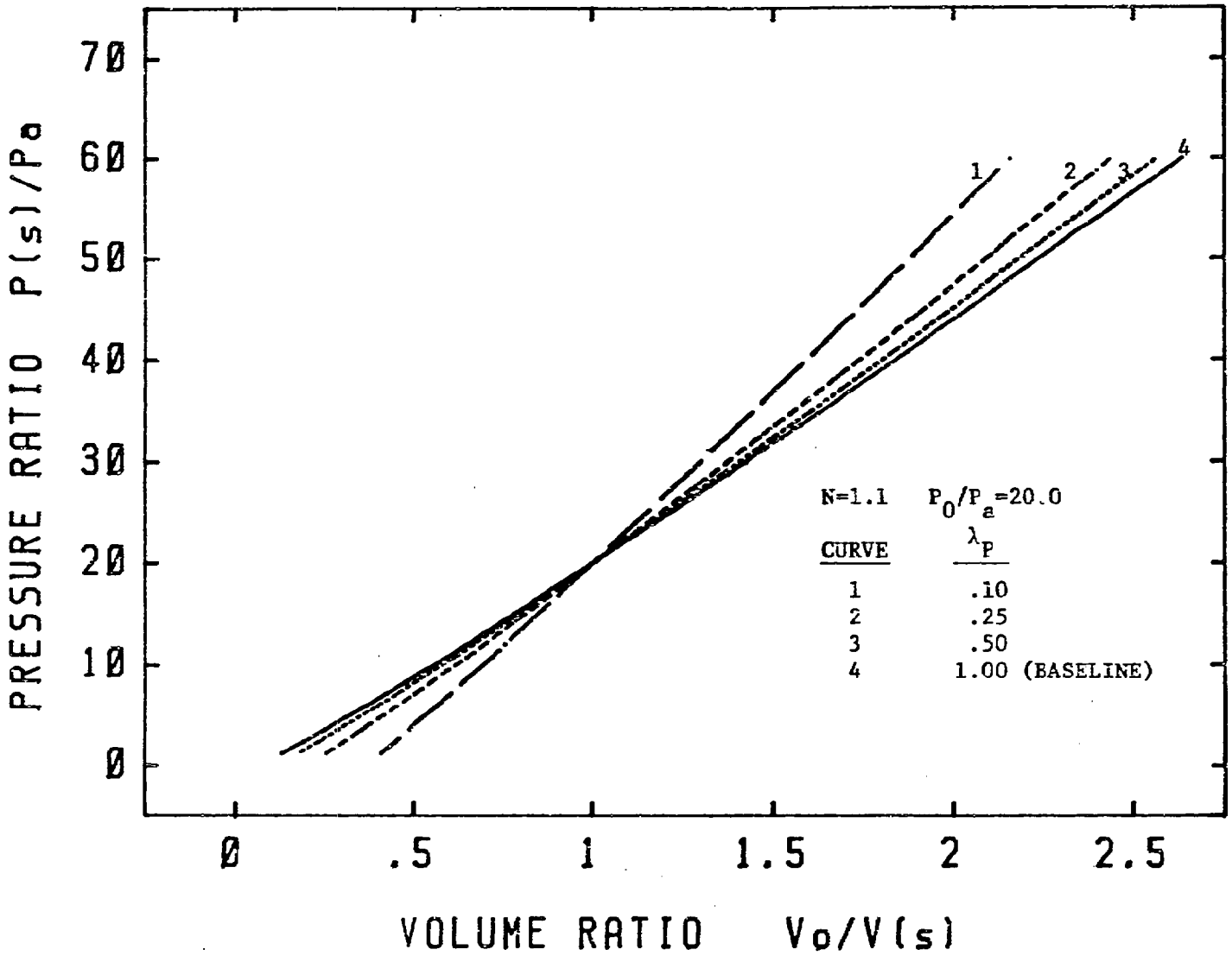

FIGURE 11. Polytrpic Curves - Effect on Dynamic Similarity of Scaling the Guage Pressure at the Static Equilibrium Position

The natural frequency of an air spring-mass system is given by

$$\omega_N = \frac{1}{2\pi}\left[\frac{A_p g\, N\left(P_{g_0} + P_a\right)}{V_0\, P_{g_0}}\right]^{\frac{1}{2}} \tag{28}$$

where ω_N: Natural frequency,

g: Gravitational acceleration,

and $P_{g_0} = W_s/A_p$,

where W_s: Sprung weight.

A_p: Pneumatic Area

A Pi number is formed by combining all terms in equation (28) on the right side, which yields

$$\pi = \frac{A_p g\, N}{V_0 \omega_N^2}\left(\frac{P_{g_0} + P_a}{P_{g_0}}\right) \tag{29}$$

Equating Pi numbers for the model and original system, to satisfy dynamic similarity, and applying the scaling factor definition yields

$$\lambda_N\, \lambda_A \left[\frac{\left(P_{g_0} + P_a\right)_s}{\left(P_{g_0} + P_a\right)_o}\right] = \lambda_P\, \lambda_V\, \lambda_\omega^2 \tag{30}$$

Making appropriate substitutions from the model law for λ_A, λ_P, and λ_ω and then solving for λ_V gives

$$\lambda_V = \lambda_x^2\, \lambda_N \left[\frac{\left(P_{g_0} + P_a\right)_s}{\left(P_{g_0} + P_a\right)_o}\right] \tag{31}$$

In terms of full-scale pressures (realizing that ambient pressure is nonscalable), then

$$\lambda_V = \lambda_x^2\, \lambda_N \left(\frac{\lambda_P\, P_{g_0} + P_a}{P_{g_0} + P_a}\right) \tag{32}$$

This is a modified scale factor for the pneumatic volume at the static equilibrium position, which insures proper natural frequency scaling. All other parameters are scaled according to the previously defined scaling factors. If the polytropic exponent is known for each system, then λ_N can be determined. If it is assumed that the polytropic exponent for each system is the same, then $\lambda_N = 1$.

Each of the air spring scaling methods discussed in this section was evaluated analytically to determine the affects on the dynamic response of the model gear strut. Results of this evaluation are presented in Section IV.

2. ANALYSIS AND SCALING OF A CONSTANT AREA HYDRAULIC DAMPING ORIFICE

Most aircraft landing gear struts are equipped with a metered orifice, which is designed to optimize the hydraulic damping characteristics for typical landing conditions. For this program however, a constant area orifice was used, since the added complexity of a metered orifice was considered unwarranted and unnecessary for satisfying stated program objectives. Also, fabrication of a metering pin for the model gear posed a difficult machining problem.

A typical round edge constant area orifice cross section is shown in Fig. 12. During strut compression, hydraulic fluid is forced through the orifice, which results in a pressure force. The magnitude of this force is governed by the equation:

$$F_h = \frac{\rho A_h \dot{s}^2}{2 C_d^2 A_t^2 g_c} \tag{33}$$

where F_h: Hydraulic force

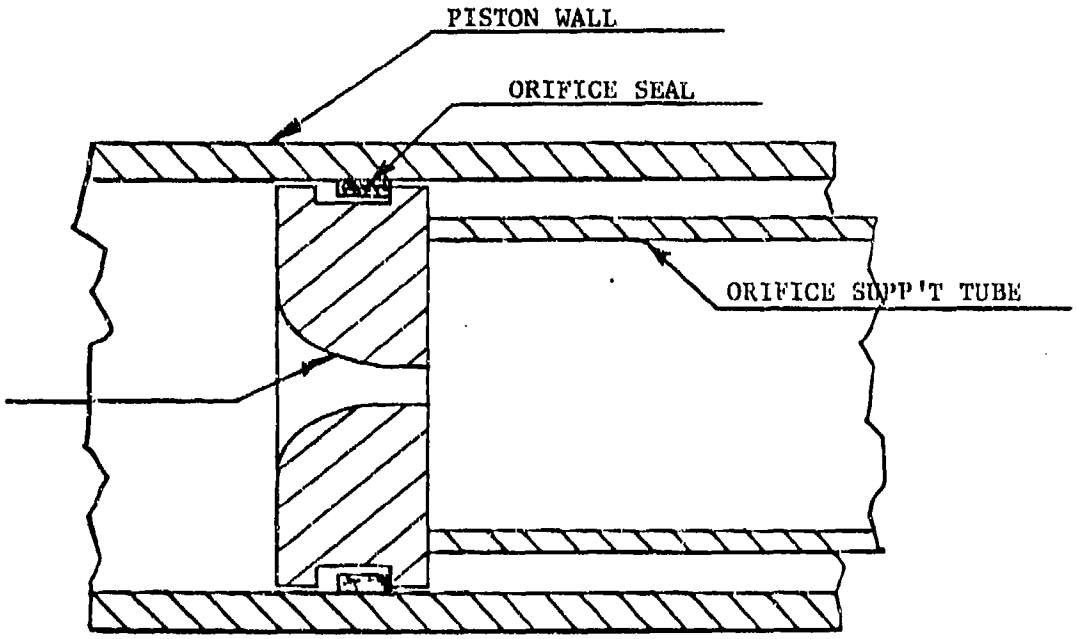

FIGURE 12. Typical Unmetered
Damping Orifice

ρ: Fluid density

A_h: Hydraulic area

A_t: Orifice throat area

C_d: Discharge coefficient

$\dot{s}$: Stroke rate

This equation is derived by applying the Bernoulli and continuity equations across the orifice, and defining an additional term, the discharge coefficient C_d, to account for boundary layer development and streamline curvature effects, which exist in any real flow. The value of C_d is determined empirically, and is generally dependent on the geometric configuration of the orifice and the expected flow regime, as defined by the Reynolds Number. Typical variation of C_d vs. R_e for various geometric configurations of round edge flow nozzle type orifices is shown in Fig. 13. It should be noted that the data in this figure is from steady flow experiments with fully developed flow upstream of the orifice entrance, standardized approach conditions, and constant fluid properties (Ref. 4, 12). Only limited data of this type was available for landing gear damping orifices, and was confined to estimated discharge coefficients for a narrow range of flow conditions (Ref. 10). Also, information concerning reverse flow discharge coefficients was not found. Specific details concerning orifice entrance geometry were not included with the data.

The design of the scaled model gear orifice and a modified full-scale orifice was based on available flow nozzle data (represented by Fig. 13). This was considered to be a rational approach, in view of the lack of available landing gear orifice design data.

In principle, scaled damping characteristics are obtained easily enough by applying the model law to equation (33), which yields the following

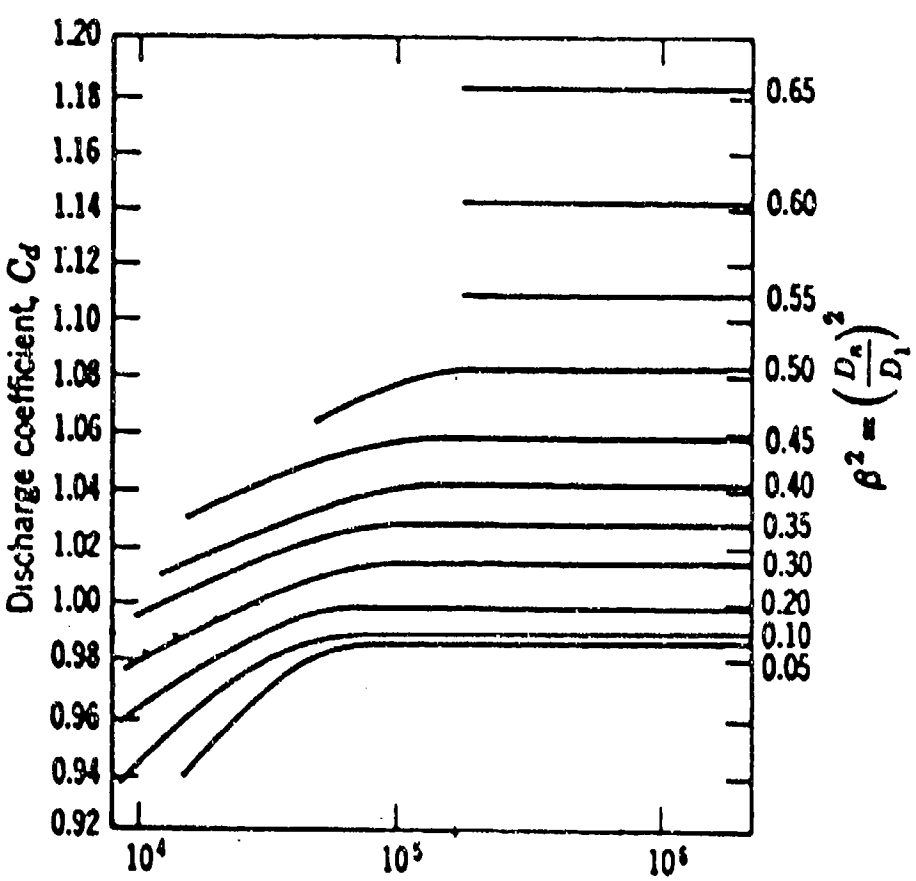

FIGURE 13. Steady Flow Characteristics For a Long Radius Flow Nozzle (Ref. 4, p. 431)

scaled parameters:

$$F_{h_s} = \lambda_F F_{h_o}$$

$$A_{h_s} = \lambda_A A_{h_o}$$

$$A_{t_s} = \lambda_A A_{t_o}$$

$$\dot{s}_s = \lambda_v \dot{s}_o$$

$$\rho_s = \rho_o$$

$$C_{d_s} = C_{d_0}$$

It is evident from Fig. 13 that two requirements must be satisfied in order to achieve identical flow characteristics for two orifices:

1. Geometric similarity, i.e.:

$$\beta_s = \beta_o \tag{34}$$

2. Flow similarity, i.e.:

$$R_{e_s} = R_{e_o}$$

or,

$$\left(\frac{\rho v d}{\mu}\right)_s = \left(\frac{\rho v d}{\mu}\right)_o \tag{35}$$

The first condition is easily satisfied, and is consistent with the model law, however, the second condition is difficult to satisfy in actual practice. Applying the scaling factor definition to (35) yields

$$\lambda_\rho \lambda_v \lambda_d = \lambda_\mu \tag{36}$$

which reduces to

$$\lambda_\mu = \lambda_x^{1.5}$$

Thus, complete flow similarity for all possible flow regimes is achievable only if the model is tested with a fluid that has properties which satisfy the model law i.e.,

$$\rho_s = \rho_o \tag{37}$$

and

$$\mu_s = \lambda_x^{1.5} \mu_o \tag{38}$$

An alternative is to maintain flow similarity by modifying the geometric configuration of the model gear orifice, and testing with the full-scale fluid. Thus, from (36), and setting $\lambda_\mu = 1$,

$$\lambda_d = \lambda_x^{-\frac{1}{2}}$$

However, this is inconsistent with the rest of the model law, since it would require an orifice throat diameter which is larger than full-scale. The result would be highly nonsimilar hydraulic pressure forces, therefore, this approach is not valid.

It has been shown that both of the orifice scaling approaches described above violate some aspect of the model law. Thus, the actual design of the model orifice was based on the approach that was least likely to cause significant deviation from similarity. Pressure forces are dominant over viscous effects in most flow regimes encountered in a landing gear strut, therefore, the model orifice was designed such that geometric similarity was maintained i.e., the throat diameter was sized according to

$$d_s = \lambda_x \cdot d_o$$

Also, the geometric configuration of the full scale and model orifices was designed such that

$$\beta_s = \beta_o$$

so that the high Reynolds Number flow characteristics of each orifice would be the same. A fluid with properties that satisfy conditions specified in the relations (37) and (38) was not available for model tests. However, tests were planned to assess the effect of fluid properties on the orifice damping charac-

teristics. These tests, and the results, are discussed in Section VII and VIII.

3. FRICTIONAL EFFECTS

Friction loads generated in a landing gear strut result from contact of internal seal and bearing surfaces, with the strut piston and cylinder walls. The seal/bearing configuration of a typical single chamber oleo-pneumatic shock strut is shown in Fig. 14. The sources of friction for this configuration are: the top bearing surface, which is in contact with the cylinder wall; the bottom seal/bearing surface, which is in contact with the outer piston wall; and the orifice seal, which contacts the inside piston wall. In general, the magnitude of the friction force depends on the magnitude of the force normal to the load bearing surface, and the coefficient of friction between the two contacting surfaces. The normal force generated at the top bearing surface and the bottom seal surface, is caused by horizontal loading conditions at the axle of the landing gear strut. The resulting frictional force, which opposes the relative motion of the strut components, is governed by the equation

$$F_f = \left[\nu_T \left(\frac{L_a}{L_s + s} - 1 \right) + \nu_B \left(\frac{L_a}{L_s + s} \right) \right] F_d \qquad (39)$$

where ν_T: Top bearing friction coefficient,

ν_B: Bottom seal/bearing friction coefficient,

F_f: Total friction force caused by horizontal axle loads,

F_d: Net horizontal load acting on the axle,

L_s: Bearing separation at zero stroke,

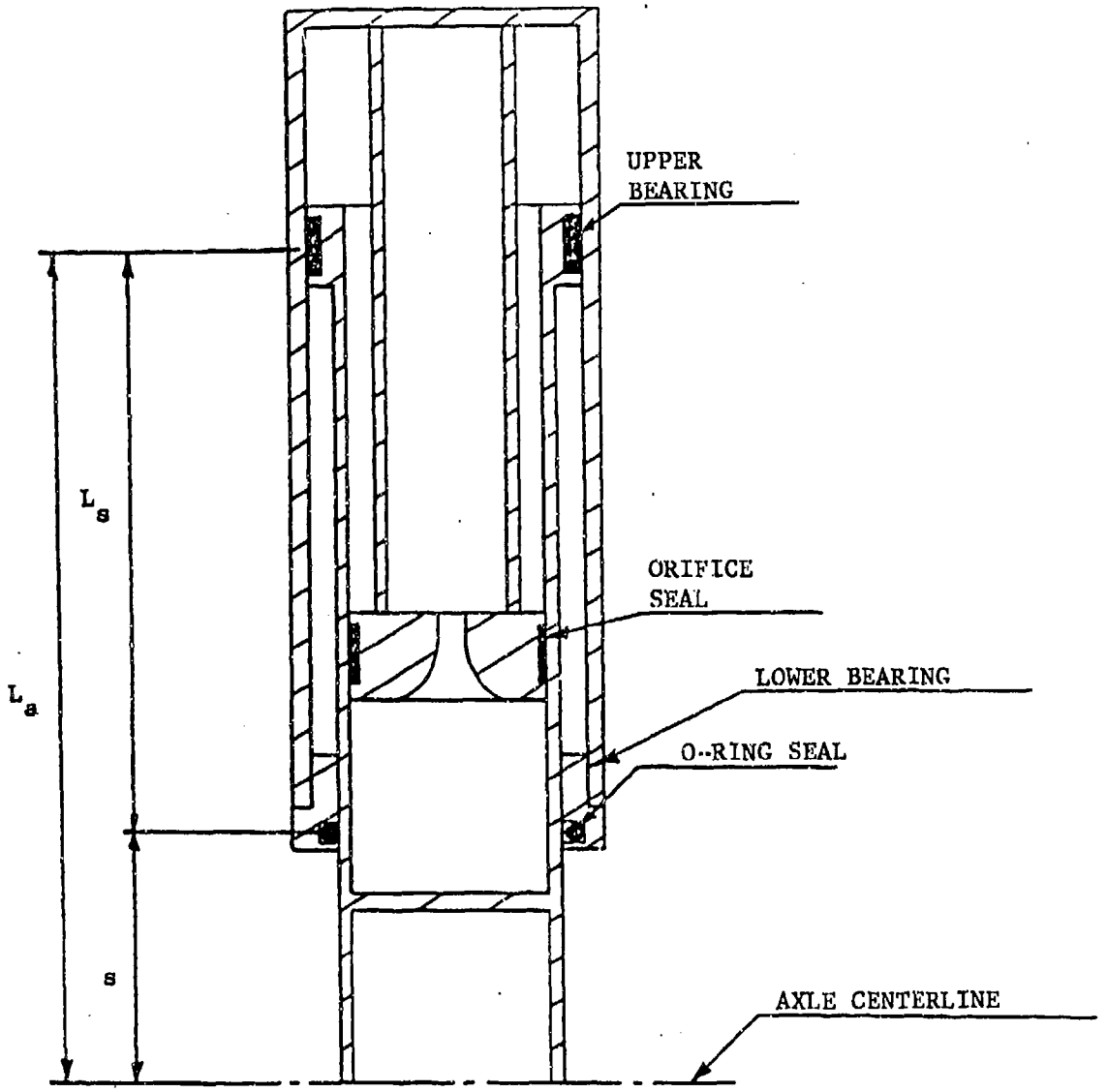

FIGURE 14. Bearing/Seal Configuration
of the A-37 NLG Strut

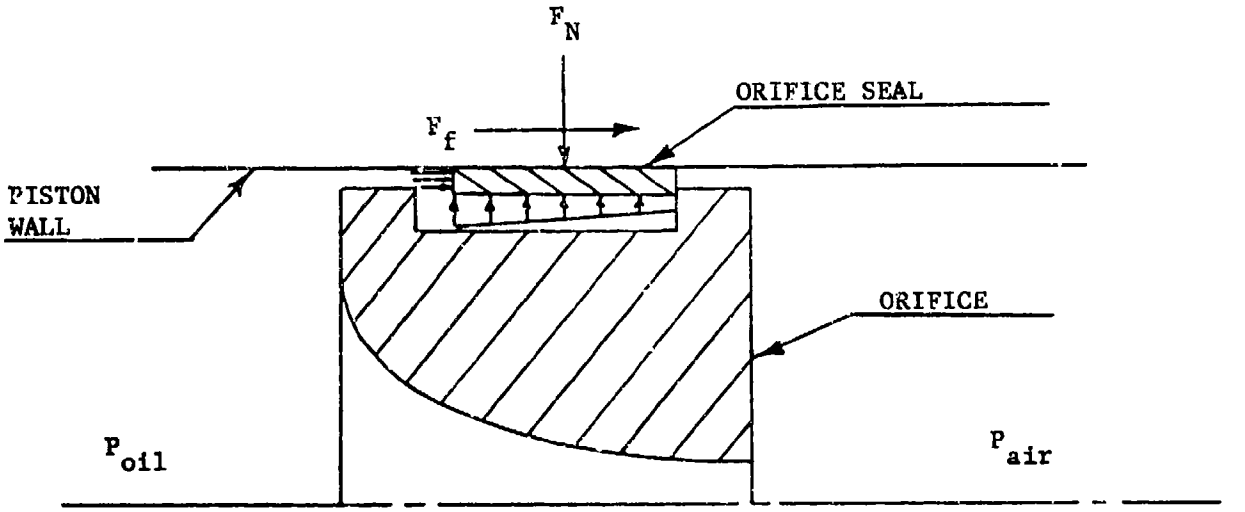

FIGURE 15. Split Ring Orifice Seal

L_a: Moment arm from center of top bearing to the axle center,

s: Moment arm from bottom seal/bearing center to the axle center.

There is an additional frictional effect at the bottom strut seal. This seal, which is typically composed of an elastometric material, must be compressed radially during assembly of the piston and cylinder components. This radial force is required prevent leakage when the strut is initially charged with pressure. The force required to compress the seal during assembly depends on seal design, spring rate, and how much radial squeeze is necessary to permit assembly of mating parts. Also, the radial force of this seal against the mating surface increases proportionally with internal strut pressure, causing a corresponding increase in seal friction. Further analysis of the many types of seals used in landing gear strut design is beyond the scope of this report. More information on various seal designs and applications can be found in Ref. 6 and 11.

The orifice seal is also a source of friction inside a landing gear strut. This seal is generally designed to be pressure energized i.e., sealing integrity is initiated and maintained by a pressure drop accross the seal (see Fig. 15). The radial force required to install this type of seal is minimal, thus, the only substantial radial force component is due to the pressure drop or,

$$F_{f_o} = \nu_o \cdot F_{N_o}$$

where

$$F_n = \Delta P \; A_o$$

and ΔP: Pressure drop across seal,

A_o: Face area of orifice seal,

ν_o: Friction Coefficient,

F_n : Seal normal force.

Dynamically similar frictional loads are obtained, as usual, by scaling the physical parameters in the governing equations. For example, parameters in equation (39) are scaled according to the model law which yields:

$$F_{d_s} = \lambda_F F_{d_o}$$

$$F_{f_s} = \lambda_F F_{f_o}$$

$$L_{a_s} = \lambda_x L_{a_o}$$

$$L_{s_s} = \lambda_x L_{s_o}$$

$$s_s = \lambda_x s_o$$

$$\nu_{T_s} = \nu_{T_o}$$

$$\nu_{B_s} = \nu_{B_o}$$

The model law is similarly applied to other frictional parameters, which yields the target values for the model gear design.

Actually obtaining the required values of all physical parameters which affect the frictional characteristics of a functional model involves detailed consideration of many aspects of component design and fabrication. Factors which may affect frictional properties of the strut include: seal/bearing type and materials, surface finish of mating parts, fabrication tolerances which could affect seal radial compressive force, lubrication conditions, etc. Precise information of the full-scale design would have to be available in order to properly represent the frictional parameters in the model strut.

It is apparent that precise friction scaling is potentially the most difficult aspect of model strut design, since so many factors are involved. The problem is compounded by the fact that, in general, full-scale system frictional characteristics would be unknown. They could, at best, be estimated based on detailed information concerning the design factors identified above.

One possible approach to simplifying the friction scaling problem would entail the use of analytical methods to estimate how frictional characteristics would affect the dynamic response of a strut, for anticipated loading conditions. If friction is predicted to be small in relation to other quantities, (such as hydraulic, pneumatic, and inertial effects) then requirements for dynamically similar friction could be relaxed. In this case, a minimum friction design would be pursued, rather than attempting to achieve the precise characteristics. This would greatly simplify the model design approach. As friction becomes more dominant, the requirement for better friction scaling is more of a consideration. In this case, an analytical method could also be used to establish an acceptable variation range of frictional properties, which could simplify model design and fabrication.

Friction control methods used in this particular program are discussed in Section V.

SECTION IV

ANALYTICAL VALIDATION OF THE MODEL LAW

The model law developed in Section II was evaluated analytically with a computerized model of a single oleo-pneumatic shock strut and tire. The computer program, called LANSIM, was developed by the Mechanical Subsystems Group (AFWAL/FIEMA) of the Air Force Wright Aeronautical Laboratories. It computes the vertical dynamic response of a single landing gear strut, by a time-step numerical integration of the governing equations of motion, using a fourth order Runge-Kutta method. A simple diagram of the tire-strut model used is depicted in Fig. 16. Pneumatic and hydraulic forces were calculated for each time-step according to equations (25) and (33) respectively. The tire force computations per time-step were based on calculated deflections of each radial element, in proximity to a user defined, two-dimensional ground obstacle model. Total horizontal and vertical force components were summed together at the axle.

The following assumptions were made in the development of LANSIM:

1. Taxi speed of the landing gear strut was constant throughout all simulations;

2. Aerodynamic damping was not modeled;

3. Only vertical dynamic response of the strut was modeled. Other possible modes of vibration were not included;

4. All strut components were modeled as rigid i.e., material strain was not considered;

5. Rolling, braking and tire envelopment effects were not modeled;

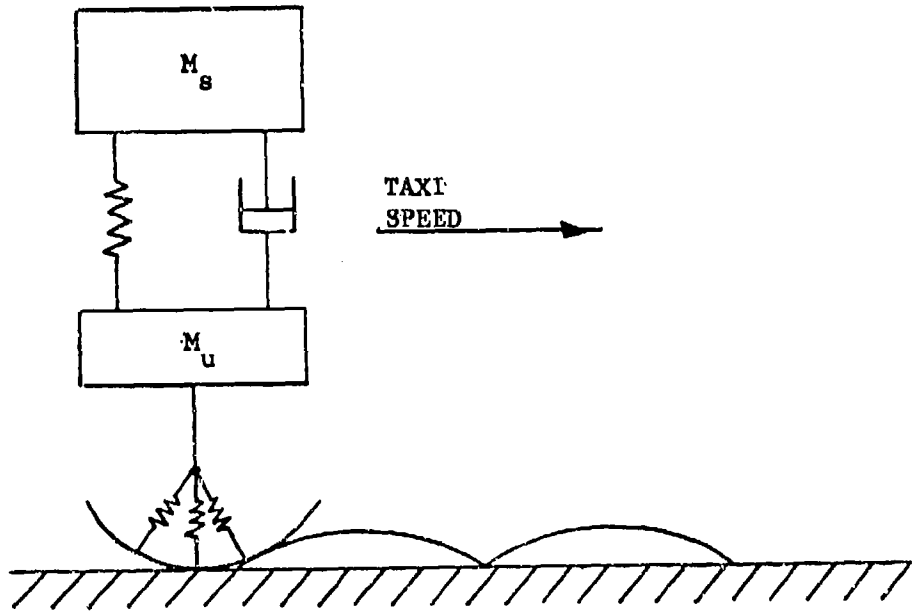

FIGURE 16. LANSIM Strut/Tire Model

6. Stroking friction was not included in these initial simulations. (An adequate friction model was not developed and incorporated into the model until late in this program. Simulations with friction are discussed in Appendix B);

7. A constant area orifice was modeled. The discharge coefficient was not varied with Reynolds Number; a constant value was used for forward and reverse flows. Viscous forces were not modeled;

8. The polytropic exponent was constant for all pneumatic force calculations.

Verification of the model law was accomplished by making a direct comparison of time history data from independent simulations of the full-scale A-37 NLG, and a dynamically scaled model of this strut. The full-scale A-37 NLG was simulated first to establish a data baseline for later comparisons with model gear simulation results. All strut parameters and other simulation parameters were scaled according to the model law developed in Section II, for corresponding model gear simulations.

The model gear strut and tire parameters were calculated from the model law, and corresponding full-scale A-37 NLG parameters, using a scaling factor of one-third, i.e.,

$$\lambda_x = 1/3$$

There were a total of four separate simulations conducted. The first simulation was of the full-scale A-37 NLG; the second was of an "exact" scale model of this strut (including properly scaled ambient pressure); and the third simulation was of the model gear for nonscaled ambient pressure conditions. Simulation #4 was similar to Simulation #3 in that the ambient pressure component was not scaled. However, the pneumatic volume at the static equilibrium position for simulation #4 was calculated according to equation (32), to insure proper natural frequency scaling of the air spring. The static stroke position

for this case was determined by scaling the corresponding full-scale static stroke position, according to λ_x. Input parameters for each simulation are listed in Tables 2 and 3. The forcing function for all simulations was a sequence of two 1-cosine bumps placed end to end. The dimensions of the bumps are shown in Fig. 17.

Each simulation was repeated for two "taxi" speeds, over the 1-cosine bumps. These speeds are also listed in Table 2. The model gear speeds were determined by scaling the full-scale speeds in Simulation #1, according to $_v$.

Model gear simulation results were scaled up by applying the appropriate scaling factors to each output parameter. Time history data for each model gear simulation was then plotted against corresponding baseline data from the full-scale gear simulation. All simulation data is located at the end of this section, due to the amount of data presented.

Data from simulation #2 is presented in Fig. 18 through 21. Scaled up results are identical to full-scale gear simulation results for this case in which all input parameters were scaled correctly according to the model law, (including the ambient pressure component of the air spring.)

Data from simulation #3 is presented in Fig. 22 through 25. All input parameters for this simulation were scaled as in Simulation #2, with the exception of the ambient pressure. The full-scale value was used. All parameters clearly show some deviation of peak values during bump traversal, as well as a phase shift during the free response after clearing the bumps.

Data from Simulation #4 is presented in Fig. 26 through 29. All input parameters for this simulation were scaled as in the previous model gear runs, with the exception of the ambient pressure component which was full-scale, and

INPUT PARAMETERS	SIMULATION #1	SIMULATION #2	SIMULATION #3	SIMULATION #4
m_{sp} (lb) :	660.00	24.44	24.44	24.44
m_u (lb) :	44.00	1.63	1.63	1.63
V_0 (in) :	19.29	0.715	0.715	0.731
A_p (in) :	2.71	0.30	0.30	0.30
N :	1.25	1.25	1.25	1.25
P_0 (psig) :	18.45	6.15	6.15	-0.99
P_a (psia) :	14.70	4.90	14.70	14.70
A_h (in) :	2.09	0.23	0.23	0.23
A_o (in) :	0.02	0.002	0.002	0.002
C_d :	0.90	0.90	0.90	0.90
C_d :	1.10	1.10	1.10	1.10
v (FPS) :	7.00	4.00	4.00	4.00
	10.00	5.77	5.77	5.77
	20.00	11.40	11.40	11.40

TABLE 2. LANSIM Inputs (Strut Model)

SIMULATION #1		SIMULATION #2-4	
F_t (lb)	δ (in)	F_t (lb)	δ (in)
100.0	0.10	3.70	0.033
425.0	0.30	15.74	0.10
860.0	0.50	31.85	0.167
1462.0	0.75	54.15	0.250
2200.0	1.00	81.48	0.333
Tire Free Radius:	8.0 in	Tire Free Radius:	2.667 in
Section Height :	3.4 in	Section Height :	1.133 in

TABLE 3. LANSIN Inputs (Tire Model)

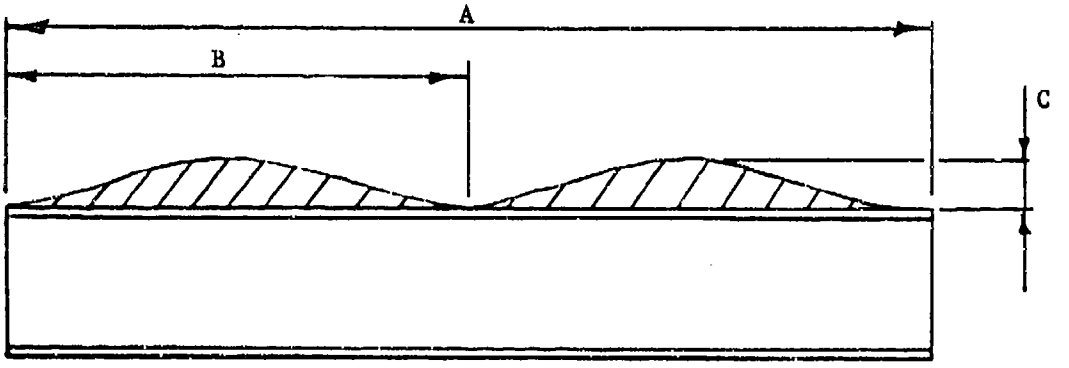

	A(ft.)	B(ft.)	C(in)
PHASE I :	6.0	3.0	1.5
PHASE II :	2.0	1.0	0.5

FIGURE 17. Ground Feature Dimensions

the static equilibrium pneumatic volume, which was scaled according to equation (32). Very good agreement was obtained for all output parameters.

Fig. 30 shows the difference in the static pneumatic force-stroke characteristics for each simulation. Note that all stroke values are referenced to the static equilibrium strut position.

In summary, the analytical simulations proved the basic validity of the model law as formulated in Section II. It was shown that good results are possible, despite the unscaled ambient pressure, if the volume at the static equilibrium position is scaled according to Equation (32).

(An additional fact concerning the computer runs was noted. On the average, the model gear simulations required 30 to 40 percent less CPU time than corresponding full-scale A-37 NLG simulations, and yielded equivalent results. Thus, from a computational point-of-view, scale model simulations were considerably more efficient than full-scale simulations.)

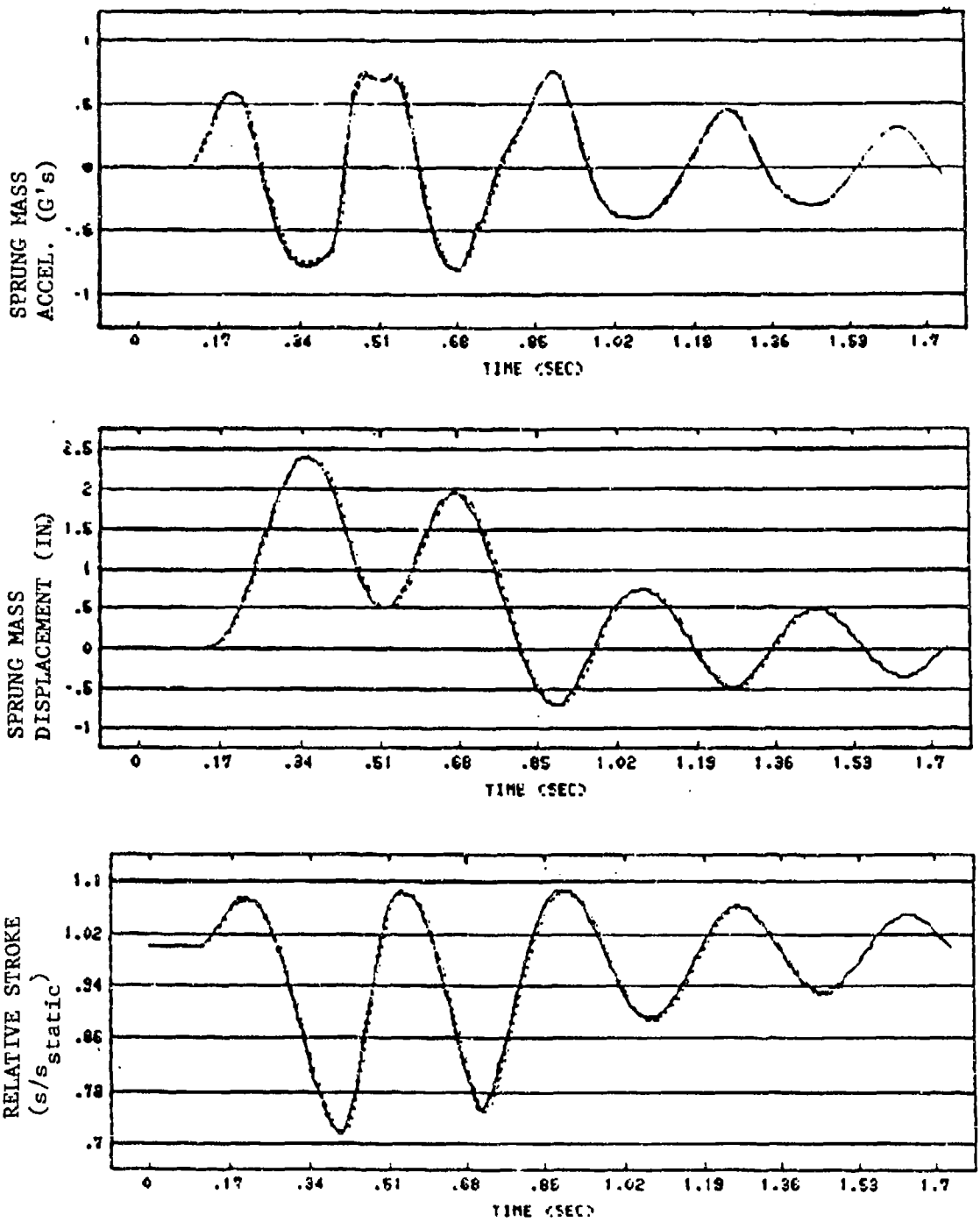

	TAXI SPEED	LEGEND
FIGURE 18. Model Gear (Sim. #2)	5.7 Ft/s	———
vs.		
A-37 NLG (Sim. #1)	10.0 Ft/s	·····

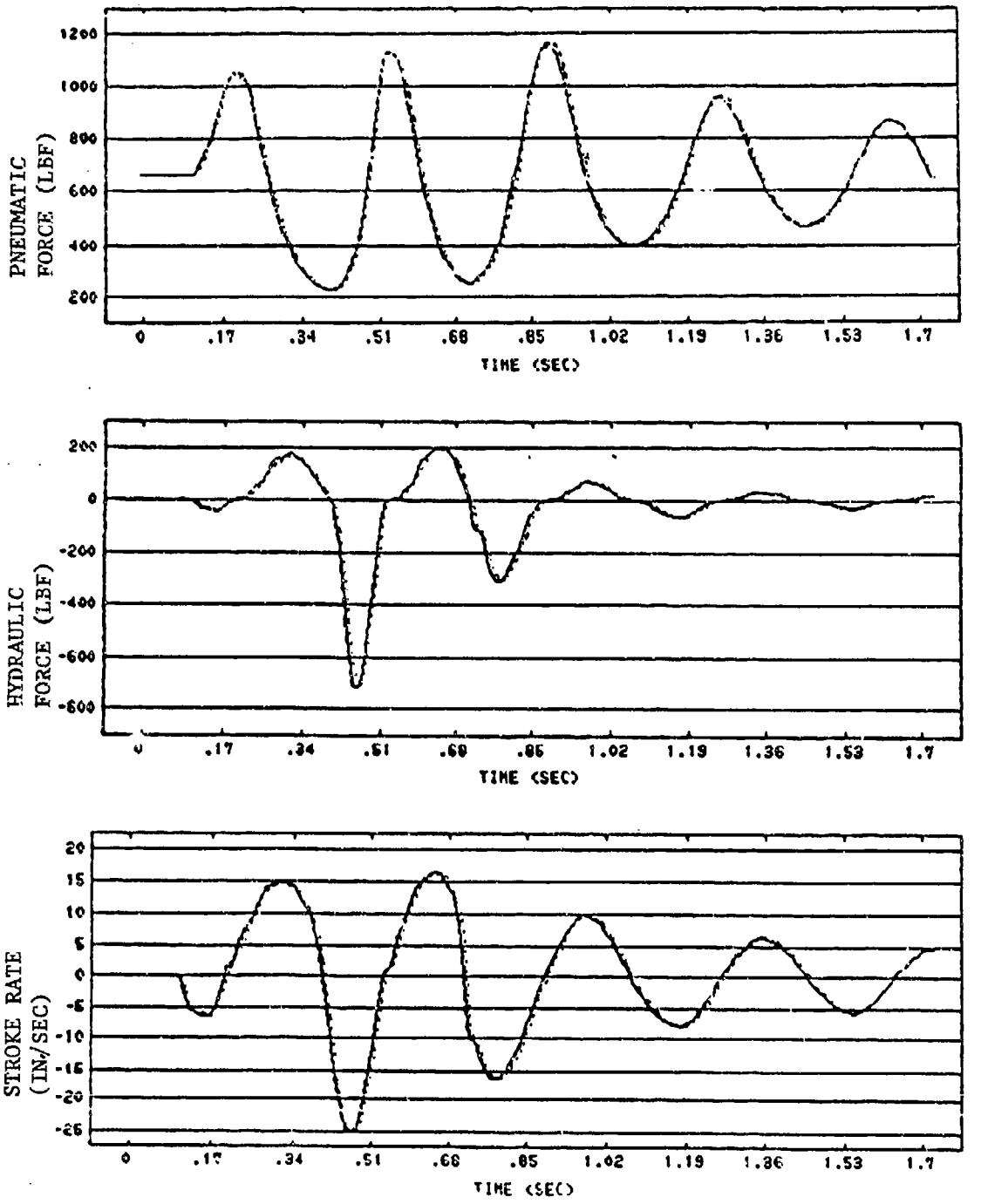

TAXI SPEED	LEGEND
5.7 Ft/s	———
10.0 Ft/s	·····

FIGURE 19. Model Gear (Sim. #2)

vs.

A-37 NLG

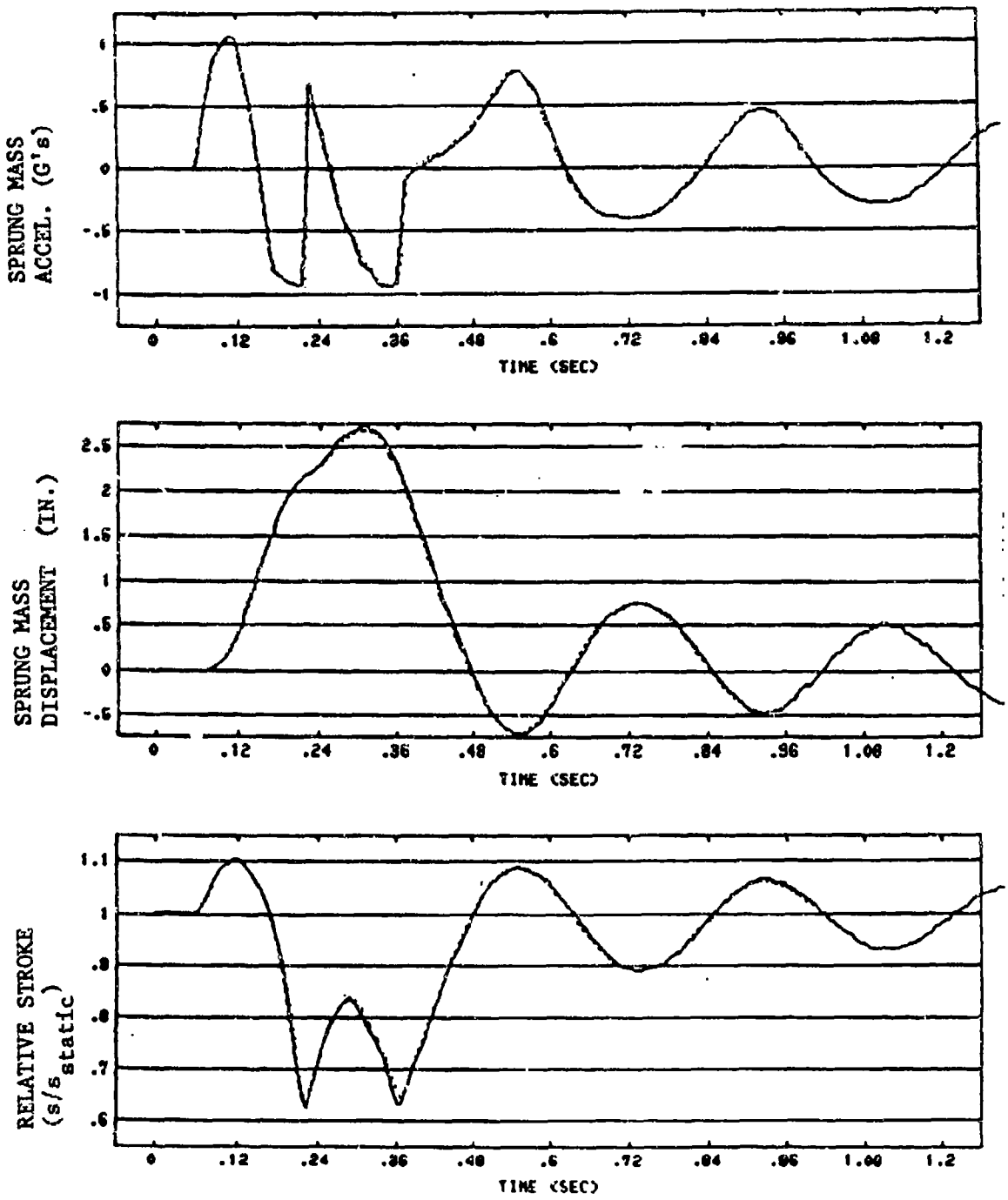

	TAXI SPEED	LEGEND
Model Gear (Sim. #2)	11.5 Ft/s	_____
vs.		
A-37 NLG (Sim. #1)	20.0 Ft/s	.....

FIGURE 20.

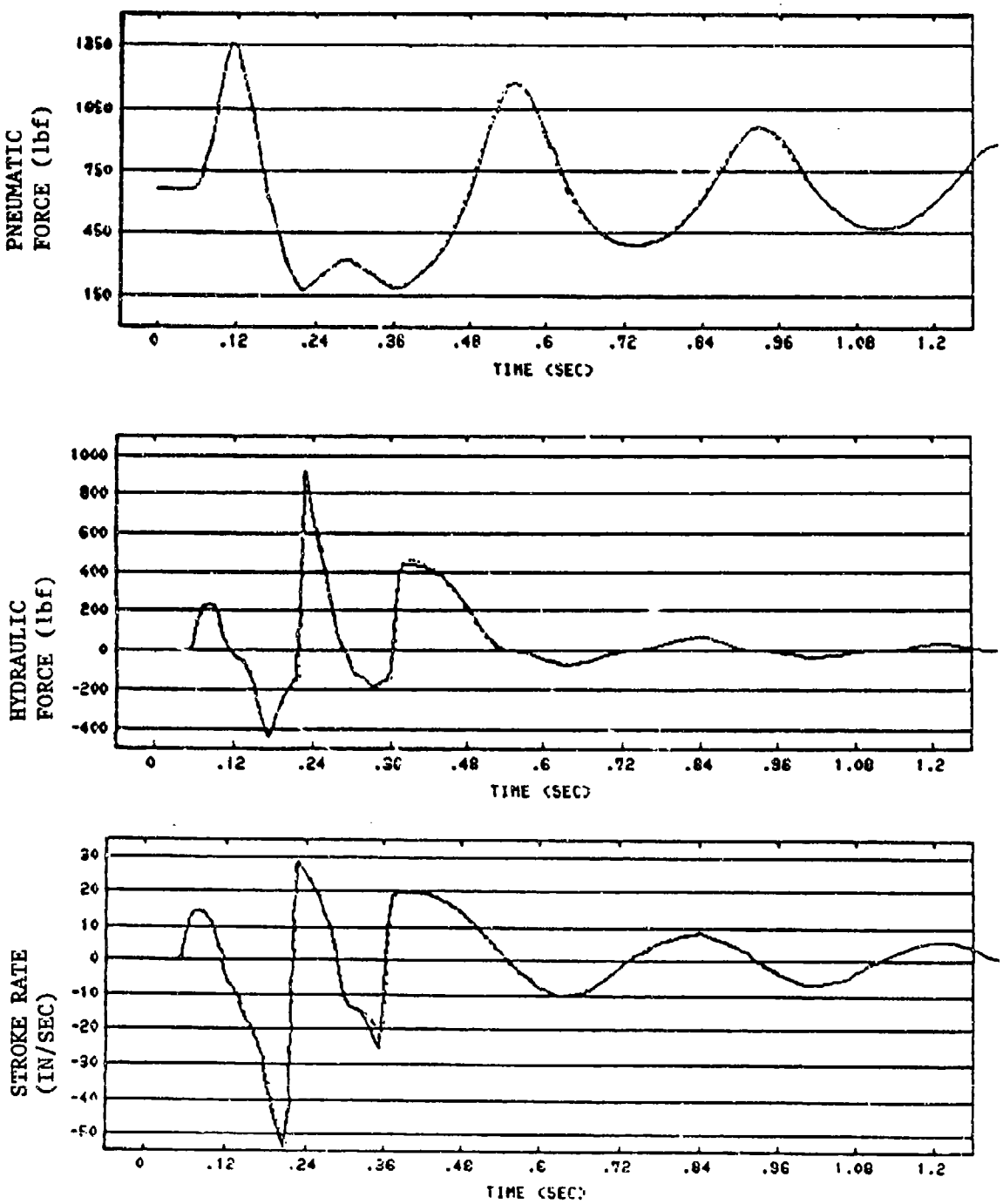

TAXI SPEED	LEGEND
11.5 Ft/s	———
20.0 Ft/s	.....

FIGURE 21. Model Gear (Sim. #2) vs. A-37 NLG (Sim. #1)

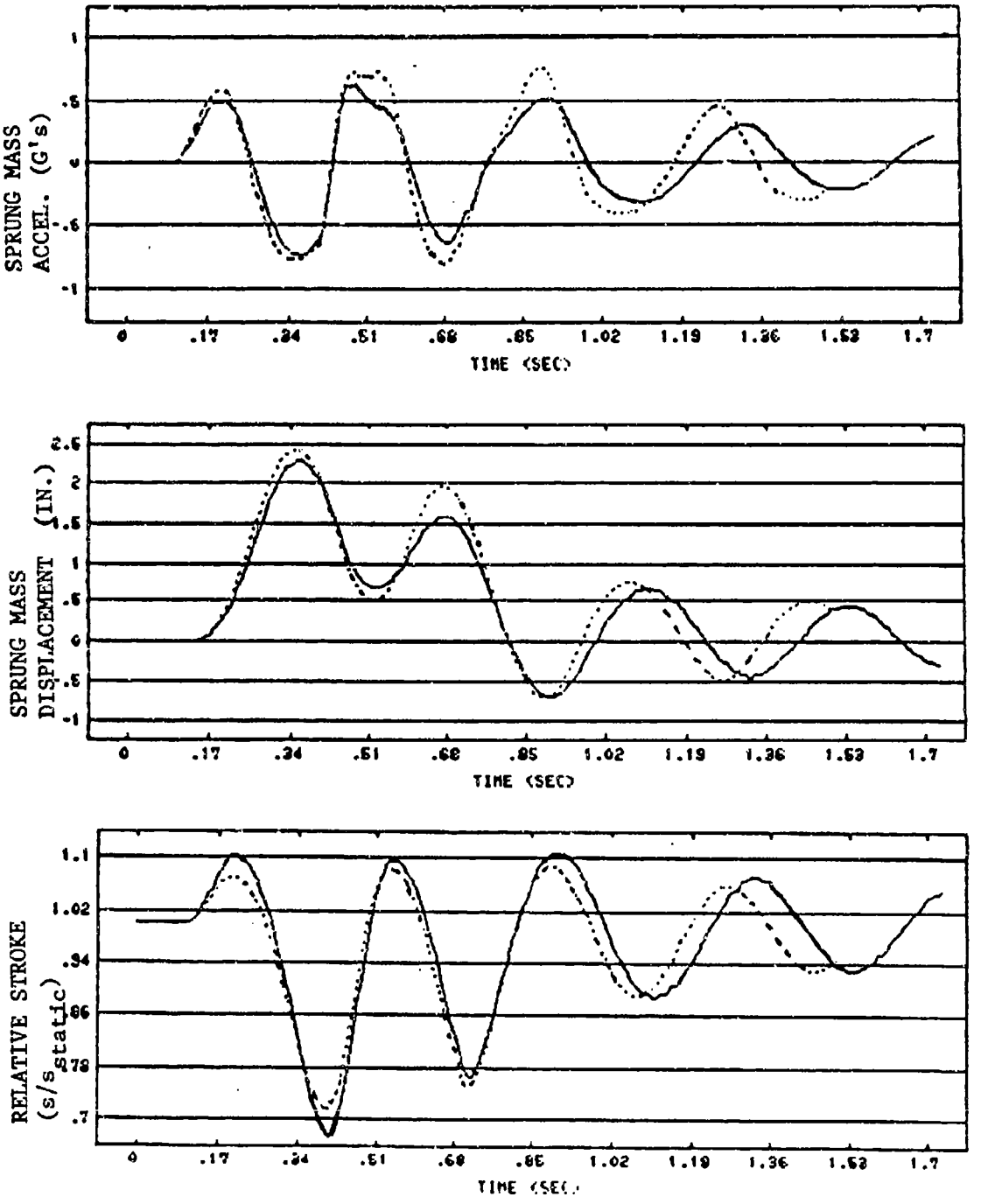

	TAXI SPEED	LEGEND
Model Gear (Sim. #3)	5.7 Ft/s	———
vs.		
A-37 NLG (Sim. #1)	10.0 Ft/s	.....

FIGURE 22.

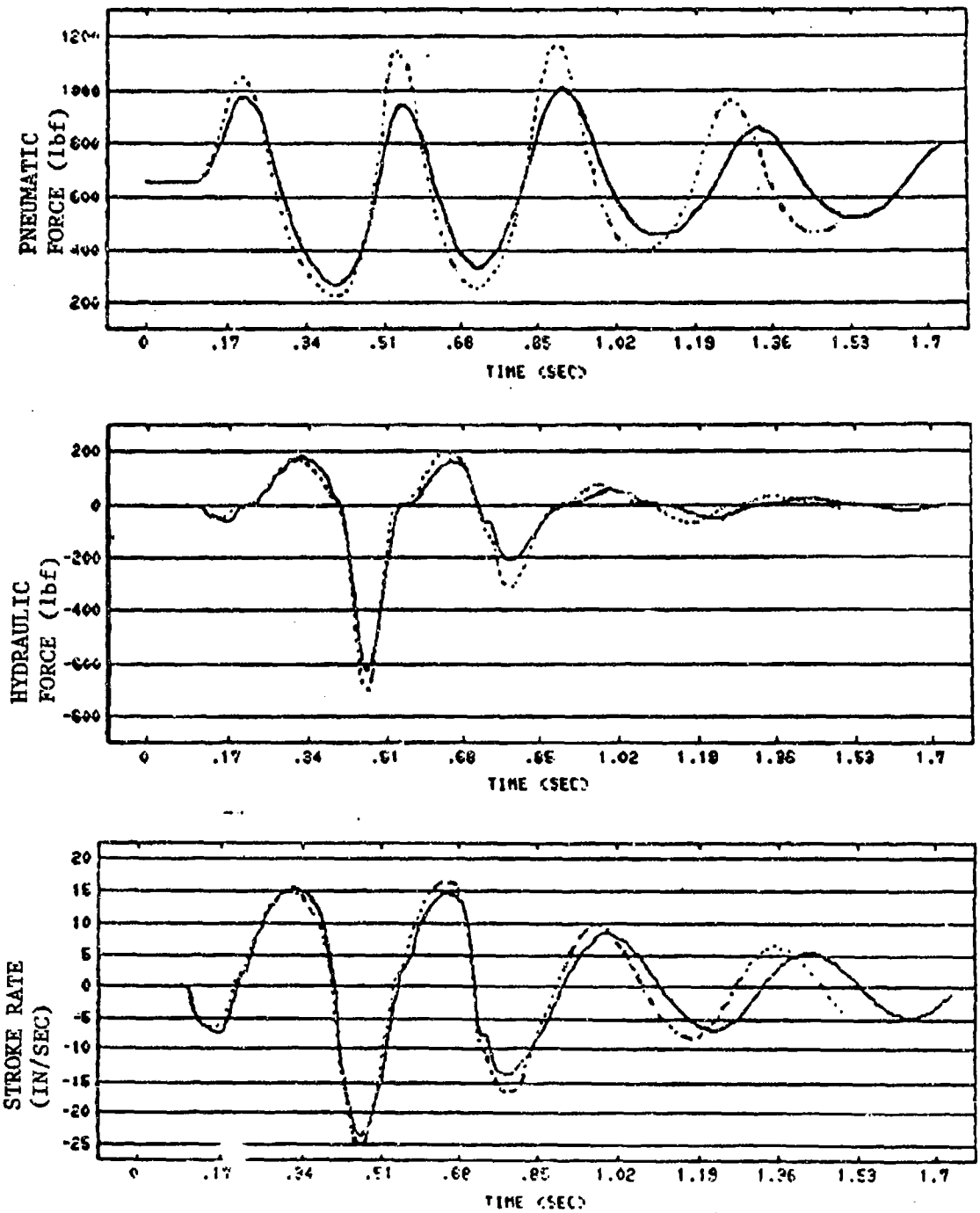

	TAXI SPEED	LEGEND
Model Gear (Sim. #3)	5.7 Ft/s	———
vs.		
A-37 NLG (Sim. #1)	10.0 Ft/s	.....

FIGURE 23.

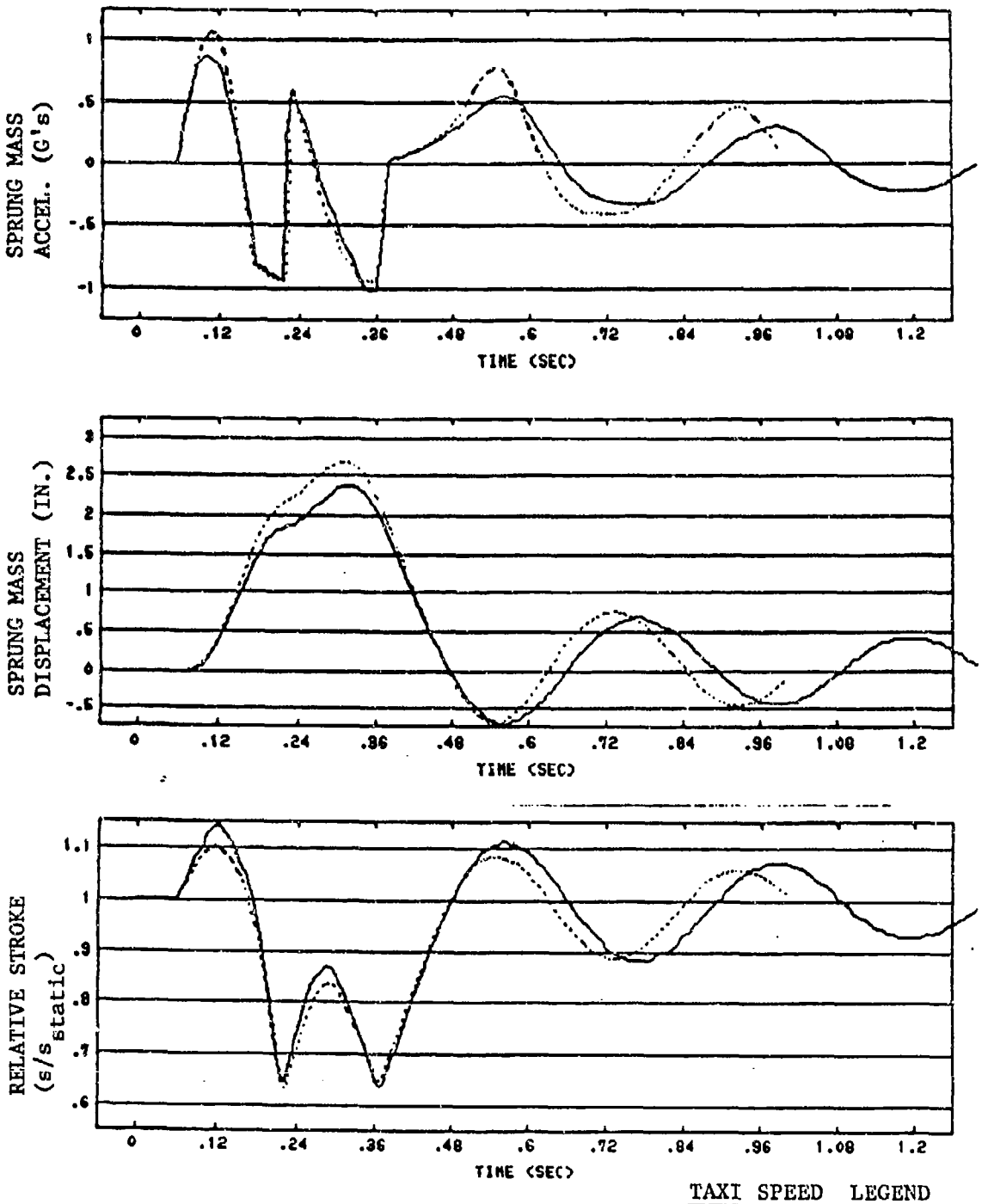

	TAXI SPEED	LEGEND
FIGURE 24. Model Gear (Sim. #3)	11.5 Ft/s	_____
vs.		
A-37 NLG (Sim. #1)	20.0 Ft/s	.....

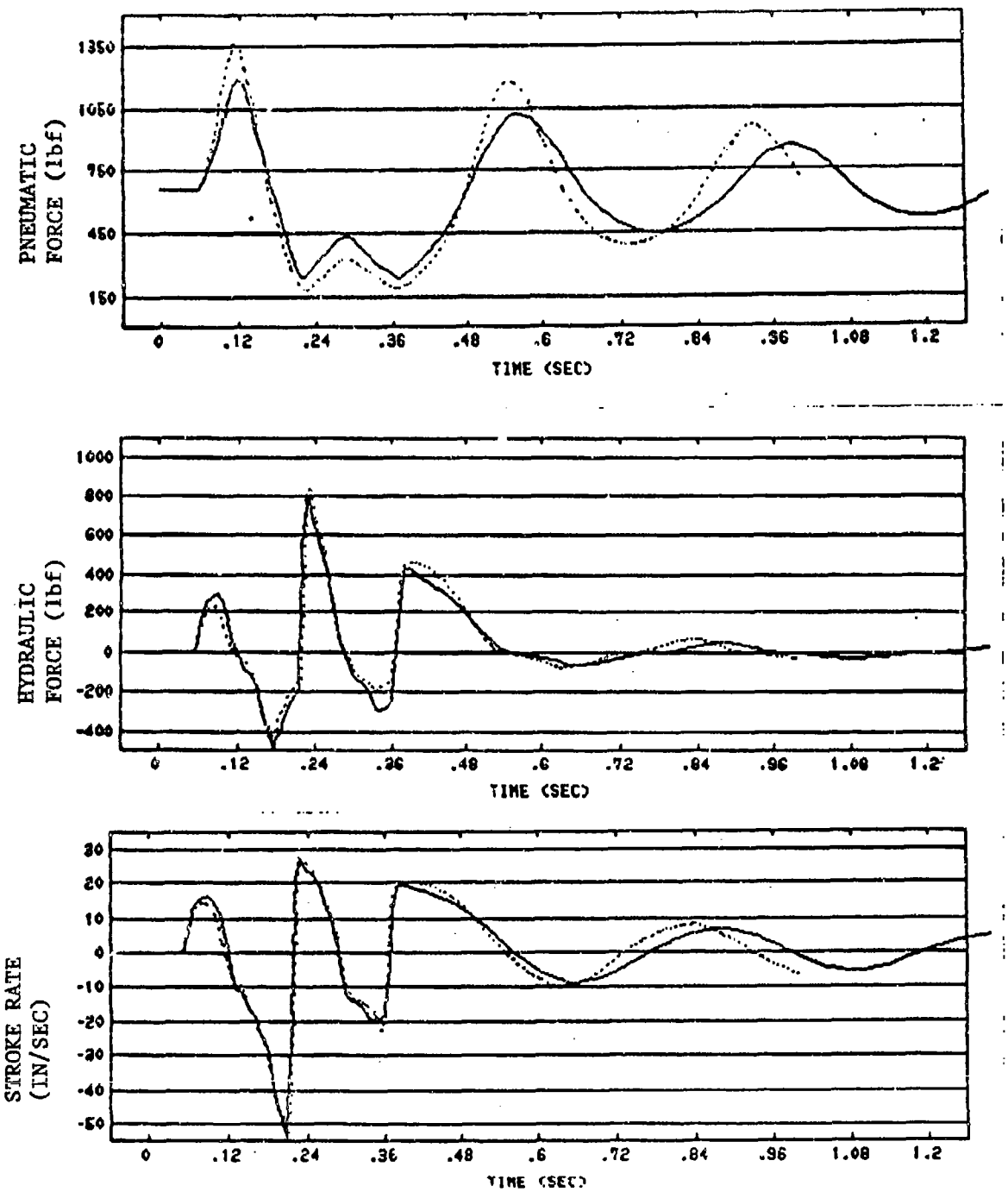

TAXI SPEED LEGEND

11.5 Ft/s _____

20.0 Ft/s .....

FIGURE 25. Model Gear (Sim. #3) vs. A-37 NLG (Sim. #1)

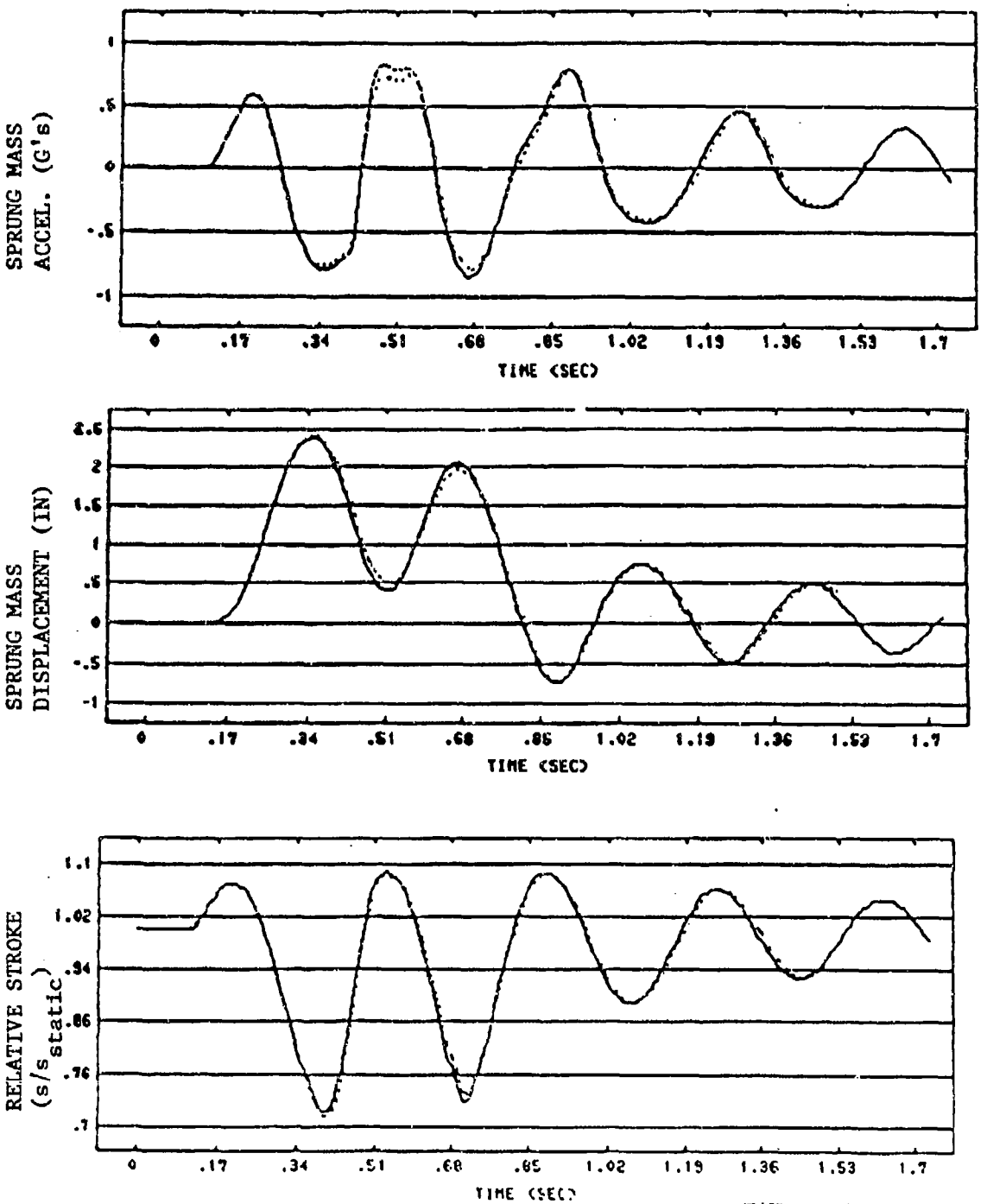

	TAXI SPEED	LEGEND
Model Gear (Sim. #4)	5.7 Ft/s	———
vs.		
A-37 NLG (Sim. #1)	10.0 Ft/s	.....

FIGURE 26.

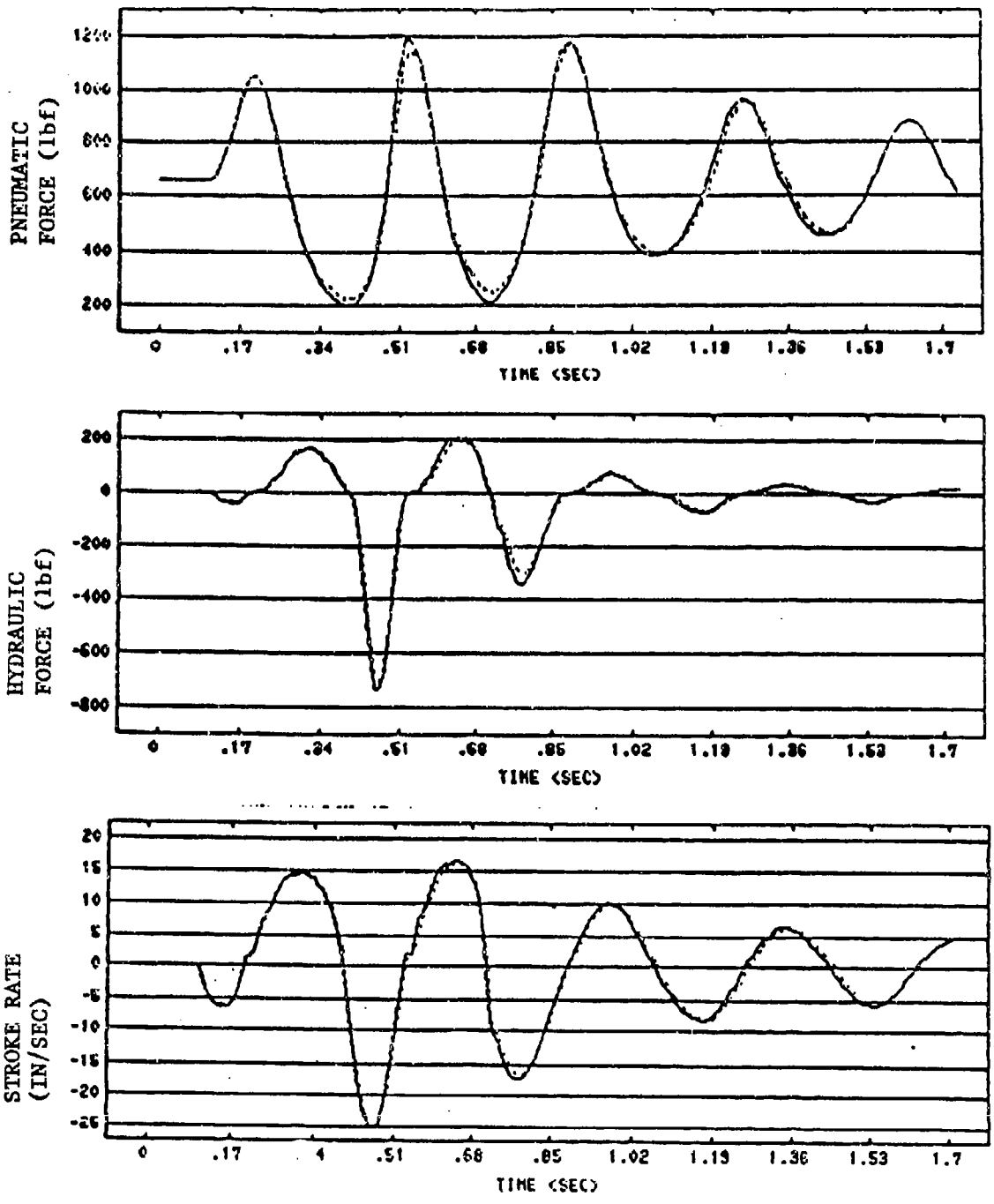

	TAXI SPEED	LEGEND
FIGURE 27. Model Gear (Sim. #4)	5.7 Ft/s	———
vs.		
A-37 NLG (Sim. #1)	10.0 Ft/s	.....

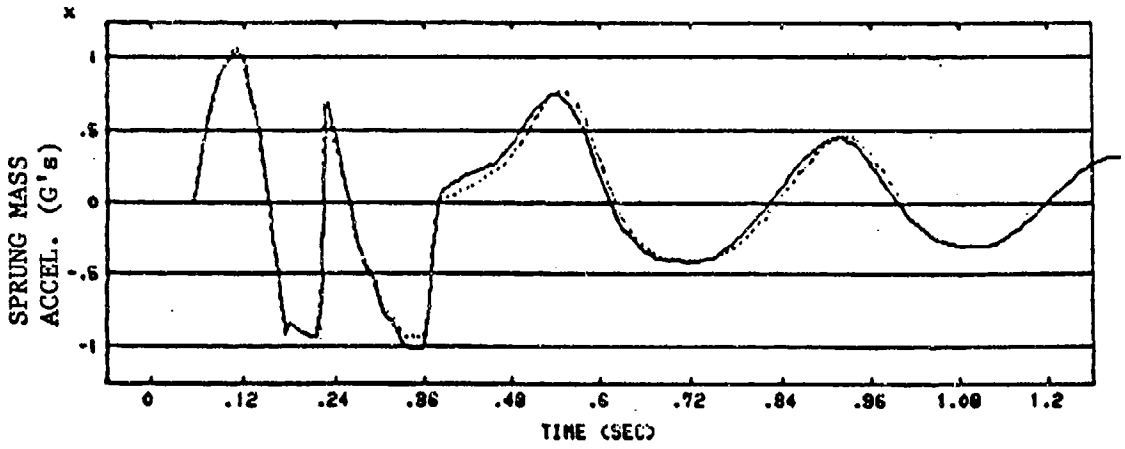

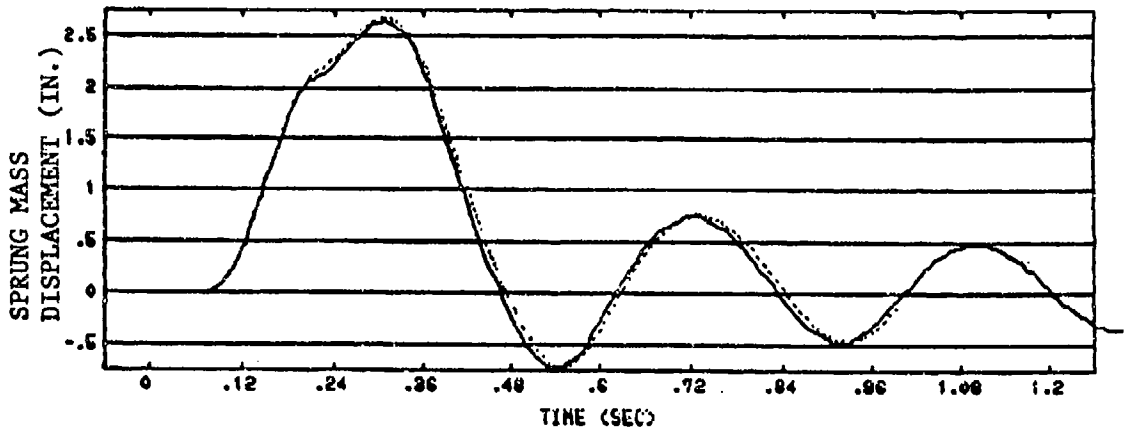

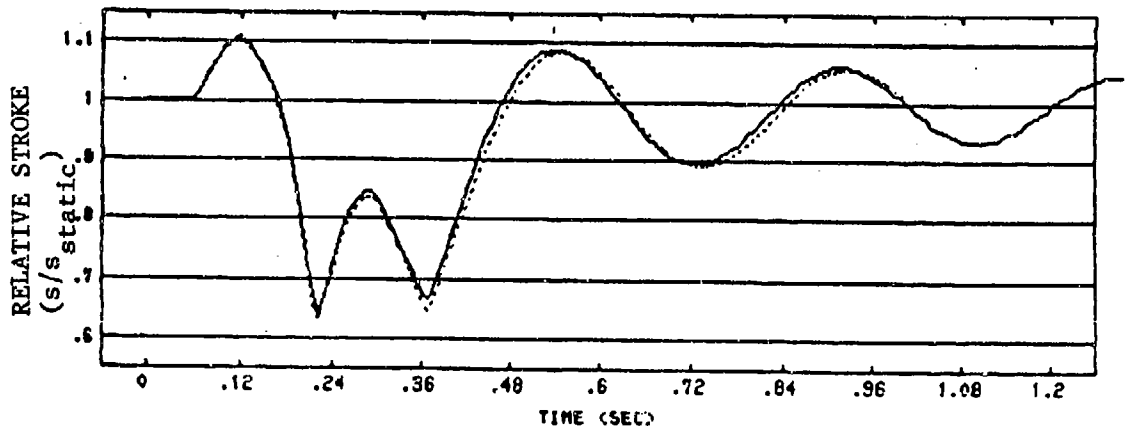

	TAXI SPEED	LEGEND
FIGURE 28. Model Gear (Sim. #4)	11.5 Ft/s	_____
vs.		
A-37 NLG (Sim. #1)	20.0 Ft/s	.....

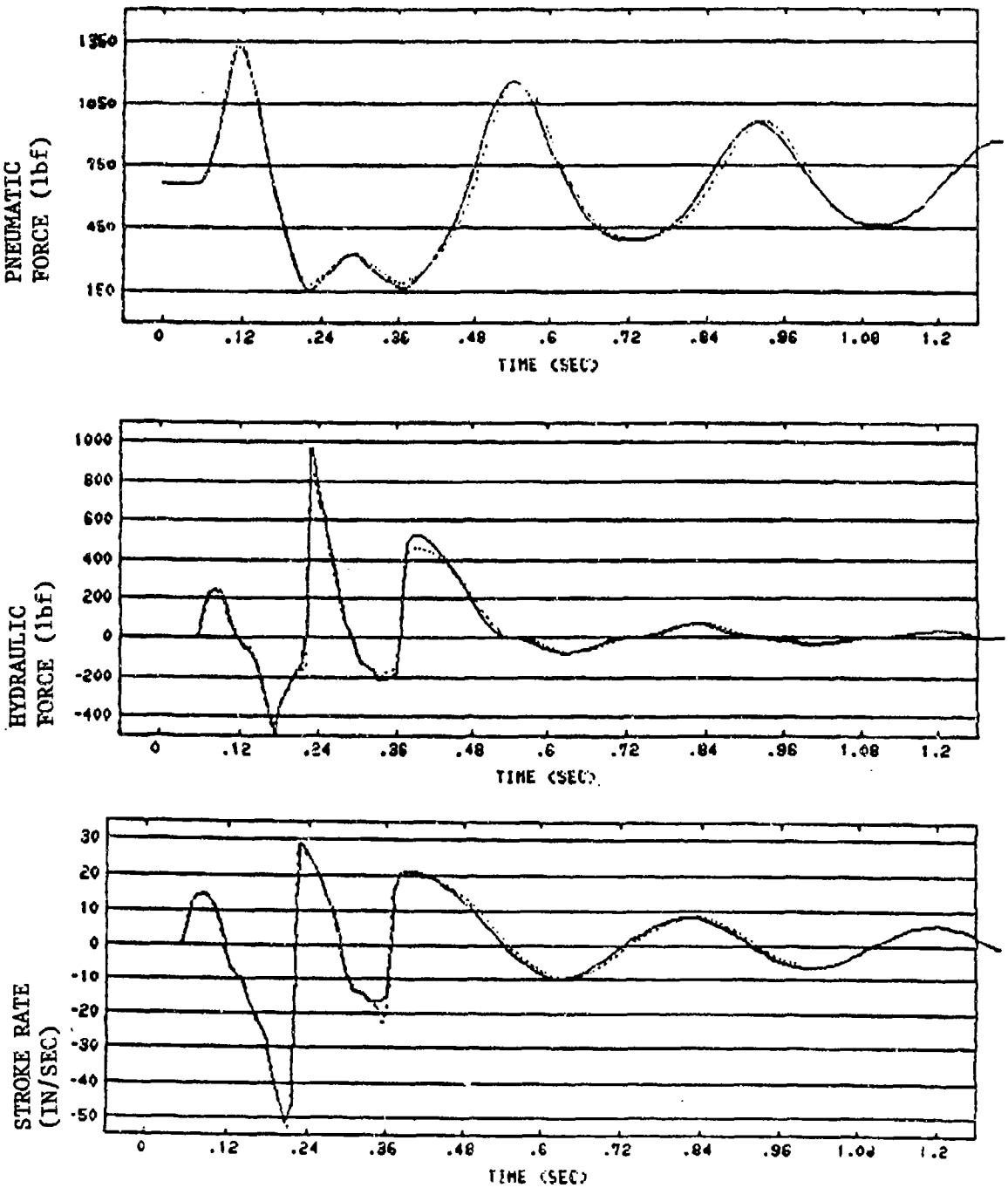

	TAXI SPEED	LEGEND
FIGURE 29. Model Gear (Sim. #4)	11.5 Ft/s	_____
vs.		
A-37 NLG (Sim. #1)	20.0 Ft/s	.....

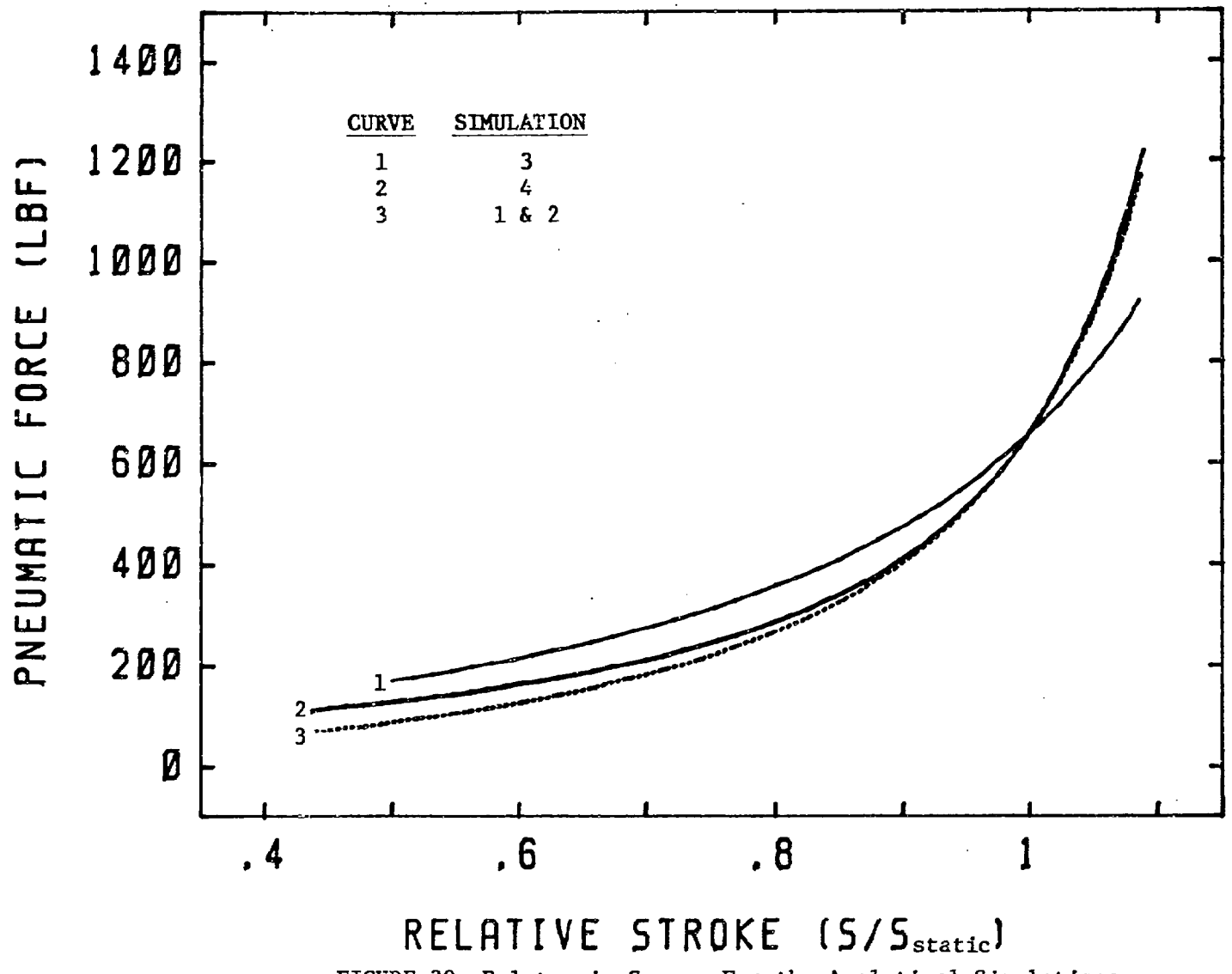

FIGURE 30. Polytropic Curves For the Analytical Simulations

SECTION V

THE SCALE MODEL STRUT

The computerized analysis of the preceding section was sufficient to validate the model law from a theoretical point-of-view, however, the results were subject to the idealized assumptions inherent in the analytical model. An empirical approach to investigate the feasibility and practicality of using the developed scaling techniques in a realistic hardware application, was the primary objective of the overall program. This phase involved design, fabrication, testing, and evaluation of a one-third dynamically scaled model of the A-37 NLG strut.

1. GENERAL DESIGN PARAMETERS

The model gear design parameters were calculated by applying the scaling factors to corresponding full-scale strut parameters. The A-37 NLG strut parameters were obtained from measurements made of individual components of the disassembled strut. This method was used because detailed fabrication drawings of the strut were not available. Results of the measurements, and target values for model gear design parameters, are presented in Table 4. Table 5 lists the strut components which were lumped together into representative sprung and unsprung weights. The weights of the instrumentation devices were also included.

The relatively small A-37 NLG unsprung weight, and the large degree of weight scaling required to satisfy the model law (based on the chosen scaling factor $\lambda_W = 1/27$), yielded an unsprung weight for the model gear which was difficult to obtain. The dimensions of the model gear strut components re-

PARAMETER	A-37 NLG	SCALE FACTOR	MODEL GEAR PARAMETER
M_{sp} (lb) :	660.00	1/27	24.44
M_u (lb) :	44.00	1/27	1.63
V (in) :	42.90 (Dry)	1/27	1.59
A_p (in) :	2.71	1/9	0.30
A_h (in) :	2.09	1/9	0.23
S_{max} (in):	7.25	1/3	2.42
L_a (in) :	24.19	1/3	8.06
L_s (in) :	4.88	1/3	1.63

TABLE 4. Measured A-37 NLG Parameters and Target Model Gear Design Parameters

SPRUNG WEIGHT	UNSPRUNG WEIGHT
- Dead Weight Supported by Gear	- Piston
- Cylinder	- Fork
- Orifice Support Tube	- Axle Assembly
- Orifice	- Wheel
- Lower Bearing/Seal Block	- Tire
- Trunion	- Pressure Transducer
- Displacement Pot.	
- Accelerometer	
- Pressure Transducer	
- Heave Post	

TABLE 5. Individual Strut Components

quired to ensure structural integrity for expected loading conditions, led to an unsprung weight figure that exceeded the value required to maintain dynamic similarity. This problem was circumvented by increasing the unsprung weight of the full-scale A-37 NLG enough to compensate for the excessive weight of the model unsprung components. This was accomplished by adding circular lead disks to the A-37 NLG strut axle (these weights are visible in Fig. 40 on page).

2. FRICTIONAL CHARACTERISTICS

A requirement for obtaining precise frictional scaling was not included in the design specifications of the model gear strut. This was primarily due to two considerations: 1) detailed full-scale friction data for the loading conditions which could be expected during the tests was not available for verification of model gear friction, and 2) there was no comprehensive approach for designing the model strut components to yield properly scaled friction. The factors which would have to be included in such an approach were previously identified in Section III.

The approach used in this program was to design a seal/bearing configuration in the model, which was similar to that of the A-37 NLG. An o-ring design was used for the strut seal (Ref. Fig. 7), which is the same type of seal used in the A-37 NLG strut. Details of the model gear o-ring seal design are shown in Fig. 31. The specifications for this design were consistent with standard practice used in the design of a typical reciprocating rod type seal. Also, the top bearing and the orifice seal were of similar designs as those used in the A-37 NLG strut.

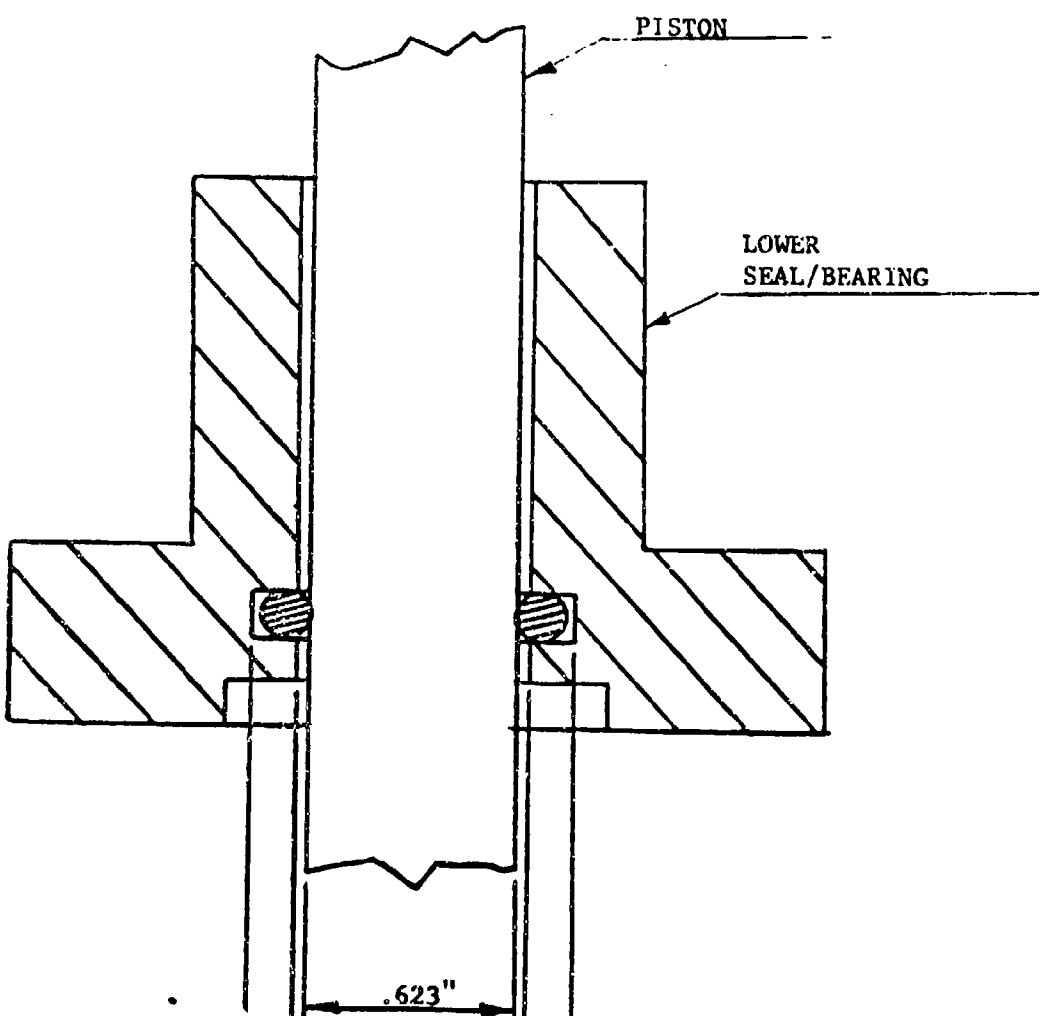

O-RING

CROSS SEC.: .103"
WIDTH

I.D. : .612"

MATERIAL : BUNA-N

HARDNESS : 70 (SHORE)

FIGURE 31. Model Gear Strut Seal
Design Details

The model gear orifice seal was a split ring design. Several of these seals, each with a different uninstalled gap width, were supplied with the model gear as a means of increasing or decreasing stroking friction as required (see Fig. 32). The seals with a larger uninstalled gap width required a larger radial compressive force for installation, which caused a corresponding increase in friction. The seals with the smaller gap widths required less force for installation, which resulted in less friction.

3. ORIFICE DESIGN

The A-37 NLG strut was originally equipped with a metering pin, which tailors damping forces during a landing impact. For purposes of this program, however, the metering pin was removed, and the original orifice was replaced with a fixed area orifice. The throat area was sized according to the estimated annular area of the original metered orifice, at the static equilibrium strut position. The shape of the full-scale and model gear orifices was designed according to the method outlined in Section III. Design details for each orifice are presented in Fig. 33.

Photographs of various full-scale and model gear strut components are presented in Fig. 34 and 35. These photos relate the small physical size of the model gear strut components. The fully assembled model gear strut is shown, in comparison with the full-scale A-37 NLG, in Fig. 5.

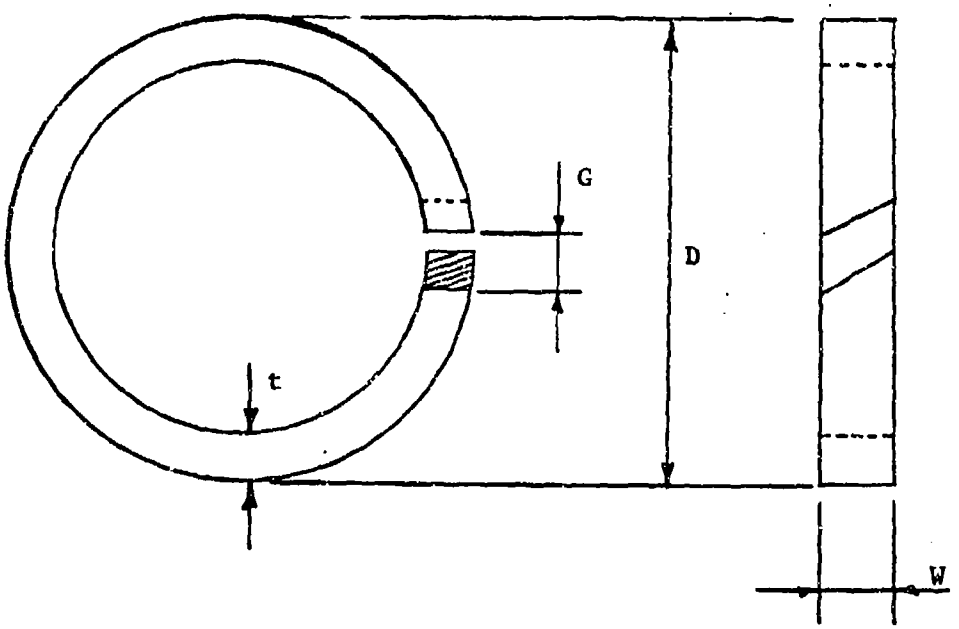

D : Installed Diameter

G : Uninstalled Gap Width

t : Minimum Thickness

W : Ring Width

FIGURE 32. Split Ring Seal Design Parameters

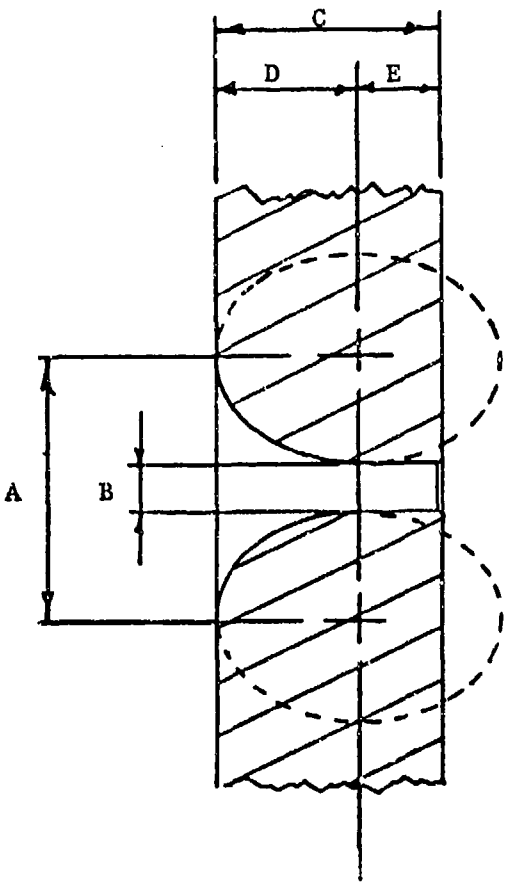

ORIFICE	A	B	C	D	E
A-37	.500	.160	.275	.250	.025
MODEL	.167	.053	.092	.083	.008

FIGURE 33. A-37 NLG and Model Gear Damping Orifice Design Details

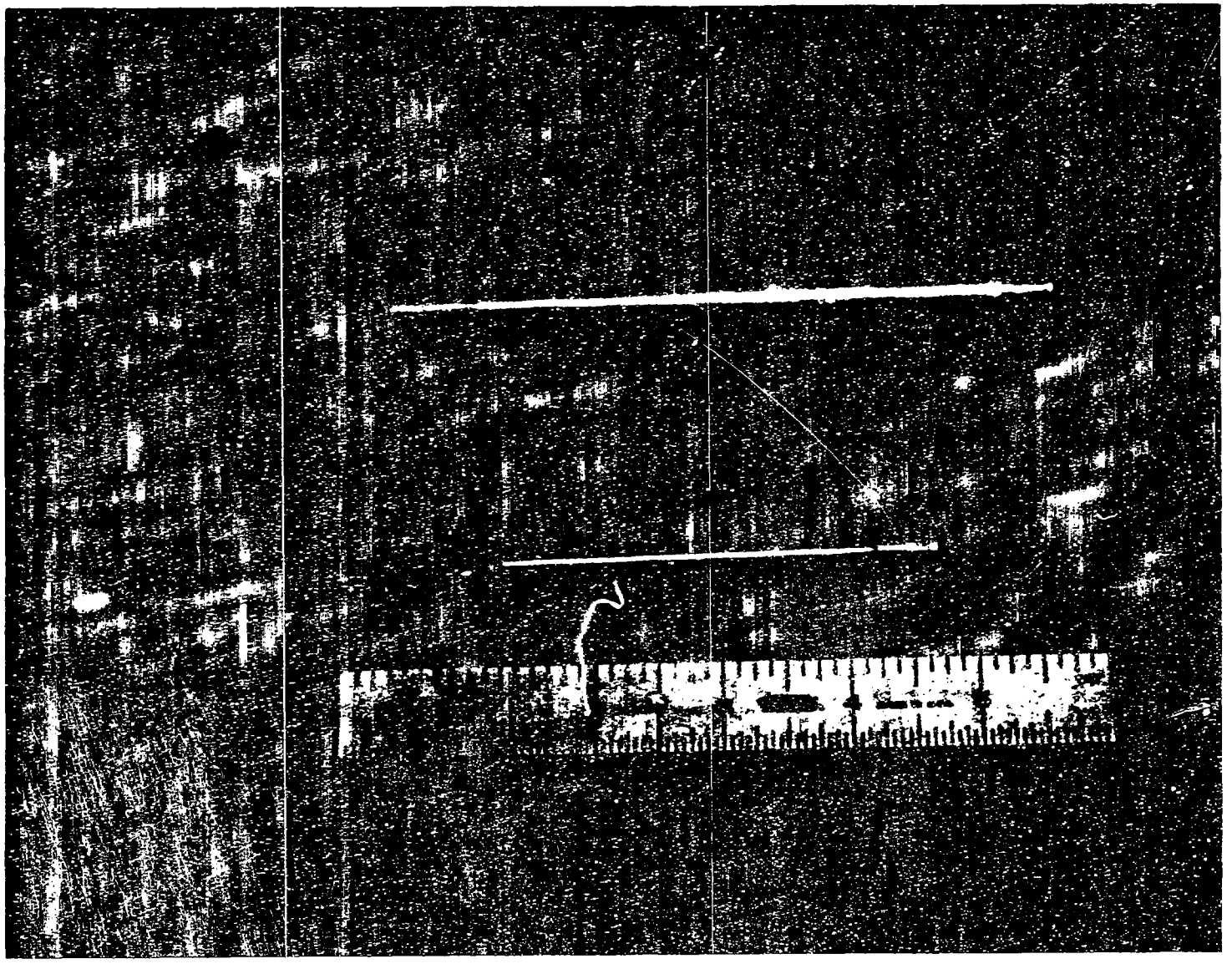

FIGURE 34. Model Gear Components

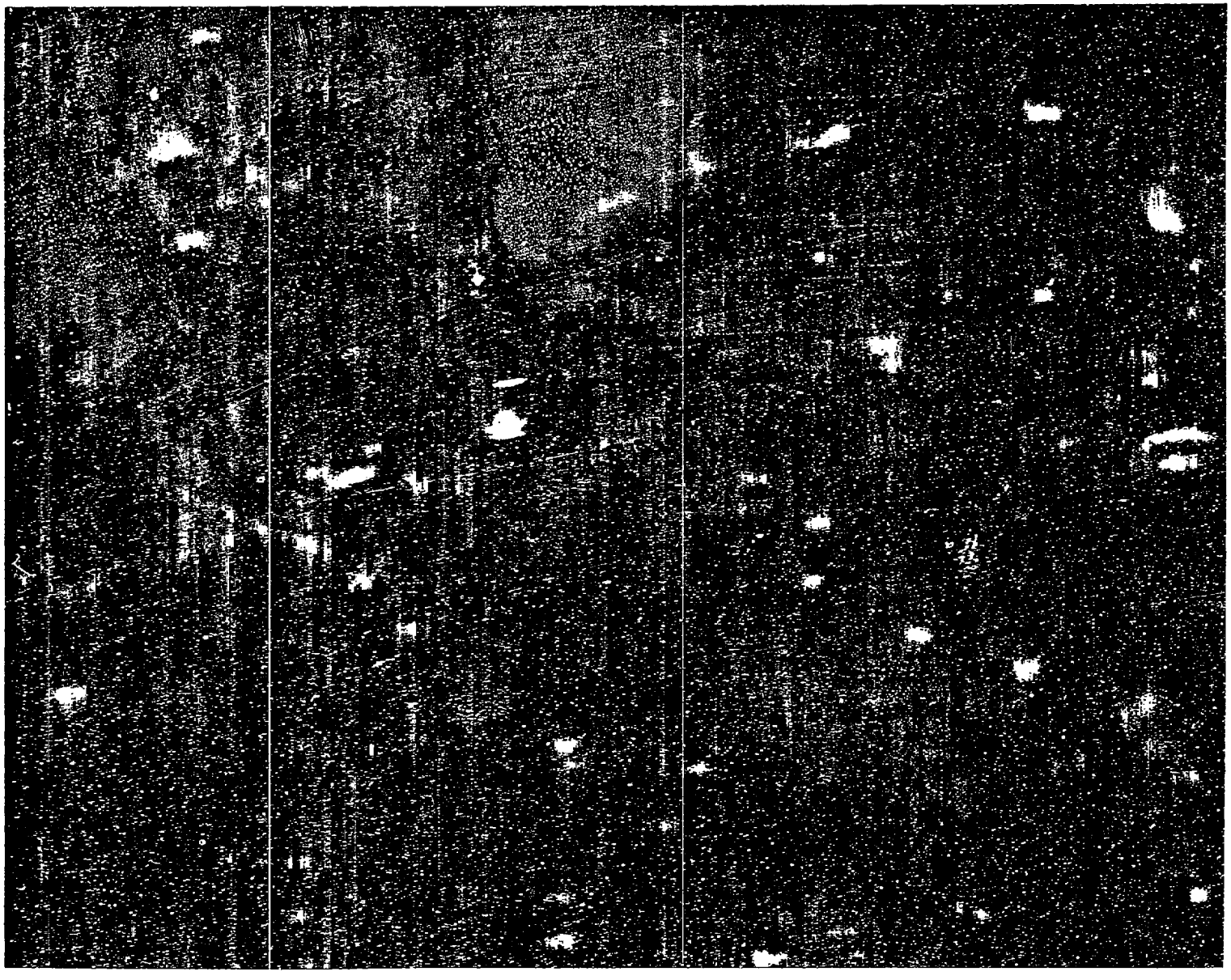

FIGURE 35. A-37 NLG and Model Gear Damping Orifices

SECTION VI

THE SCALE MODEL WHEEL AND TIRE

The availability of the technology to fabricate a scale model tire with the characteristics required to satisfy the model law was a key factor in the conception and successful implementation of the test portion of this program. The techniques for designing and fabricating dynamically scaled model aircraft tires were developed and proven during programs conducted in 1970 and 1981 at the University of Michigan. These techniques are not discussed in this report. Information concerning basic tire scaling techniques are discussed in Ref. 1 and 3.

The specifications for the model tires that were used in this program called for dynamic scaling of the vertical load-deflection characteristics only i.e.,

$$F_T = \lambda_F \cdot F_T \quad @ \quad \delta_s = \lambda_x \cdot \delta_o$$

where F_T: Vertical tire force

δ: Vertical tire deflection

and, λ_F: 1/27

λ_x: 1/3,

for all points on the load-deflection curve. Scaling of other tire properties including lateral, torsional, and fore-aft stiffness was not specified. Accurate scaling of these properties was considered as beyond the scope of this initial attempt at scaling a landing gear strut. Averaged vertical load-deflection data from static tests of model and full-scale A-37 NLG tires is presented in Fig. 36. The model tire data was scaled up with the appropriate scaling factors for this comparison.

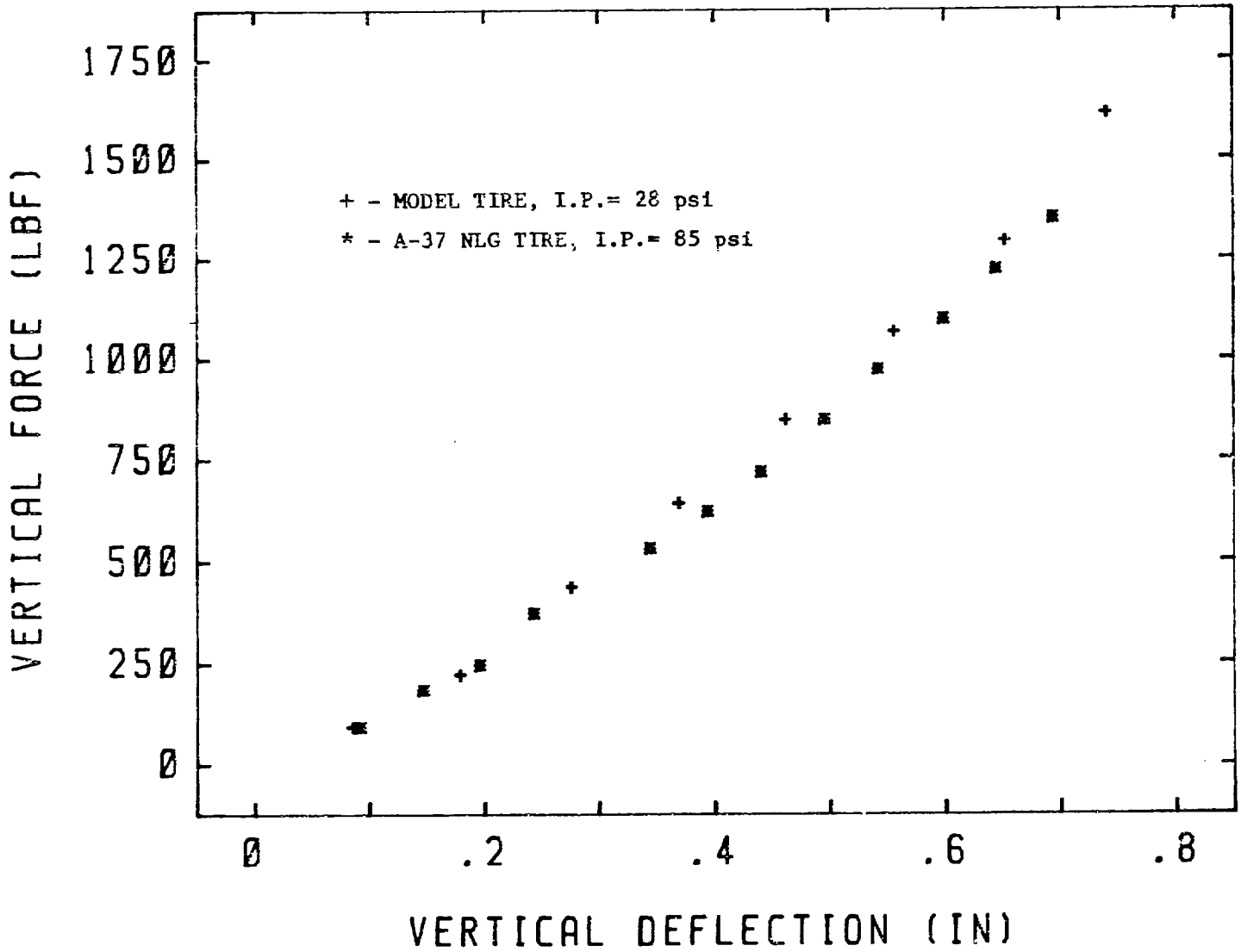

FIGURE 36. Comparison of A-37 NLG Tire and the Model Gear Tire Load-Deflection Curves

Fig. 37 is a photograph of a model tire, which was cut in half to show the tire cross-section, and how the tire interfaced with the model wheel. The tire design included a bead design that is similar to the bead design used in aircraft tires. This is the first time this feature has been used in small scale model tire design.

The components of the model wheel are shown in Fig. 38. The wheel is assembled by placing the model tire over one wheel half, and then bolting the second wheel half in place. Sealing integrity is maintained by the tire bead, which seats against the wheel rim, and an o-ring which prevents pressure loss between the two wheel halves.

The mass of the wheel and tire is included as part of the overall unsprung mass. Individual mass scaling of the tire and wheel, with their respective full-scale A-37 NLG conterparts, was not accomplished for this program. Scaling of other mass properties, such as various wheel/tire moments of inertia, was not attempted.

FIGURE 37. Model Tire Cross-Section

FIGURE 38. Model Wheel Components

SECTION VII

THE TEST PROGRAM

A two-phase test program was planned to acquire the data needed for a comprehensive evaluation of the model gear dynamic performance, relative to that of the A-37 NLG, and the model law. The A-37 NLG was tested during Phase I to establish a data baseline for a given set of test parameters. Follow-on tests of the model gear strut were then conducted in Phase IIa and Phase IIb. Scaled conditions for model gear tests were determined from the model law, and corresponding Phase I test conditions. Phase I and II test parameters are presented in Table 6.

Model gear tests were conducted for two different hydraulic fluids to investigate the effect of fluid properties on the hydraulic force characteristics of the model damping orifice. The first series of model tests were run with full-scale hydraulic fluid, i.e., MIL-H-5606 standard fluid. The second model test series was run with a fluid that had essentially the same density as MIL-H-5606. The viscosity of this fluid was considerably less than MIL-H-5606, but it was still approximately 17.6 percent greater than the value required by the model law, for complete flow similarity. Fluid properties for each test phase are summarized in Table 6. All other test conditions were identical to those of the Phase IIa test series. The model gear pneumatic volume was calculated from the equation (32).

All Phase I and Phase II tests were conducted on the Dynamic Test Machine (DTM), at the Mobility Development Laboratory (MDL). The capabilities and basic specifications of the DTM are listed in Table 7. This device (shown in Figure 39) was originally designed for air cushion model testing, but was later

SECTION VII

THE TEST PROGRAM

A two-phase test program was planned to acquire the data needed for a comprehensive evaluation of the model gear dynamic performance, relative to that of the A-37 NLG, and the model law. The A-37 NLG was tested during Phase I to establish a data baseline for a given set of test parameters. Follow-on tests of the model gear strut were then conducted in Phase IIa and Phase IIb. Scaled conditions for model gear tests were determined from the model law, and corresponding Phase I test conditions. Phase I and II test parameters are presented in Table 6.

Model gear tests were conducted for two different hydraulic fluids to investigate the effect of fluid properties on the hydraulic force characteristics of the model damping orifice. The first series of model tests were run with full-scale hydraulic fluid, i.e., MIL-H-5606 standard fluid. The second model test series was run with a fluid that had essentially the same density as MIL-H-5606. The viscosity of this fluid was considerably less than MIL-H-5606, but it was still approximately 17.6 percent greater than the value required by the model law, for complete flow similarity. Fluid properties for each test phase are summarized in Table 6. All other test conditions were identical to those of the Phase IIa test series. The model gear pneumatic volume was calculated from the equation (32).

All Phase I and Phase II tests were conducted on the Dynamic Test Machine (DTM), at the Mobility Development Laboratory (MDL). The capabilities and basic specifications of the DTM are listed in Table 7. This device (shown in Figure 39) was originally designed for air cushion model testing, but was later

STRUT PARAMETERS	PHASE I		PHASE II (a)		PHASE II (b)	
	TARGET	ACTUAL	TARGET	ACTUAL	TARGET	ACTUAL
m_{sp} (lb) :	660.00	660.00	24.40	24.40	24.40	24.40
m_u (lb) :	44.00	44.00	1.63	1.63	1.63	1.63
V_0 (in^3) :	18.50	18.15	0.67	0.69	0.69	0.69
P_{g_0} (psig):	12.00	11.30	-3.68	-7.00	-7.00	-7.00
P_T (psig) :	85.00	85.00	28.00	28.00	28.00	28.00
A_p (in^2) :	—	2.71	0.301	0.297	0.297	0.297
v (FPS) :	7.00	7.00	4.00	4.00	4.00	4.00
	10.00	10.00	5.77	5.80	5.80	5.80
	20.00	20.00	11.40	11.50	11.50	11.50
Fluid Type:	MIL-H-5606		MIL-H-5606		Base Fluid for MIL-H-5606	
* μ $\frac{lb\text{-}s}{in^2}$:	2.5×10^{-6}		2.5×10^{-6}		9.2×10^{-7}	
* ρ $\frac{lb}{in^3}$:	3.0×10^{-2}		3.0×10^{-2}		3.0×10^{-2}	

TABLE 6. Target and Actual Test Conditions (Estimated)

* Estimated nominal fluid properties at 75 F and 1 atm.

Weight Range	:	20 - 1,000 lbs.
Max. Speed	:	70 FPS @ Track Centerline
Max. Accel./Decel.	:	8 FPS
Track Width	:	6 Ft
Track Height	:	1 Ft
Track Centerline Dia.	:	83.3 Ft
Boom Drive System	:	2 Water filled aircraft tires driven by a manually controlled 60 HP DC electric motor.
Max. No. of Data Channels	:	20
Data Acquisition System	:	Two VR-3700 B Analog FM Recorders

TABLE 7. Dynamic Test Machine Specifications and Features

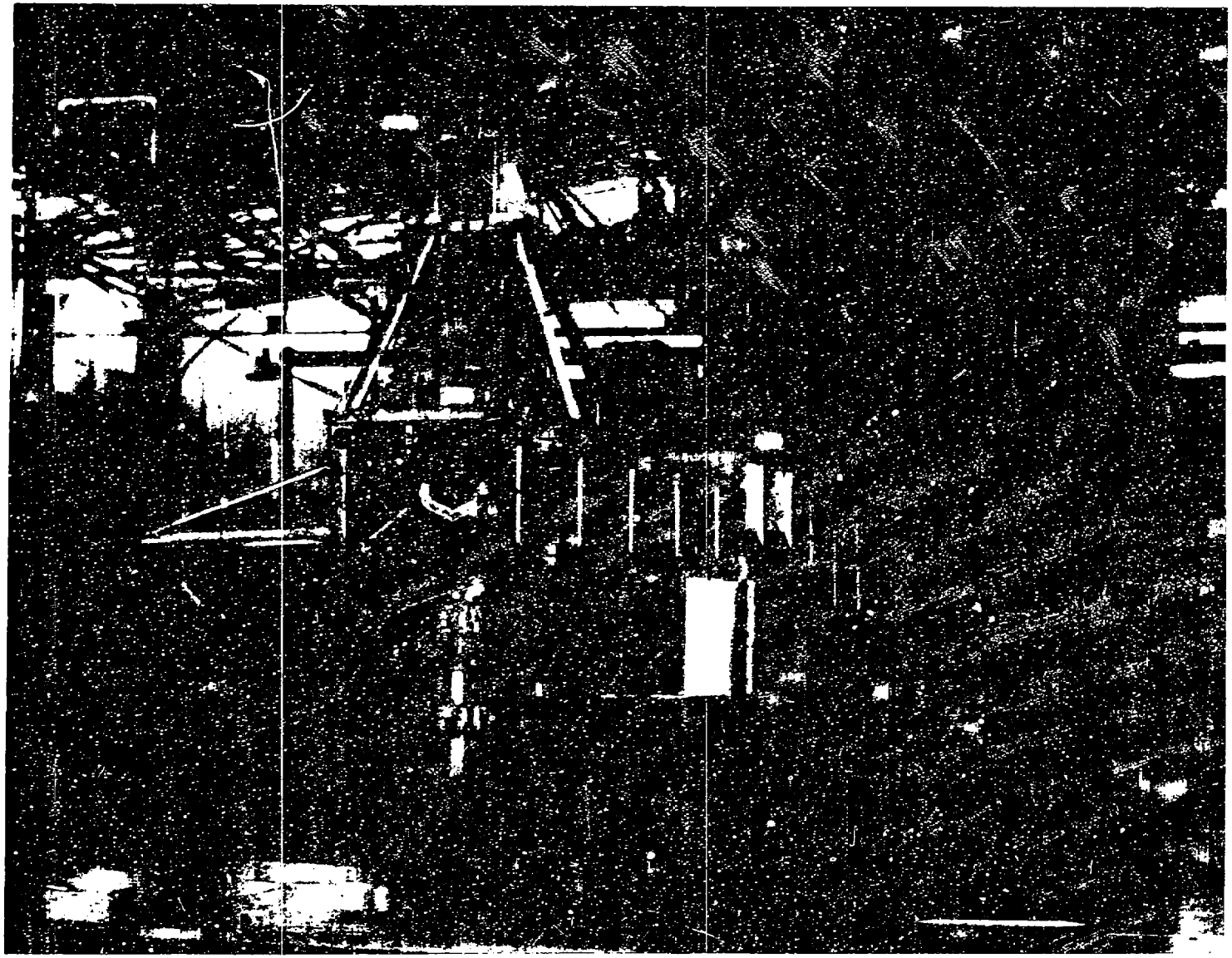

FIGURE 39. Dynamic Test Machine (DTM)

modified to add the capability of testing small landing gear struts and aircraft tires.

For Phase I tests, the A-37 NLG strut was attached to the DTM heave post, which allows free vertical motion (see Fig. 40). Fore-aft and other lateral motion is restrained by large roller bearings which are in contact with the heave post. A smaller heave post was used for Phase II tests, since the model gear sprung weight was limited to 24.44 lbs. This heave post, shown in Fig. 42 weighs only five pounds.

The motion of the DTM was manually controlled during all tests. A typical test run consisted of accelerating the DTM to a desired target velocity specified in the test plan, and continuing the test at a constant speed, until three revolutions around the test track were completed. The machine was then accelerated to the next target test velocity. Three passes around the track were planned as a check for repeatability of test data for a given condition.

A full range of data was recorded during all Phase I and Phase II tests to allow for a complete asessment of full-scale and model gear subsystem performance. Instrumentation was installed on each strut to measure sprung mass acceleration, sprung mass displacement, strut stroke, stroke rate, and pneumatic and hydraulic pressure. The installation of the A-37 NLG, with instrumentation, on the DTM, is shown in Fig. 40 and 41. Fig. 42, 43, and 44 show the installation of the instrumented model gear on the DTM. Outputs were routed through a slip ring assembly on the center post of the DTM to a Honeywell VR 3700 B F.M. analog recorder.

All Phase I and Phase II tests were conducted over a series of two cosine bumps placed end to end on a section of the DTM track surface. The bumps were designed to be identical to the bump configuration used in the analytical

simulations (Ref. Fig. 17, Section IV). The bumps used during the model gear tests are visible in Fig. 44.

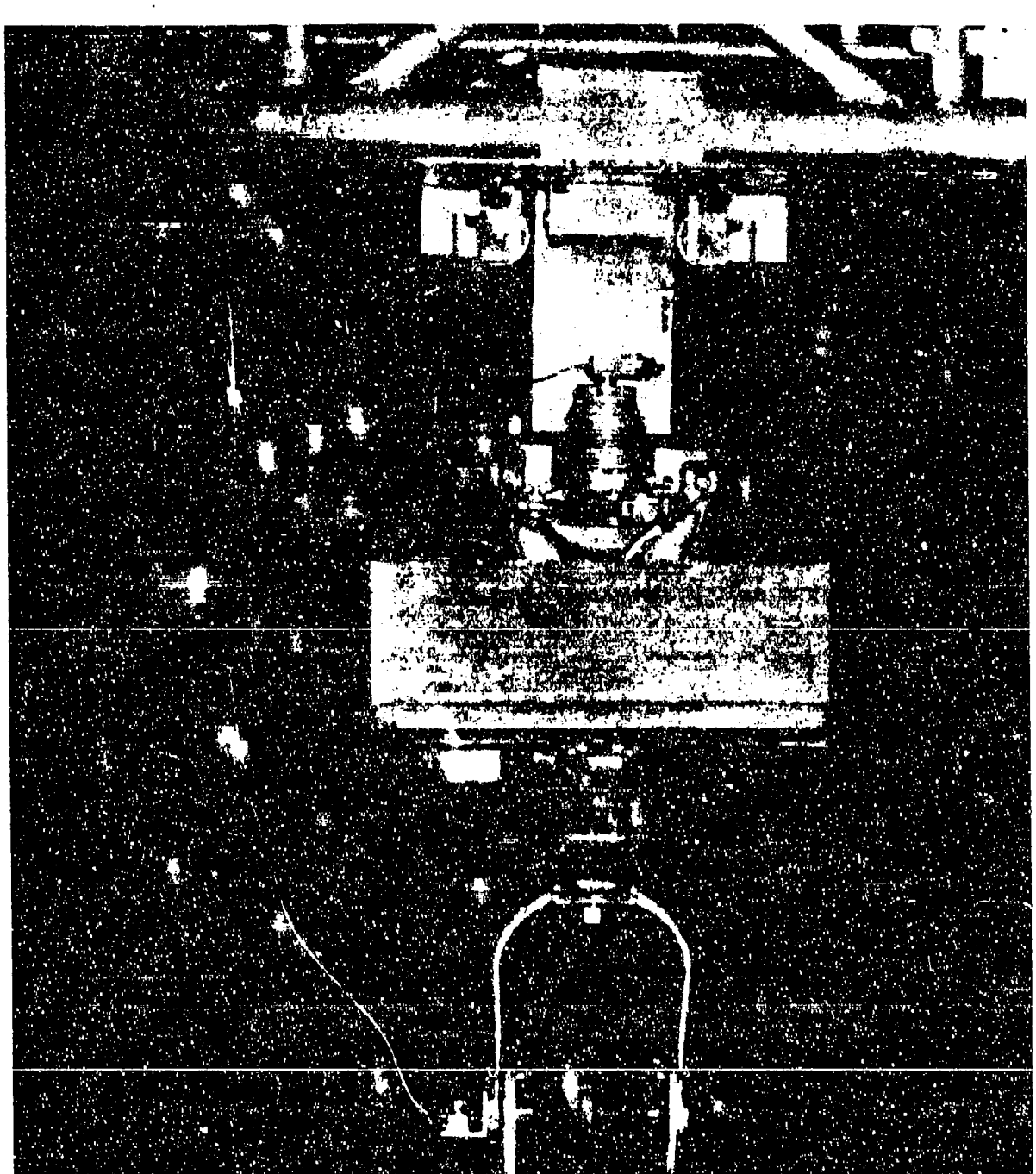

FIGURE 40. A-37 NLG Test (Back View)

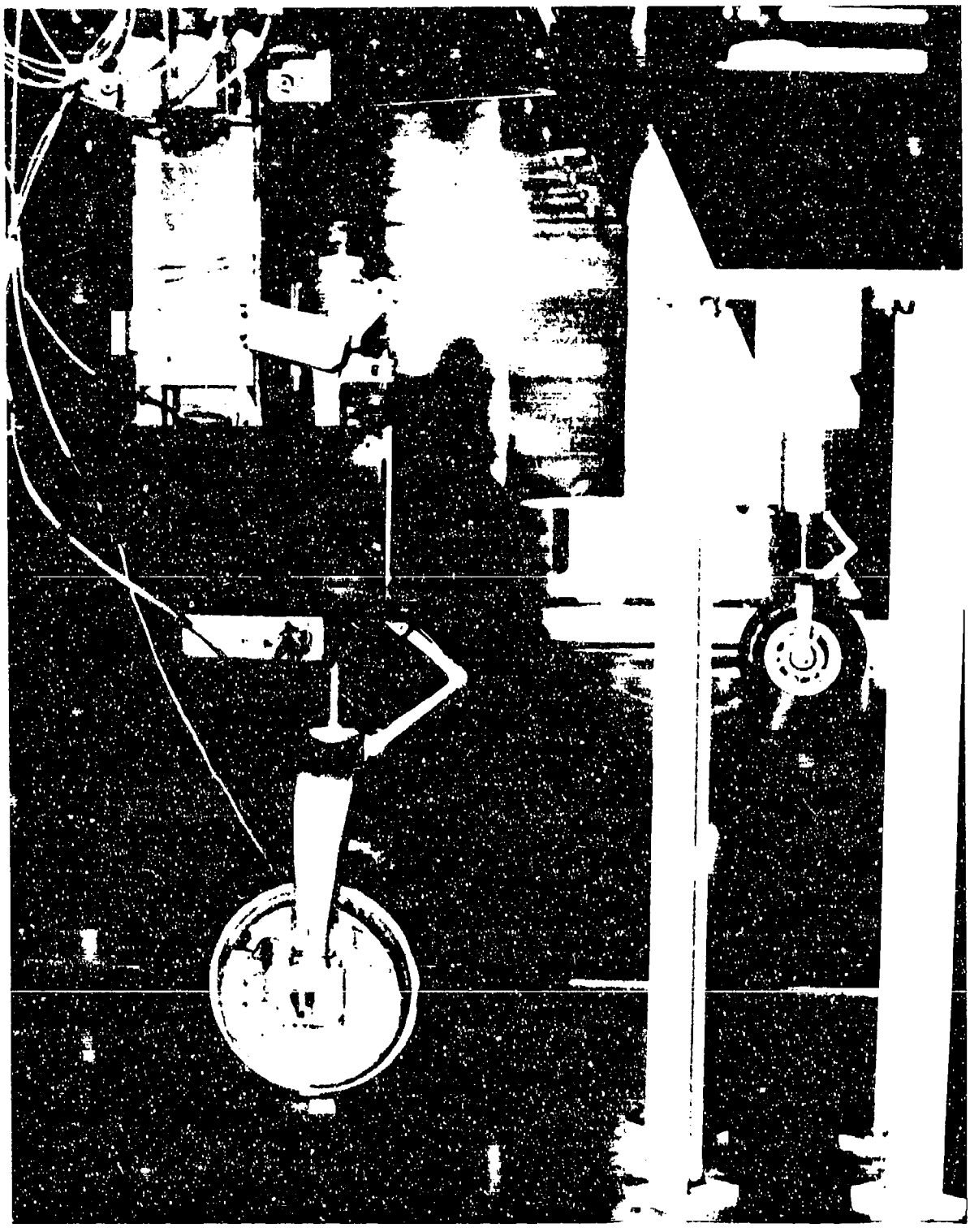

FIGURE 41. A-37 NLG Test (Side View)

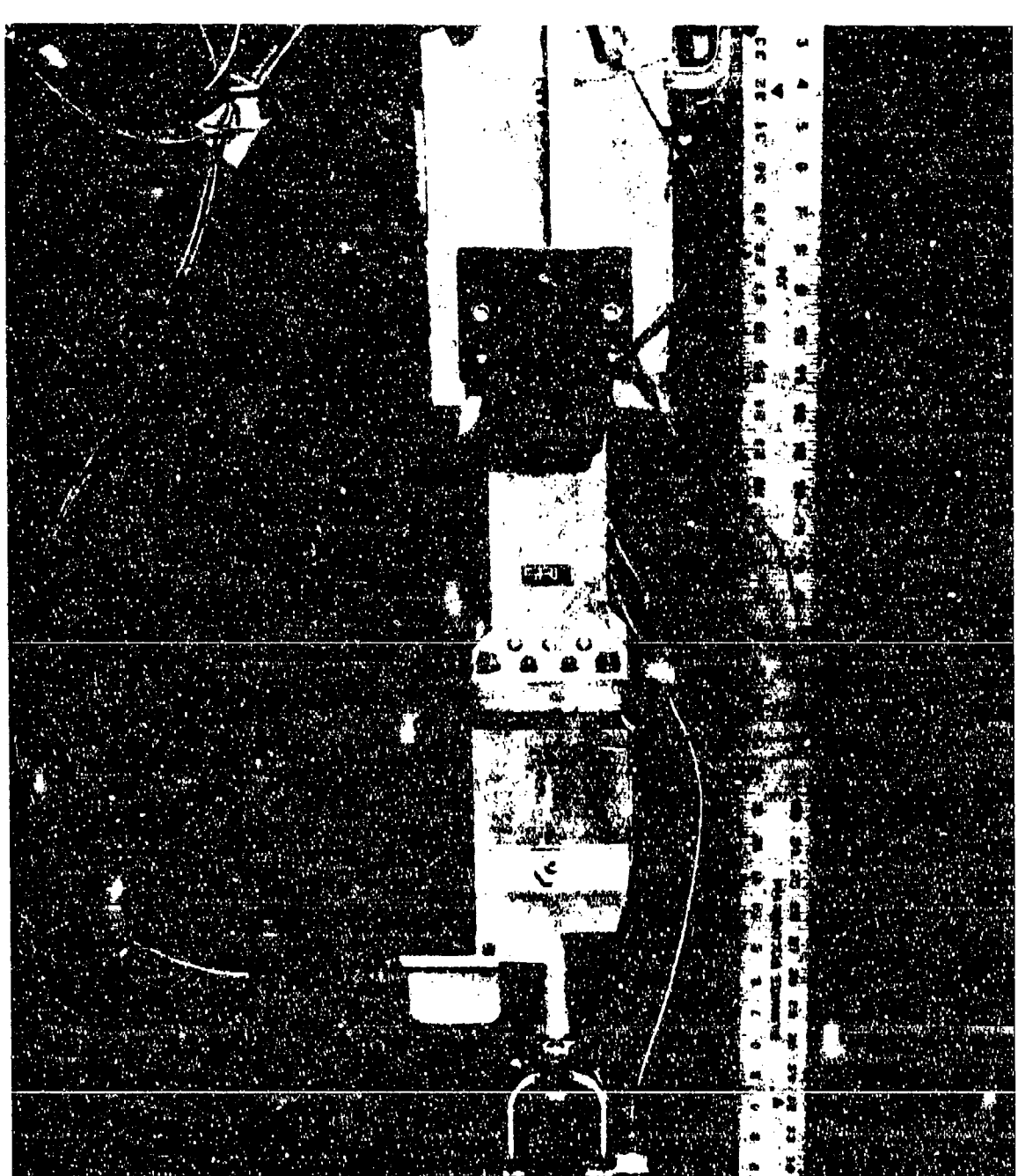

FIGURE 42. Model Gear Test (Back View)

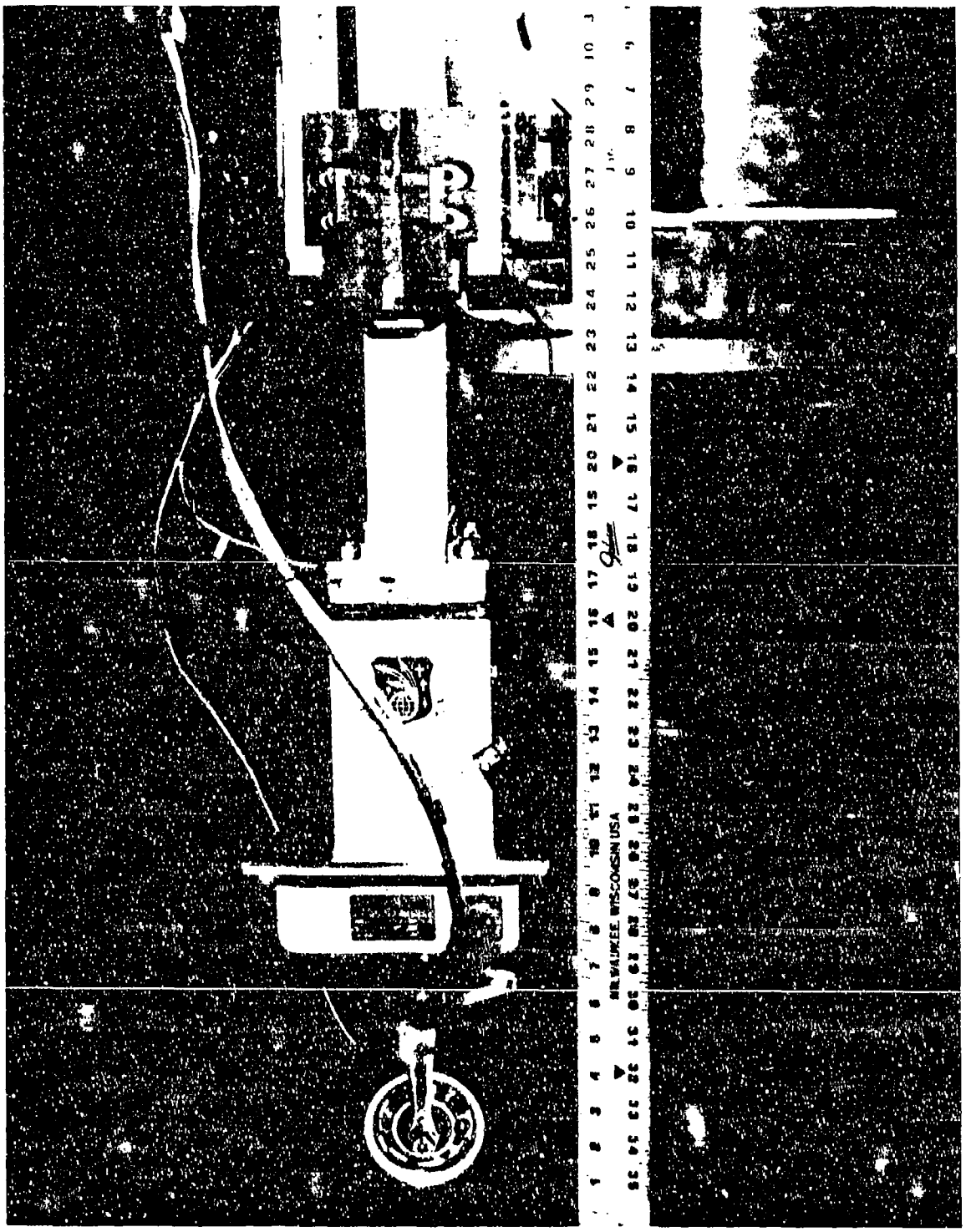

FIGURE 43. Model Gear Test (Side View)

FIGURE 44. Model Gear on Cosine Obstacle

SECTION VIII

RESULTS

Displacement and stroke data from initial test runs of the model gear on the DTM is compared in Fig. 45, to corresponding tests of the A-37 NLG conducted at dynamically similar test speeds. Apparent from an analysis of this test data, is an indication that damping in the model gear strut was considerably greater than damping in the A-37 NLG strut. This result was attributed to binding of the model gear strut, which is clearly evident from the lack of free response after it cleared the second cosine bump. Also, there was a change in the static equilibrium stroke position. The A-37 NLG strut did not exhibit this behavior.

Quasi-static load-stroke tests of both struts were conducted, following the initial DTM tests. Results of these tests confirmed that there was excessive friction in the model gear strut, which contributed to the nonsimilar dynamic response observed during the dynamic tests. The friction tests were run with the charge ports of each strut open to atmosphere, which prevented pneumatic affects on o-ring seal friction. Also, the load-stroke tests were repeated after first removing the orifice from each strut. A separate evaluation of orifice seal and o-ring friction was made from a comparison of results from both series of load-stroke tests. Upper bearing friction was considered to be negligible, since there were no side loads applied during the tests.

Orifice seal friction in the A-37 NLG strut was approximately one pound, and was essentially constant throughout the entire stroke range of the strut.

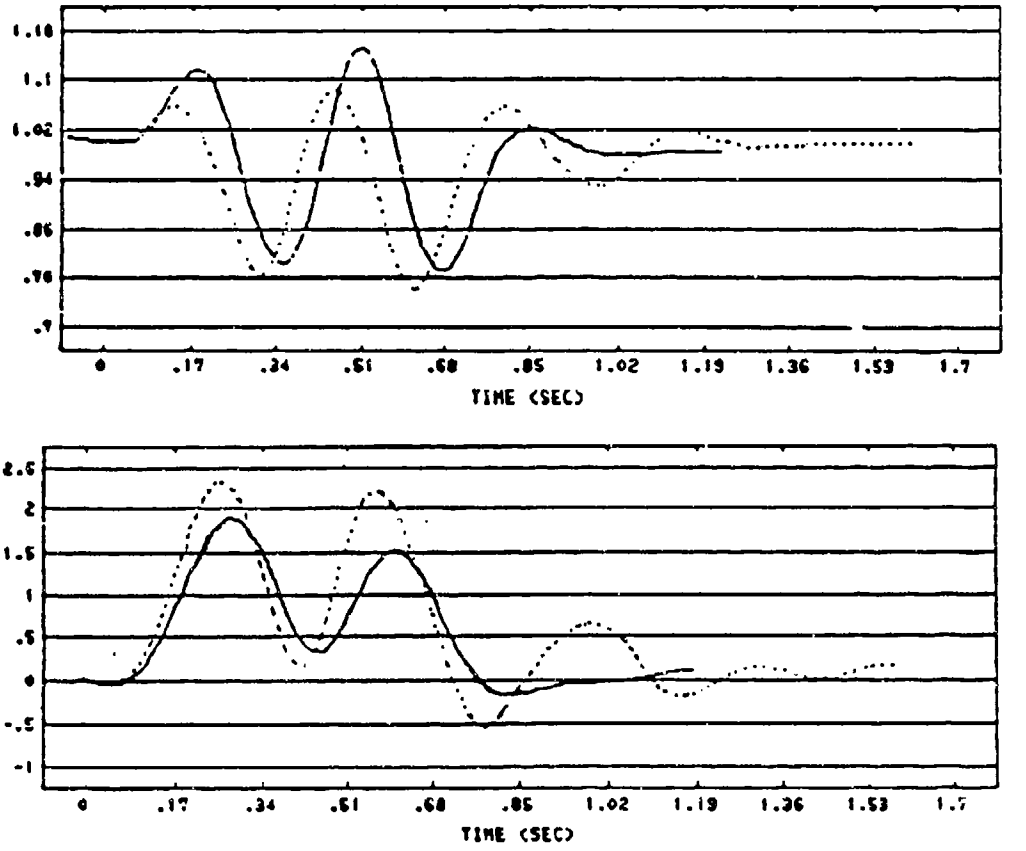

	TAXI SPEED	LEGEND
FIGURE 45. Model Gear*	5.7 Ft/s	———
vs.		
A-37 NLG	10.0 Ft/s	·····

* High Friction Orifice Seal

Ideally, dynamic similarity requires a corresponding value of 1/27 lbs (λ_F = 1/27) in the model gear strut, however, measurements of actual orifice seal friction yielded a value of 1.5 lbs (40 times the required value).

Inspection of the model gear orifice seal indicated that poor seal conformity with the cylindrical sealing surface was the cause of excessive friction. This situation is depicted in Fig. 46b, which shows how binding forces become concentrated at the points of contact between the seal and sealing surface. A secondary consequence of poor seal conformity is a loss of sealing integrity caused by excessive leakage across the seal. These problems are avoided with a properly designed seal, which is shown in Fig. 46a. In this case radial sealing forces are evenly distributed around the periphery of the seal face, and leakage past the seal is minimized. Proper split-ring seal design is briefly covered in Appendix A.

It was decided to replace the original split-ring seal design with an available teflon capped o-ring type seal, which had inherently good cylindrical conformity. Also, the seal groove machined into the orifice plate was modified to minimize radial compression of the o-ring. The surface finish of the metal sealing surface (inside piston wall) was also improved (polished to about four microinches), to further reduce friction. Another series of load-stroke tests performed on the model gear strut, following completion of the modifications, indicated that orifice seal friction had been reduced by approximately 83 percent. Overall, friction was still greater than the dynamically similar value, but the binding problem was eliminated. (There was no actual attempt at achieving precisely scaled frictional characteristics, however, the affects of stroking friction on the dynamic response of the A-37 NLG strut was evaluated analytically using LANSIM. Although this approach was considered as second

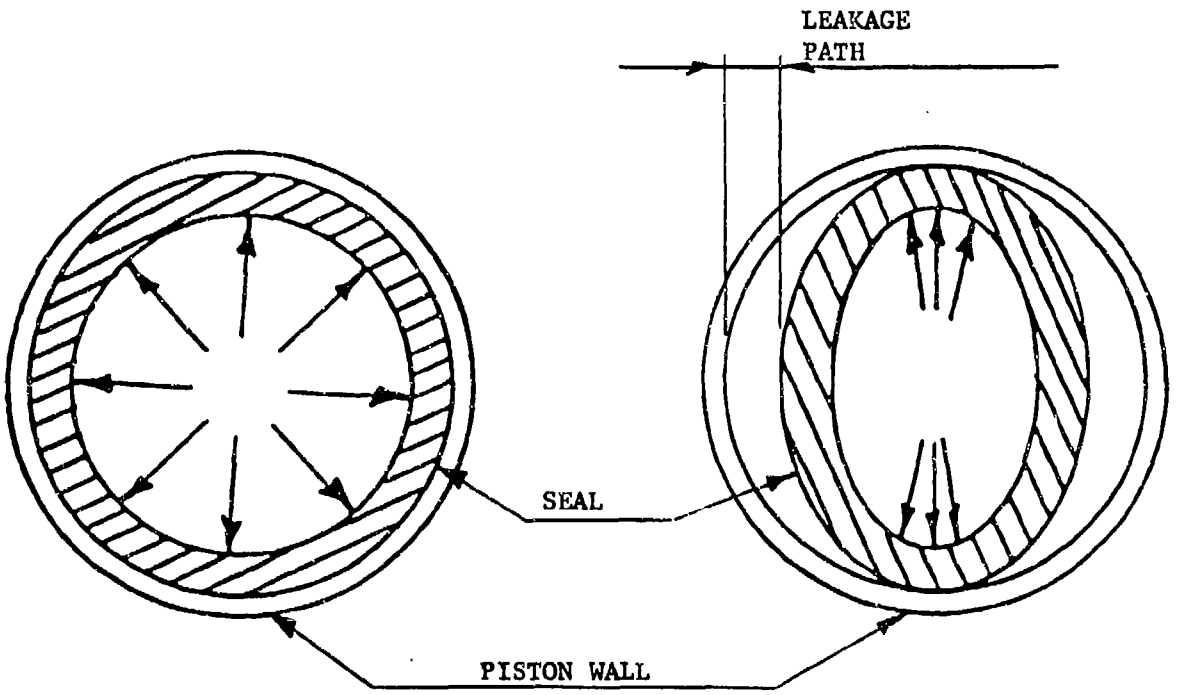

FIGURE 46. Cylindrical Conformity of a Split Ring Seal

best to obtaining dynamically similar friction in the model gear, it did provide certain valuable insights into the importance of frictional contributions for this case. The friction model used, and the results of the analysis, are presented in Appendix B.)

Phase II tests of the model gear on the DTM were repeated after the friction assessment was finished. Results from this round of testing are presented at the end of this section. In general, the dynamic response of the model gear strut was markedly improved over the initial tests run with the high friction split-ring orifice seal. Qualitatively, both struts exhibited the same dynamic response. This was true for all test parameters measured for each strut. Quantitative correlation was also considered as good for the two highest test speeds, but not good for the slowest test speed. Generally, quantitative correlation improved as the test speed was increased. This point is discussed further in the next section.

Figure 47 and 48 show time history plots of the model gear (solid curve) dynamic response against the A-37 NLG (dotted curve) at dynamically similar test speeds. (The model gear data has been scaled up with the scaling laws for all data comparisons). Obviously, quantitative agreement was not good at this speed, primarily due to greater frictional damping in the model gear strut. The stroke data in Fig. 47 indicates that the model gear was barely stroking at all compared to the A-37 NLG.

Data for the two highest test speeds is presented in Fig. 49 through 52. Correlation of model gear results with A-37 NLG results was better for these conditions, although there was some disparity in peak values of all parameters, during bump traversal. Free response of each strut after the second bump was cleared, was similar in that the number of oscillations was the same. However,

there was a difference in the phase of the dynamic response. This is primarily due to a nonsimilarity in the pneumatic force characteristics in the model gear strut, which is evident in the time history plot of this parameter (Ref. Fig. 50 and 52). Fig. 53 through 55 show the polytropic characteristics of each strut during bump traversal for each test speed.

Fig. 56 through 59 are various plots of the actual polytropic curves obtained during the tests of both struts. The test data is compared with theoretical polytropic curves in Fig. 56 and 57. Stroke data in these two plots was referenced to the static equilibrium position corresponding to a polytropic exponent of N = 1.1. The dynamic polytropic characteristics are, clearly, quite different than the theortical characteristics assumed in the analytical simulations using LANSIM. In general, the polytropic curve was considerably stiffer during a compression, and less stiff during an extension. The same physical effect was evident in both struts, but was more pronounced in the model gear.

Fig. 58 compares the polytropic curves obtained for the A-37 NLG at the two highest test speeds. Similar data is depicted in Fig. 59 for the model gear strut. The data shows that the polytropic characteristics for the A-37 NLG strut remained fairly consistent for both test speeds, although the curve was slightly softer at the higher test speed of 20 ft/sec i.e., more stroke was used to generate the same pneumatic force. There was more of a difference in the polytropic curves for the model gear strut, at the two different test speeds, as shown in Fig. 59 . There was less stroke used at the higher test speed of 11.5 ft/sec, and the overall curve at this speed tended to exhibit more of an isothermal behavior than the same curve produced at 5.7 ft/sec. The

reason for this behavior in the model gear strut was not discernable from the test data, but a relationship between the polytropic behavior of the curve and the range of stroke used seemed to be indicated.

Damping orifice characteristics are compared in Fig. 60 through 63. The orifice discharge coefficient plotted in these figures is an effective value, calculated from stroke rate and pressure data obtained from the tests. The following equation was used in these calculations:

$$C_d = \left[\frac{\rho A_h^2 \dot{s}^2}{2\Delta P A_t^2 g_c} \right]^{\frac{1}{2}} \qquad (40)$$

where ρ : Hydraulic fluid density (used as a constant for all calculations)

A_h: Hydraulic area

$\dot{s}$: Measured stroke rate

ΔP: Pressure drop across orifice (from pneumatic and hydraulic pressure measured during the tests)

A_t: Throat area of orifice

It should be kept in mind when looking at Fig. 60 through 63, that only representative data is presented, i.e. data for very low stroke rates, or of extremely short duration, was omitted from these plots. C_d data is plotted against time and relative stroke. Also, the time scales on these plots do not match the time scales in Fig. 49 through 52. The plots of C_d vs. time were included to show the dynamic behavior of the flow characteristics of each orifice.

In general, the model gear was operating at a smaller discharge coefficient than the A-37 NLG, which affected the quantitative correlation of hydraulic damping forces. Also evident from the data was a higher value of C_d for

reverse flow through the orifice (strut extension). This result was noted for all test conditions, and both struts exhibited this behavior.

The data presented in Fig. 62b and 63b for the A-37 NLG strut, shows that the effective C_d was very high at a taxi speed of 20 ft/sec, during the bump traversal. After the gear cleared the obstacle, the orifice C_d returned to a smaller value. The performance of the model gear orifice was fairly consistant at test speeds of 5.7 ft/sec and 11.5 ft/sec. There was not a significant change in the effective C_d at the highest test speed, as is evident from a comparison of Fig. 60a with 62a and also Fig. 61a with 63a.

Model gear tests were also conducted with a different hydraulic fluid, to evaluate the affects of fluid viscosity on overall dynamic response of the strut. The fluid used in this series of tests is the base fluid that is used in the manufacture of standard MIL-H-5606 hydraulic fluid. The properties of each fluid were presented in Table 6. Although the viscosity of the base fluid does not correspond to the value required for complete flow similarity, it was considerably less than that of standard MIL-H-5606. The properties of this fluid were closer to the required properties than any other readily available fluid.

Data from this series of tests is compared with the data obtained from model gear tests conducted with standard MIL-H-5606 fluid (Ref. Fig. 64 through 67). It is evident from these results that improved flow similarity had little impact on overall dynamic response of the model gear strut.

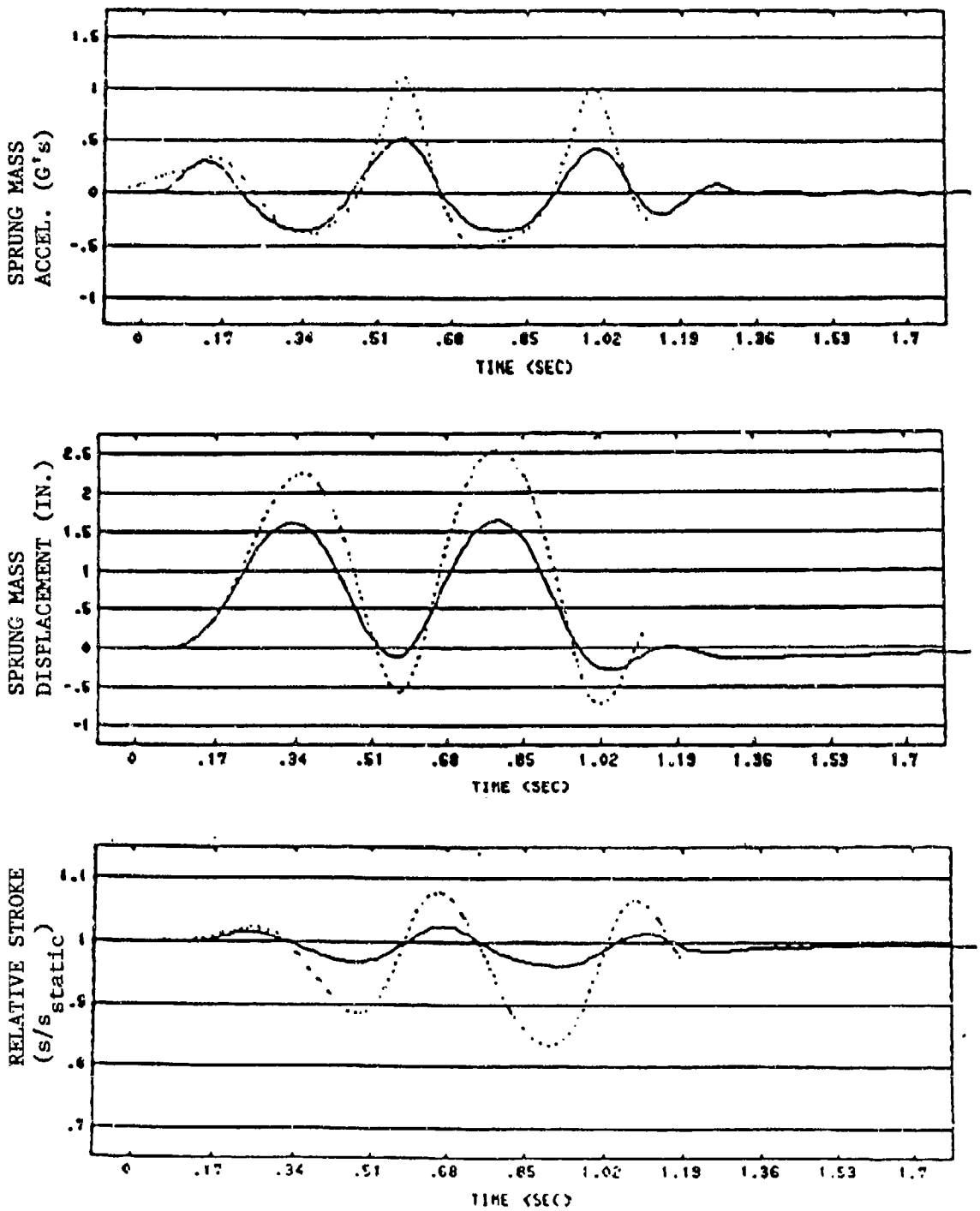

	TAXI SPEED	LEGEND
Model Gear (Phase IIa)	4.0 Ft/s	———
vs.		
A-37 NLG (Phase I)	7.0 Ft/s	.....

FIGURE 47.

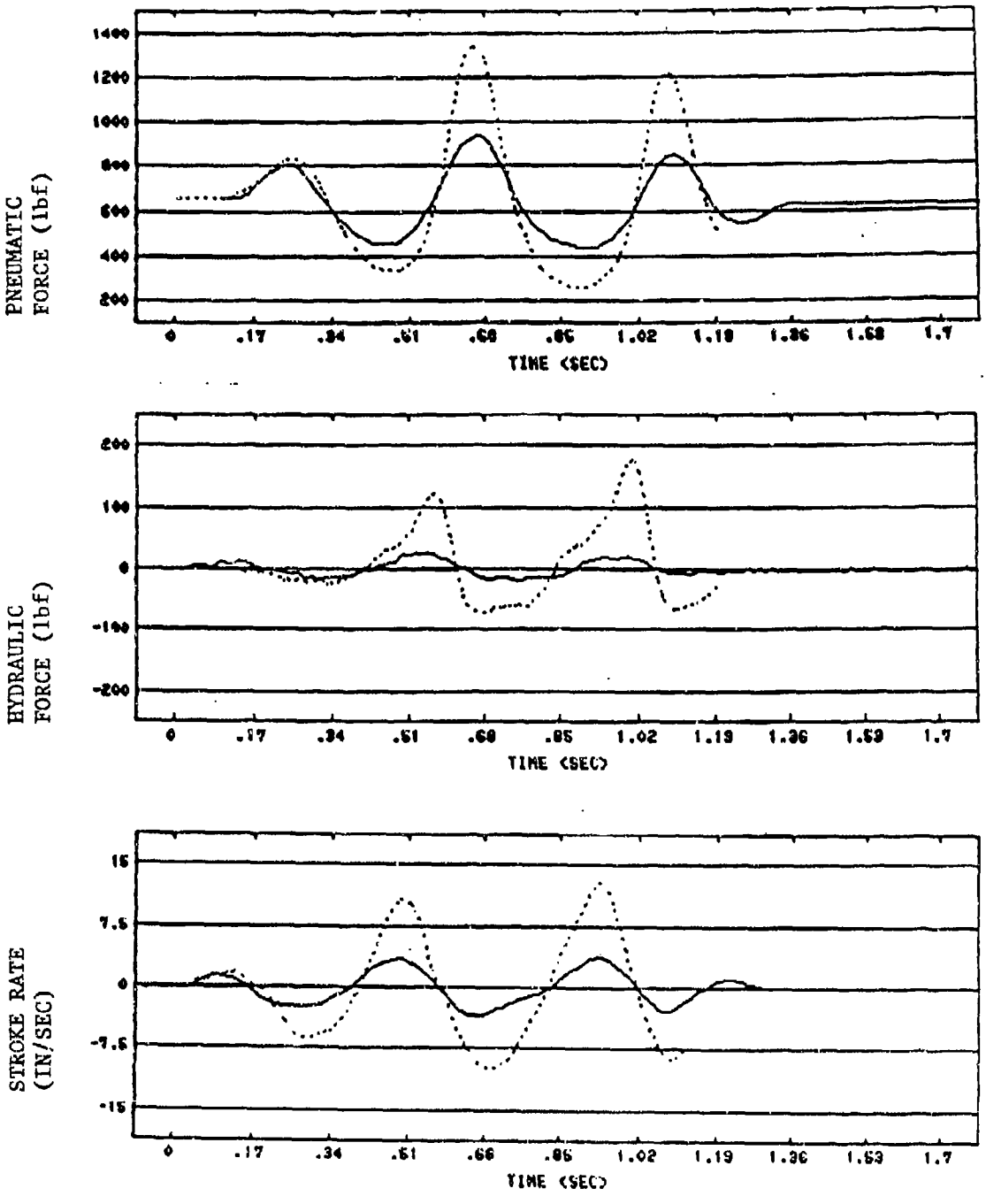

	TAXI SPEED	LEGEND
FIGURE 48. Model Gear (Phase IIa)	4.0 Ft/s	———
vs.		
A-37 NLG (Phase I)	7.0 Ft/s	.....

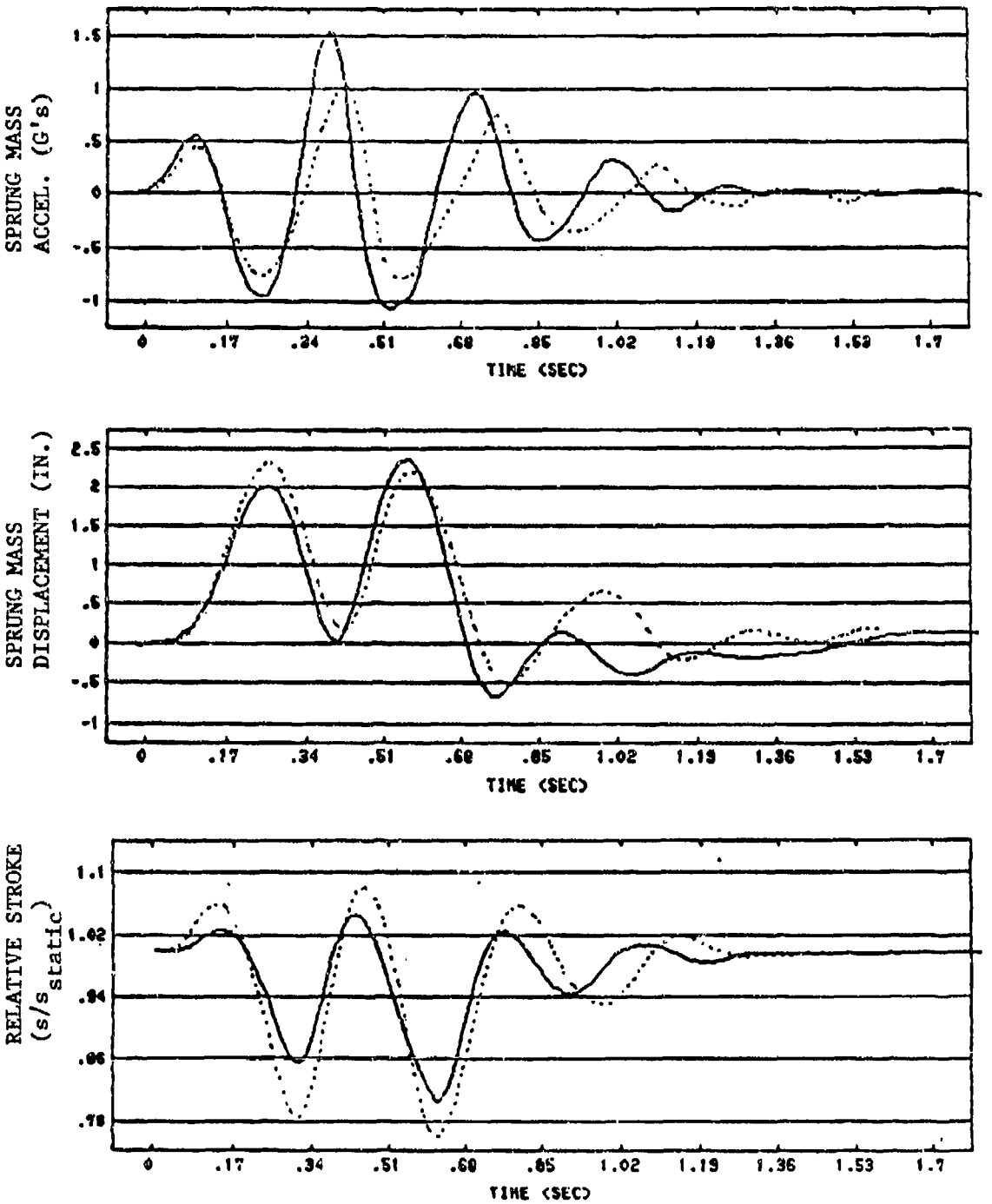

	TAXI SPEED	LEGEND
FIGURE 49. Model Gear (Phase IIa)	5.7 Ft/s	———
vs.		
A-37 NLG (Phase I)	10.0 Ft/s	.....

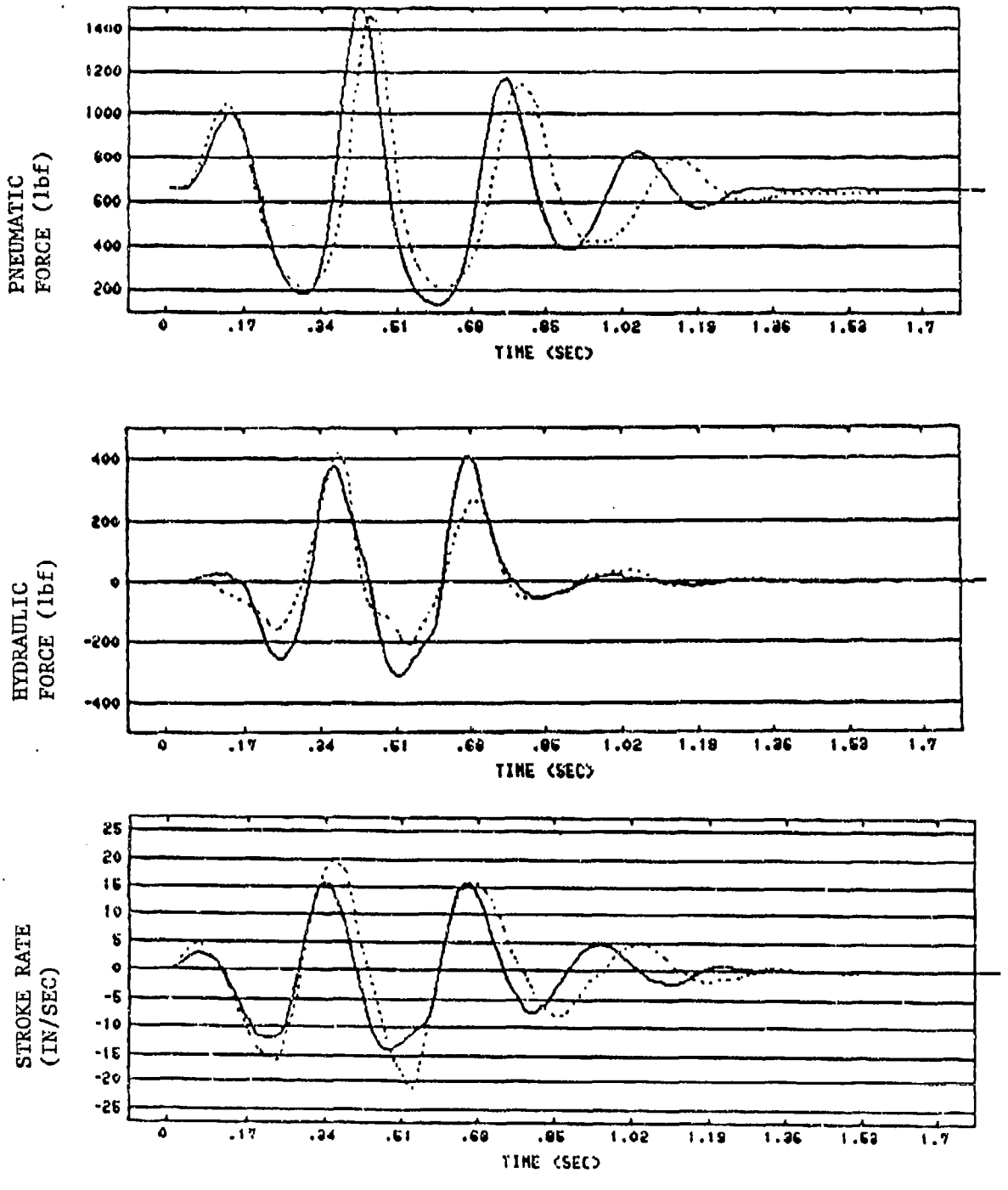

	TAXI SPEED	LEGEND
Model Gear (Phase 11a)	5.7 Ft/s	_____
vs.		
A-37 NLG (Phase 1)	10.0 Ft/s	.....

FIGURE 50.

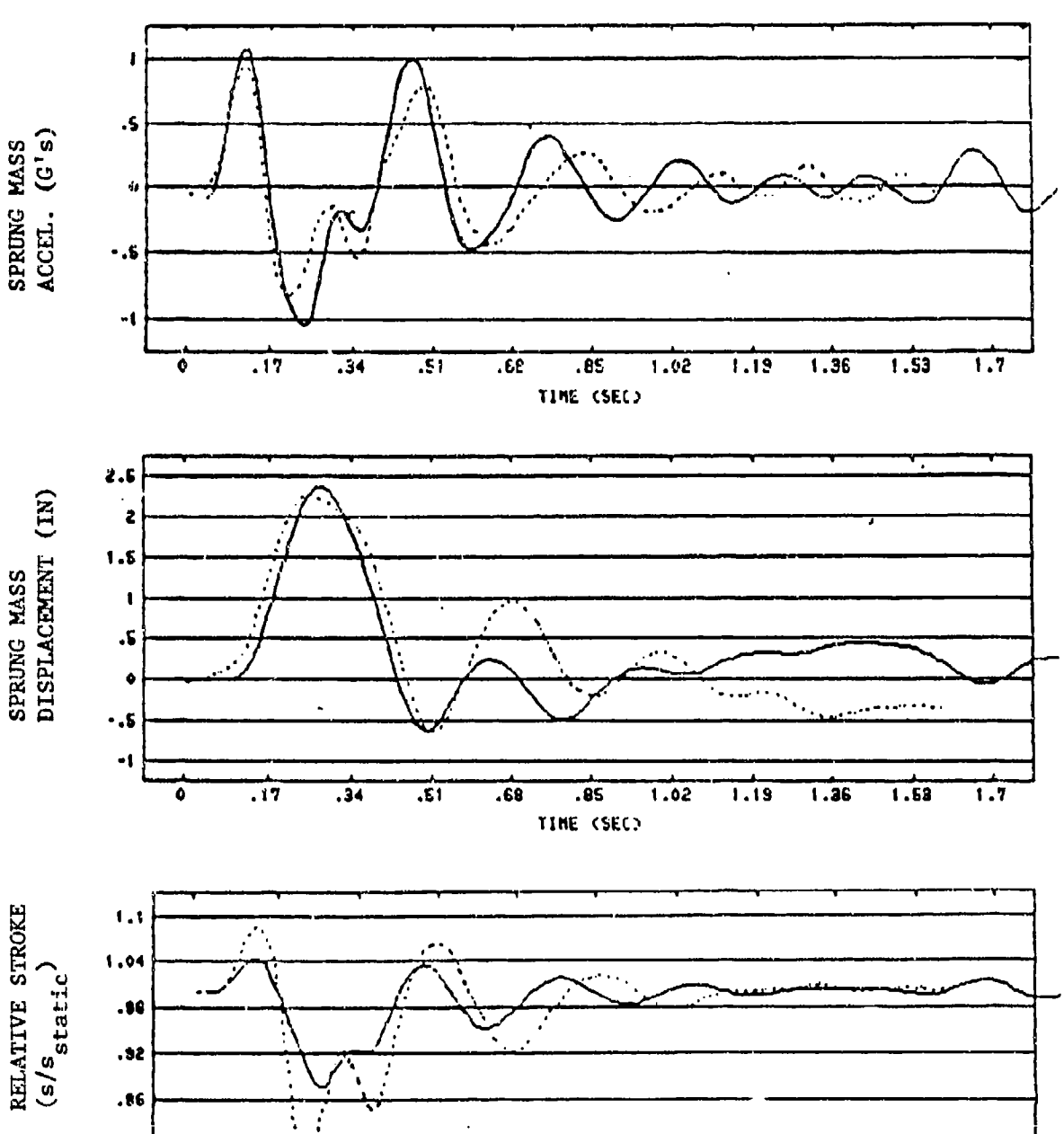

	TAXI SPEED	LEGEND
FIGURE 51. Model Gear (Phase IIa)	11.5 Ft/s	_____
vs.		
A-37 NLG (Phase I)	20.0 Ft/s	.....

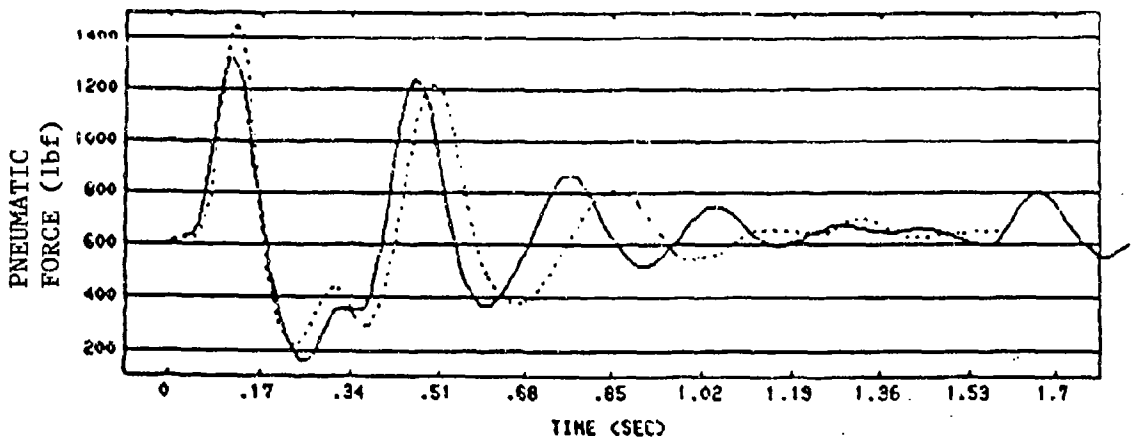

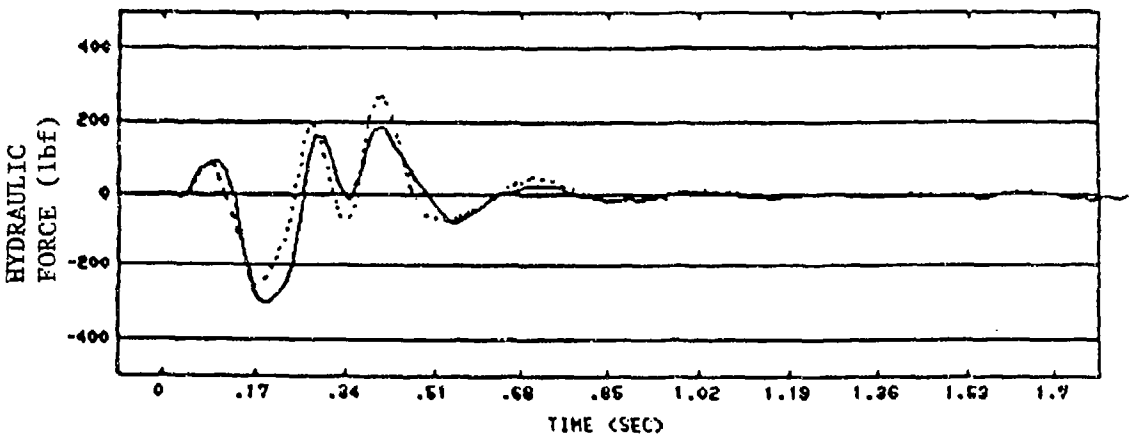

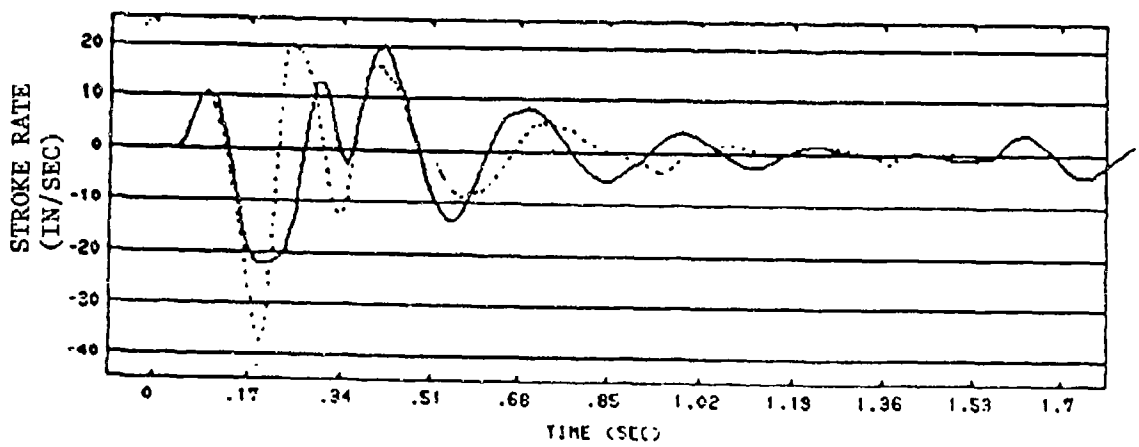

	TAXI SPEED	LEGEND
FIGURE 52. Model Gear (Phase IIa)	11.5 Ft/s	———
vs.		
A-37 NLG (Phase I)	20.0 Ft/s	.....

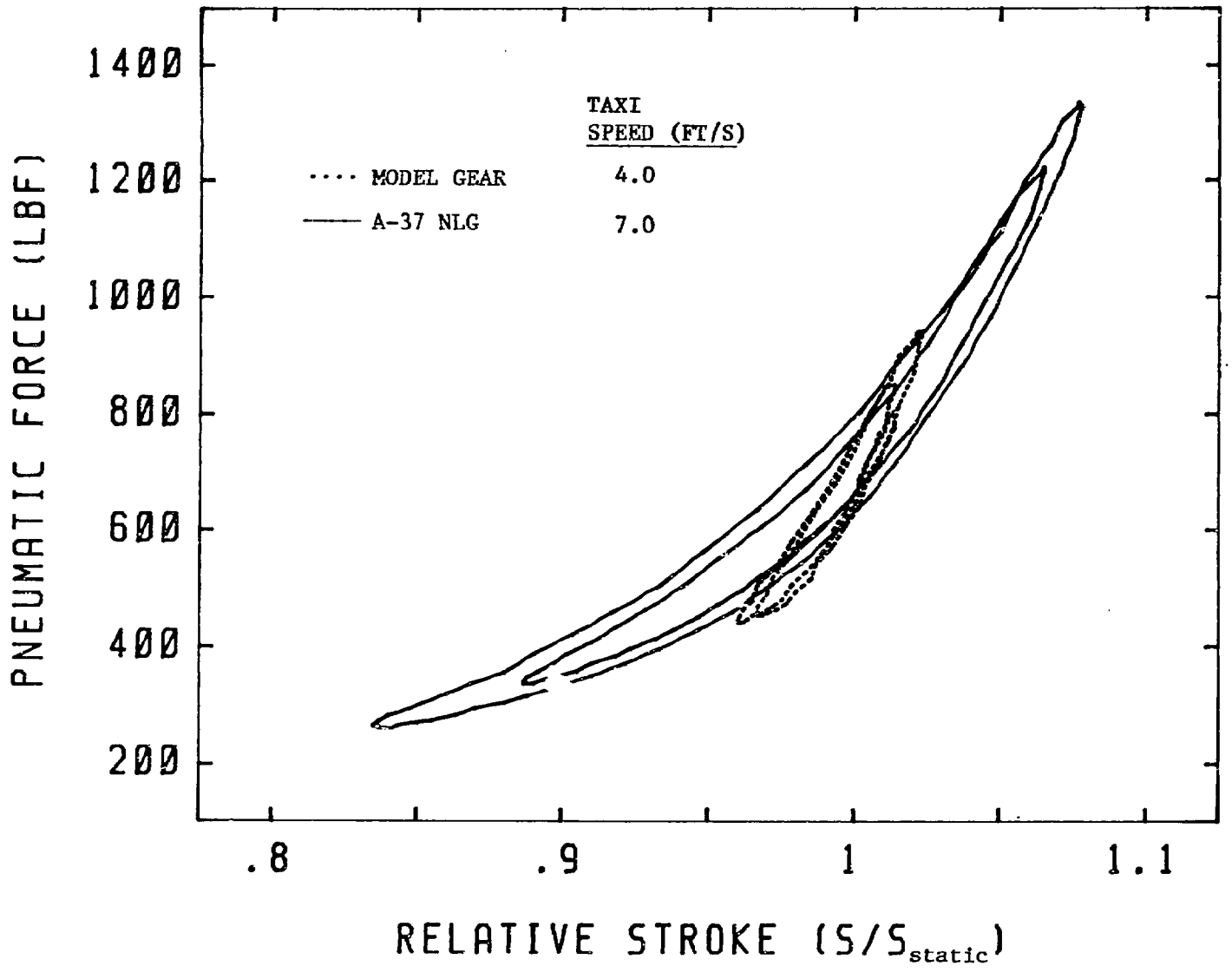

FIGURE 53. Polytropic Curves 1 - Model Gear vs. A-37 NLG

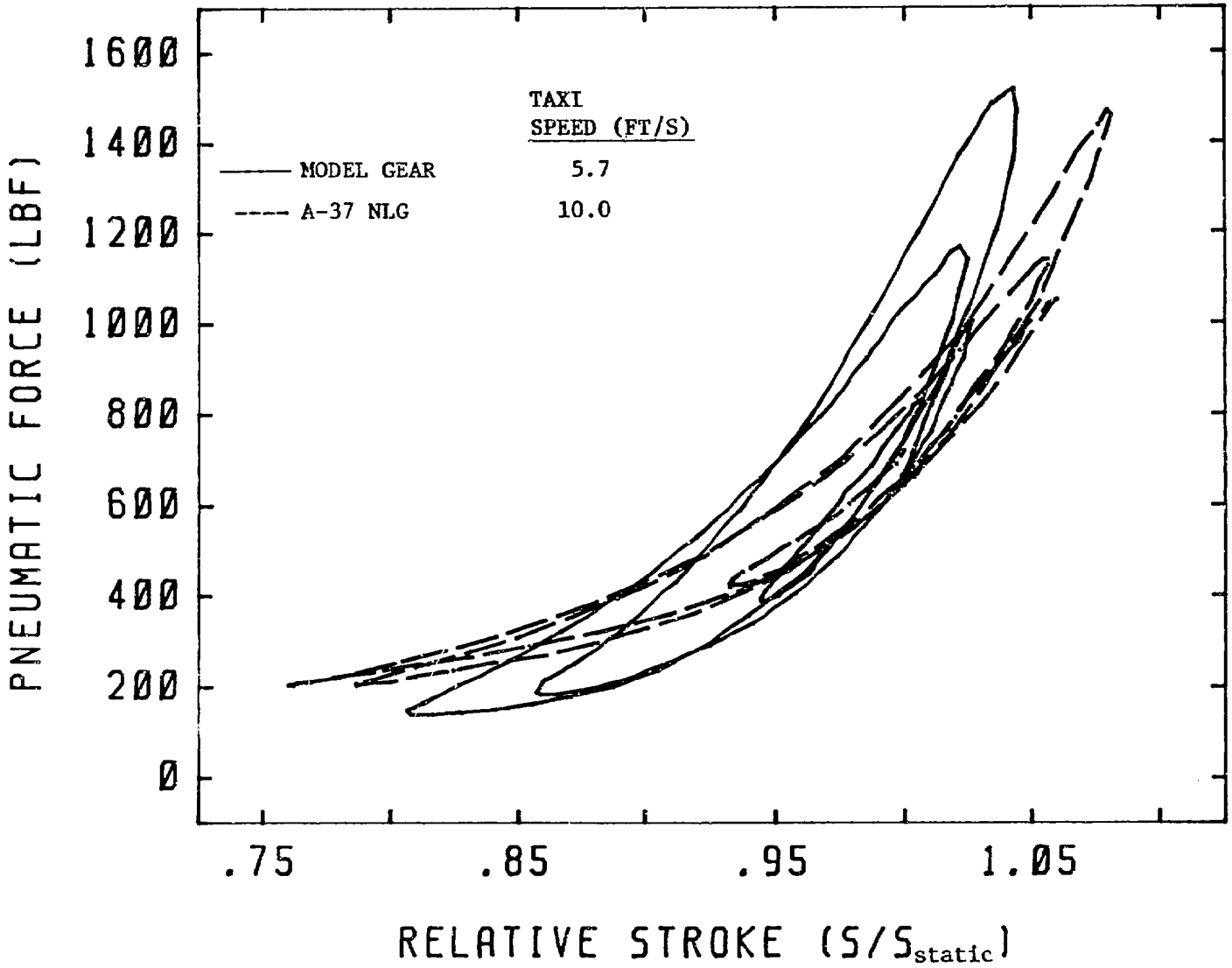

FIGURE 54. Polytropic Curves 2 - Model Gear vs. A-37 NLG

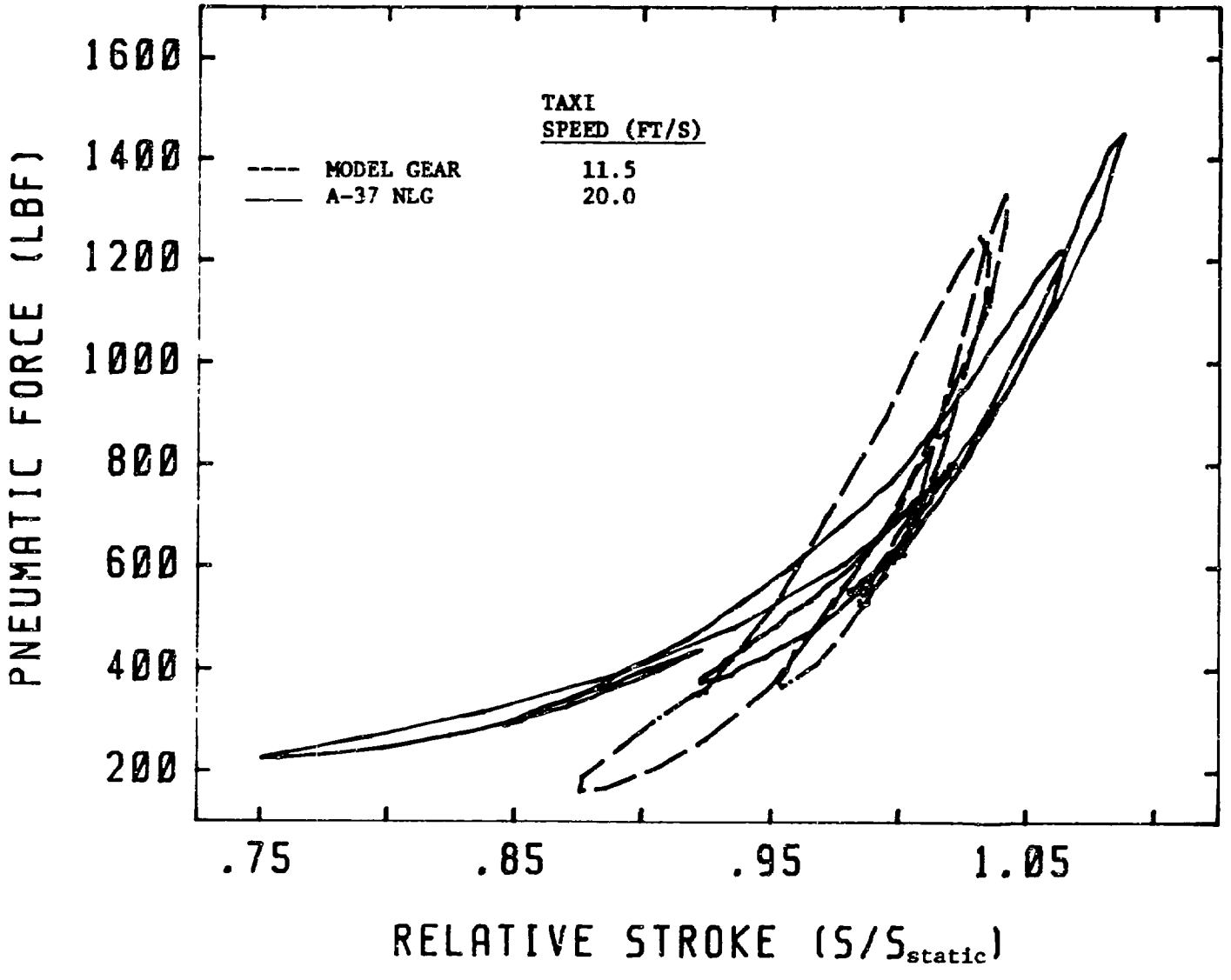

FIGURE 55. Polytropic Curves 3 - Model Gear vs. A-37 NLG

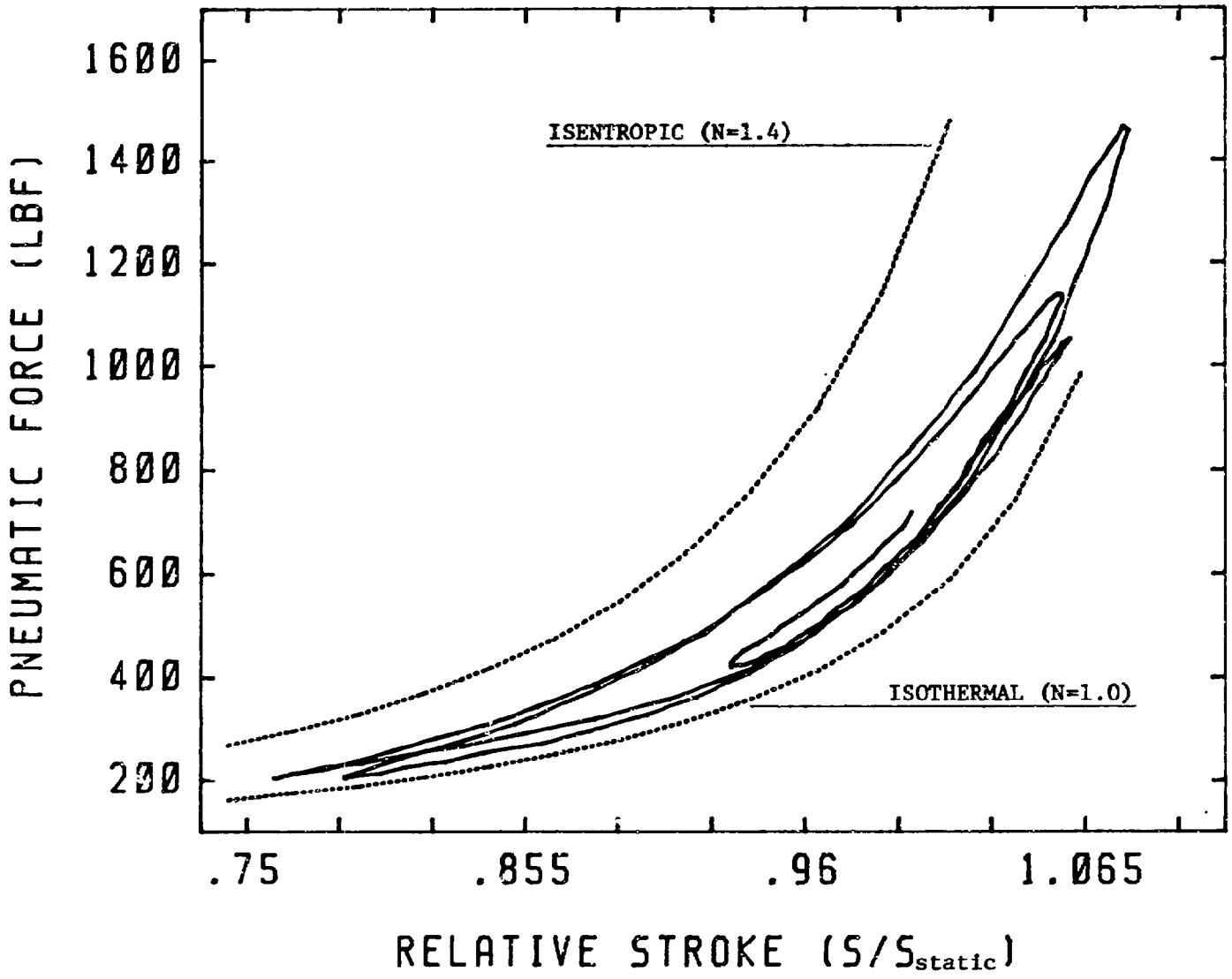

FIGURE 56. Comparison of A-37 NLG Polytropic Data With Isothermal and Isentropic Polytropic Curves

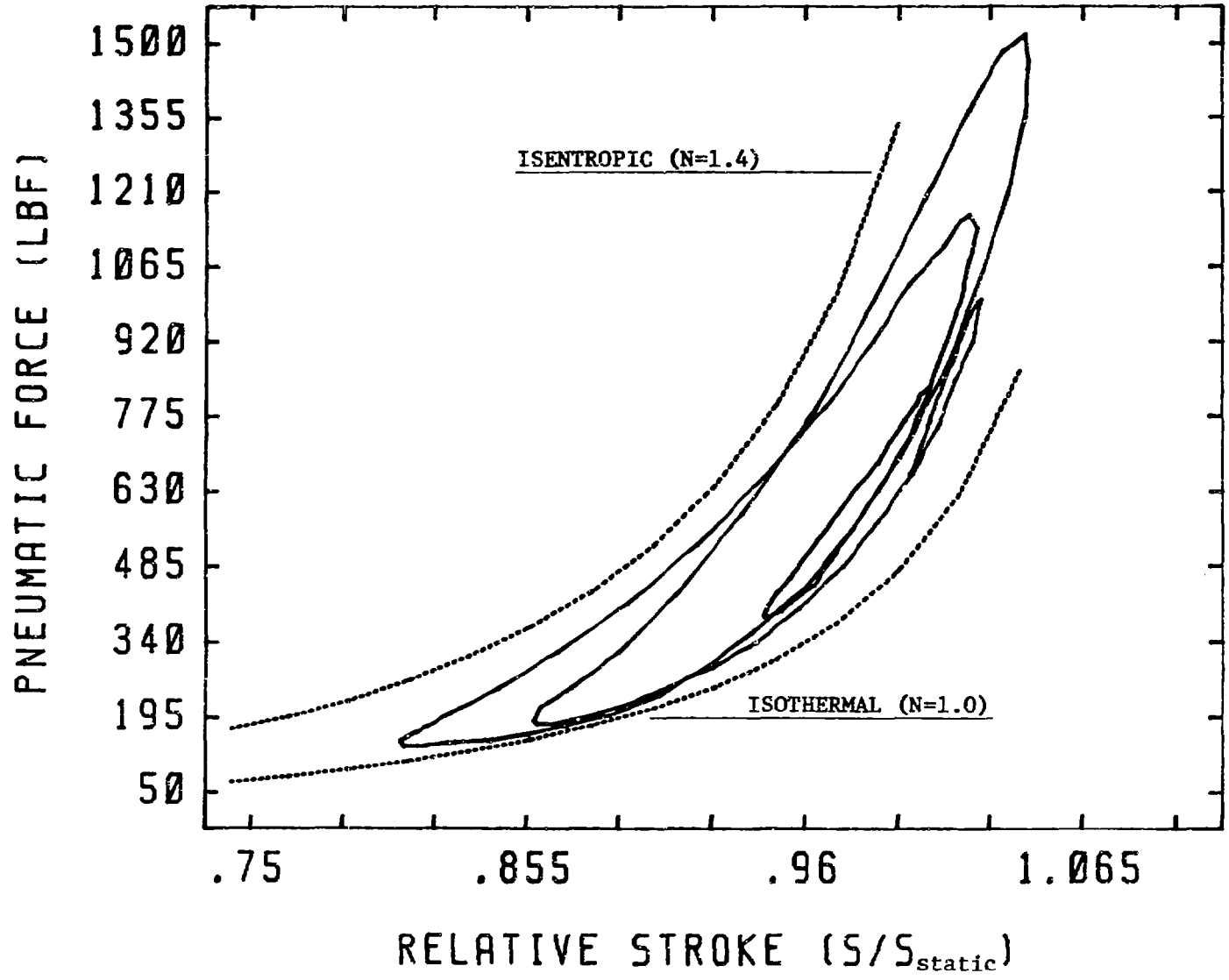

FIGURE 57. Comparison of Model Gear Polytropic Data With Isothermal and Isentropic Polytropic Curves

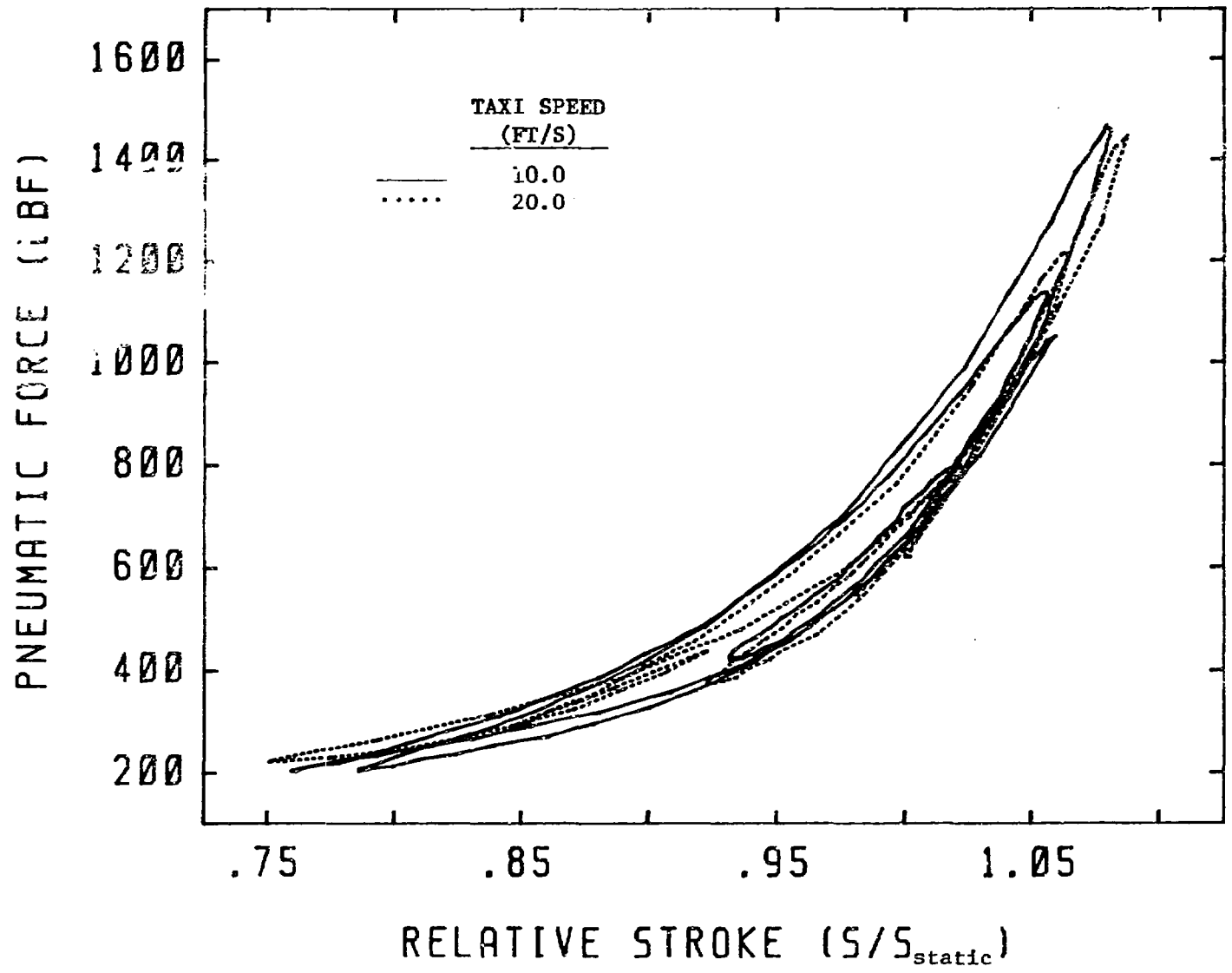

FIGURE 58. Comparison of A-37 NLG Polytropic Curves For Two Different Test Speeds

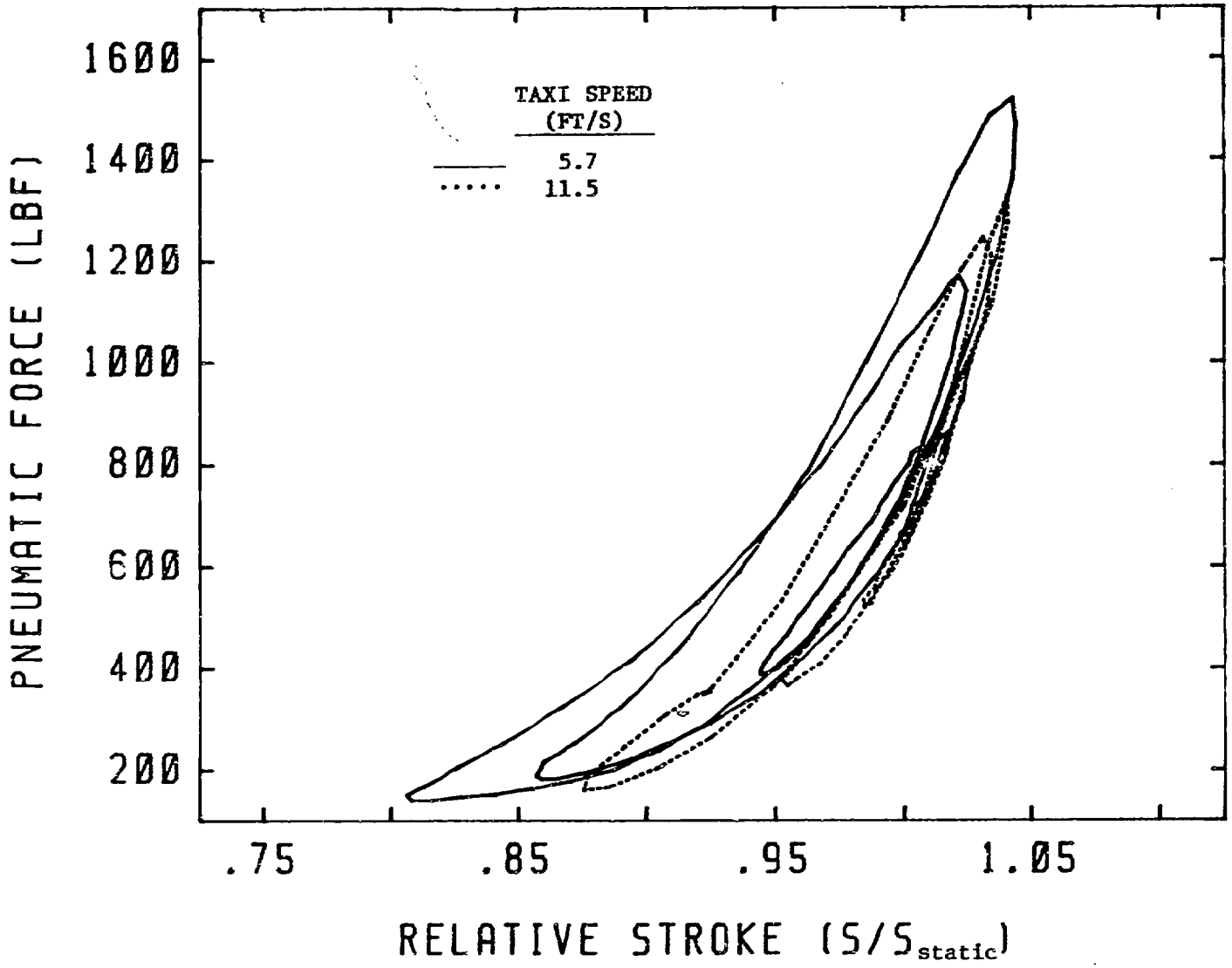

FIGURE 59. Comparison of Model Gear Polytropic Curves For Two Different Test Speeds

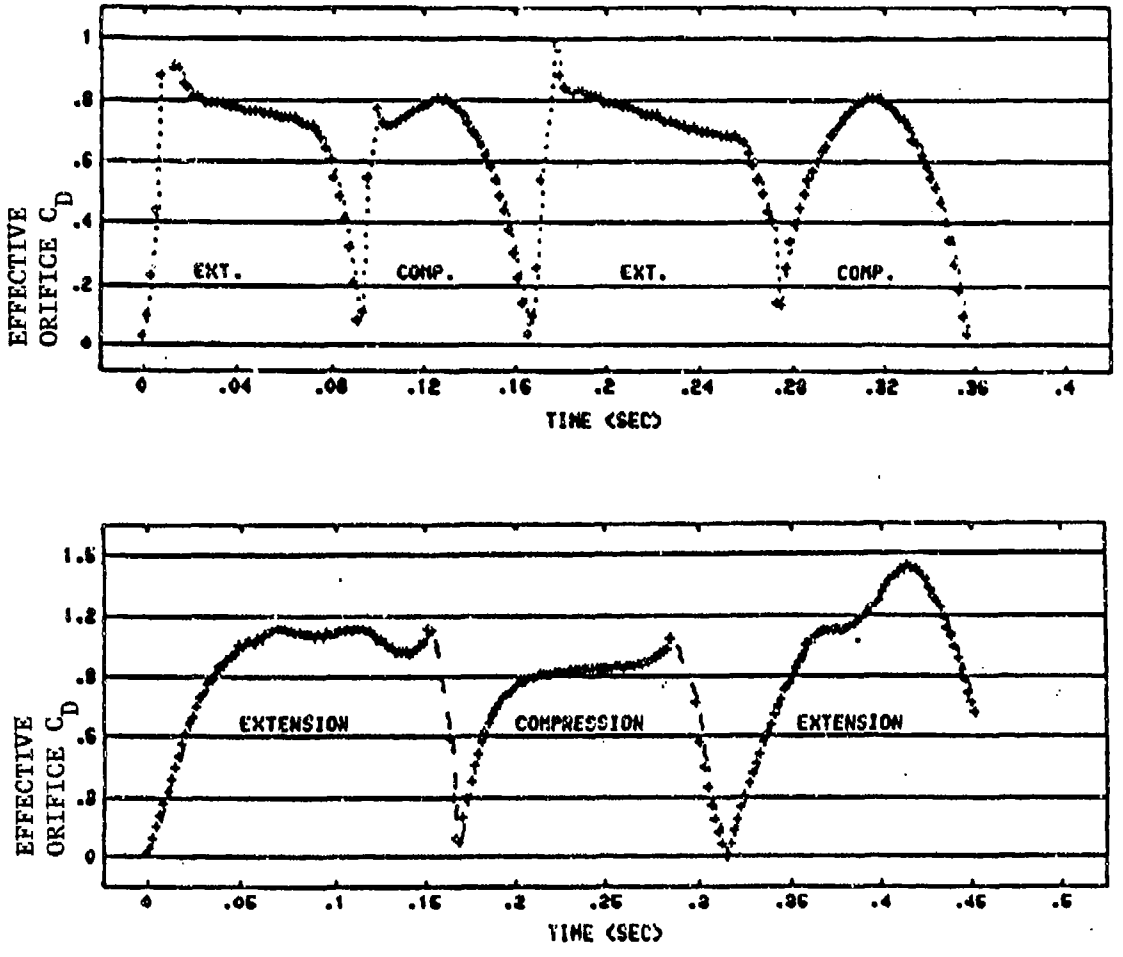

FIGURE 60. Effective Orifice C_d [1]

	TAXI SPEED
(A) Model Gear (Phase IIa)	5.7 Ft/s
(B) A-37 NLG (Phase I)	10.0 Ft/s

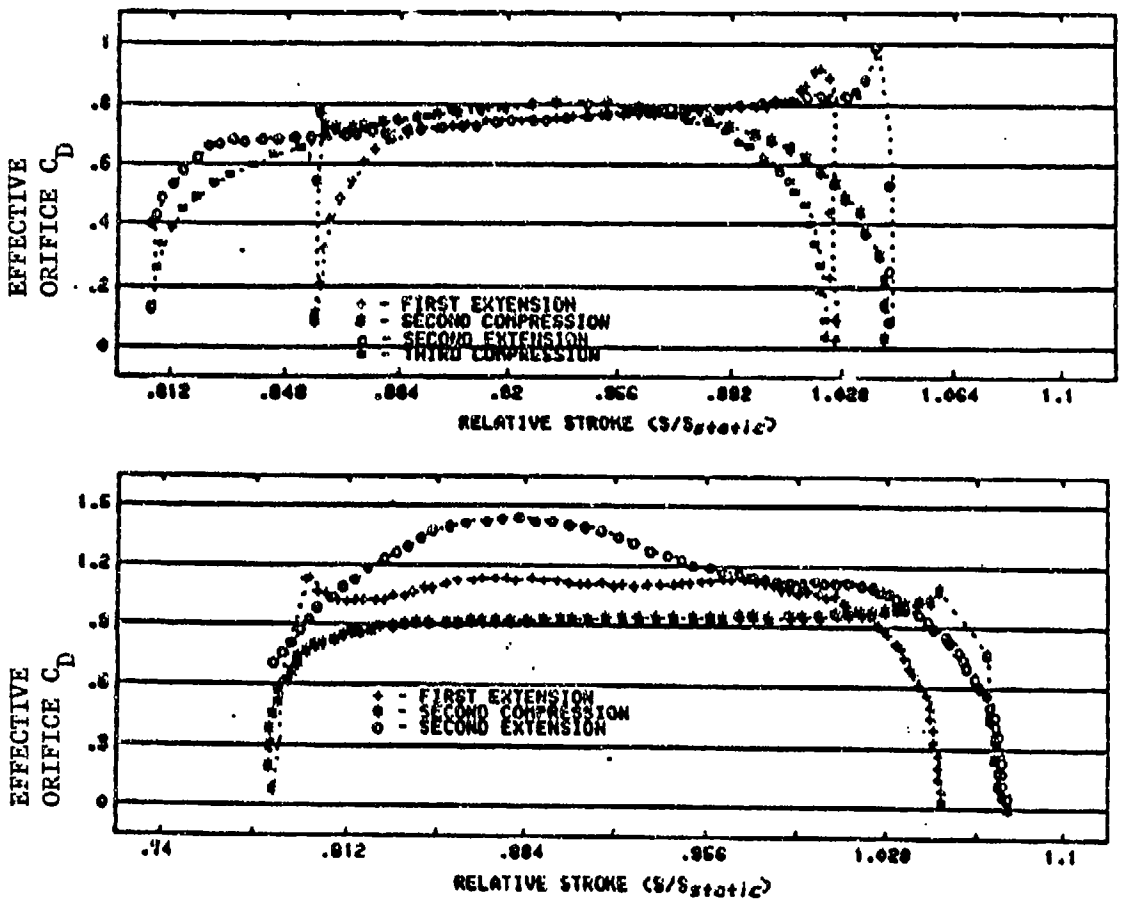

FIGURE 61. Effective Orifice C_d 2

	TAXI SPEED
(A) Model Gear (Phase IIa)	5.7 Ft/s
(B) A-37 NLG (Phase I)	10.0 Ft/s

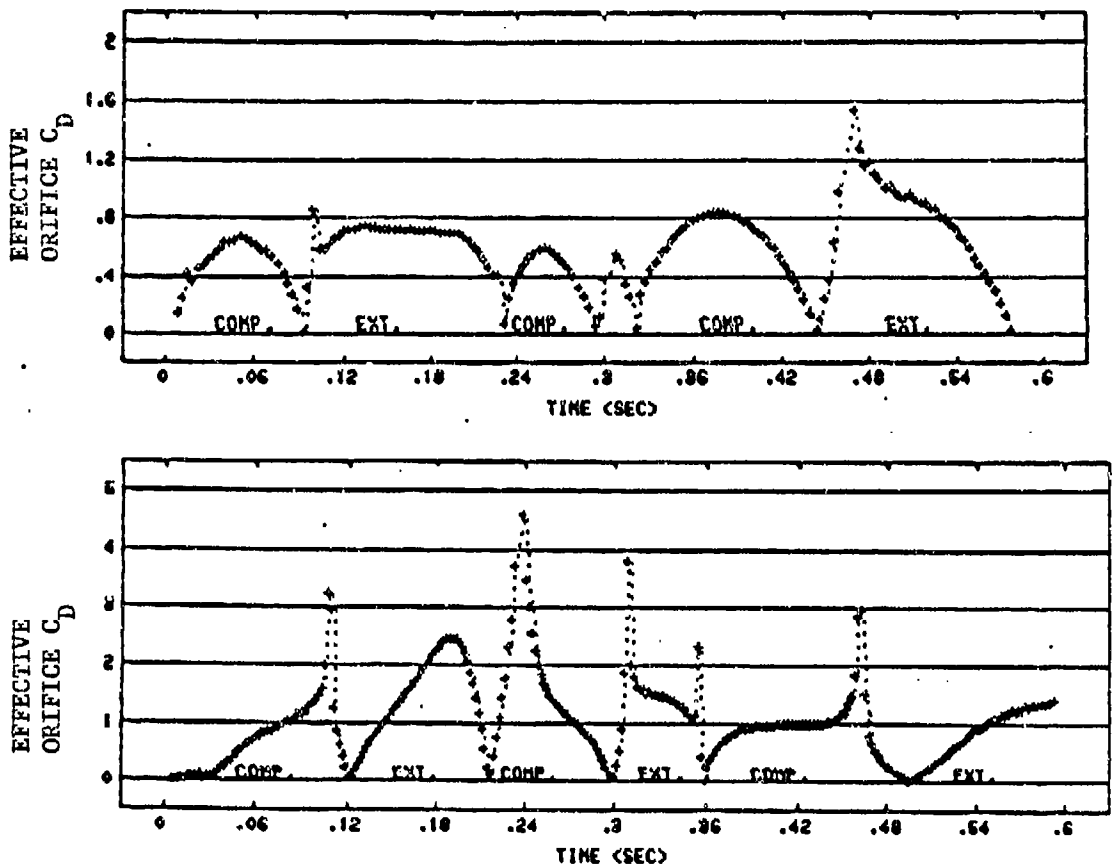

FIGURE 62. Effective Orifice C_d 3

	TAXI SPEED
(A) Model Gear (Phase IIa)	11.5 Ft/s
(B) A-37 NLG (Phase I)	20.0 Ft/s

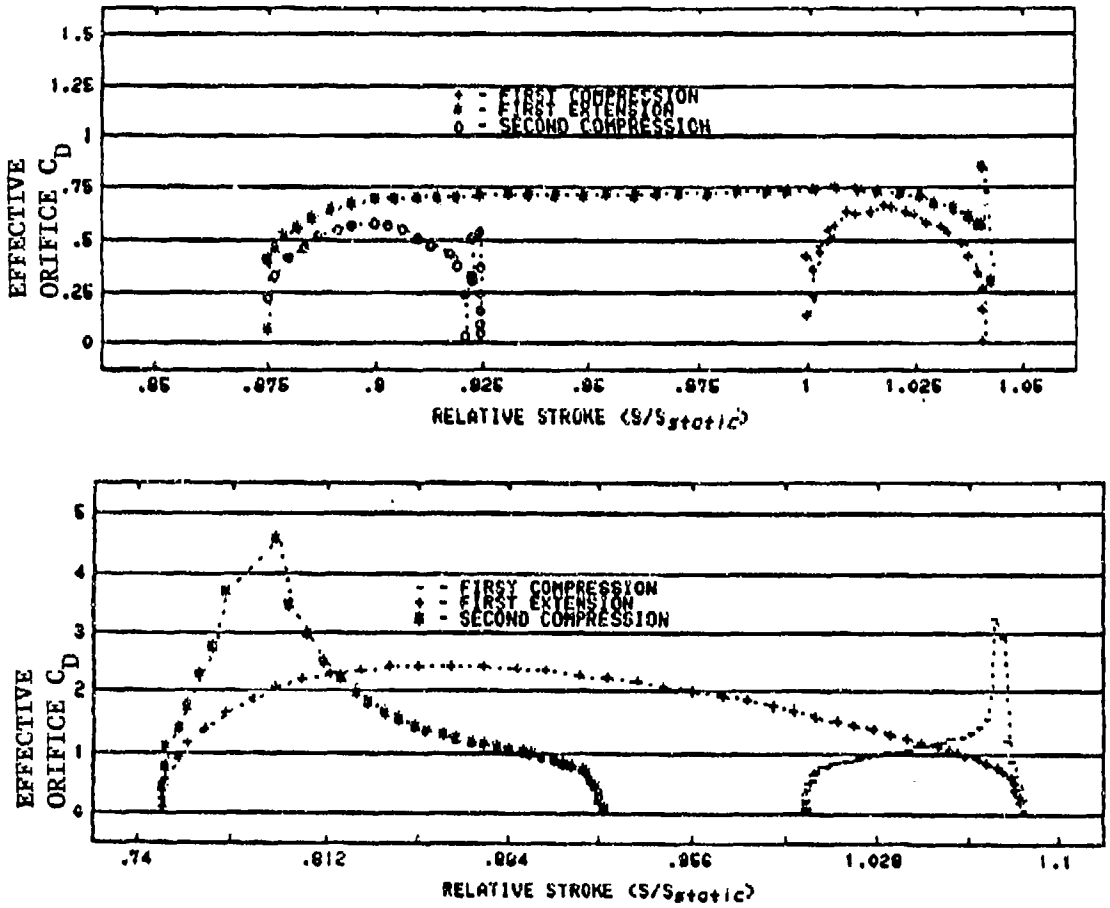

FIGURE 63. Effective Orifice C_d 4

	TAXI SPEED
(A) Model Gear (Phase IIa)	11.5 Ft/s
(B) A-37 NLG (Phase I)	20.0 Ft/s

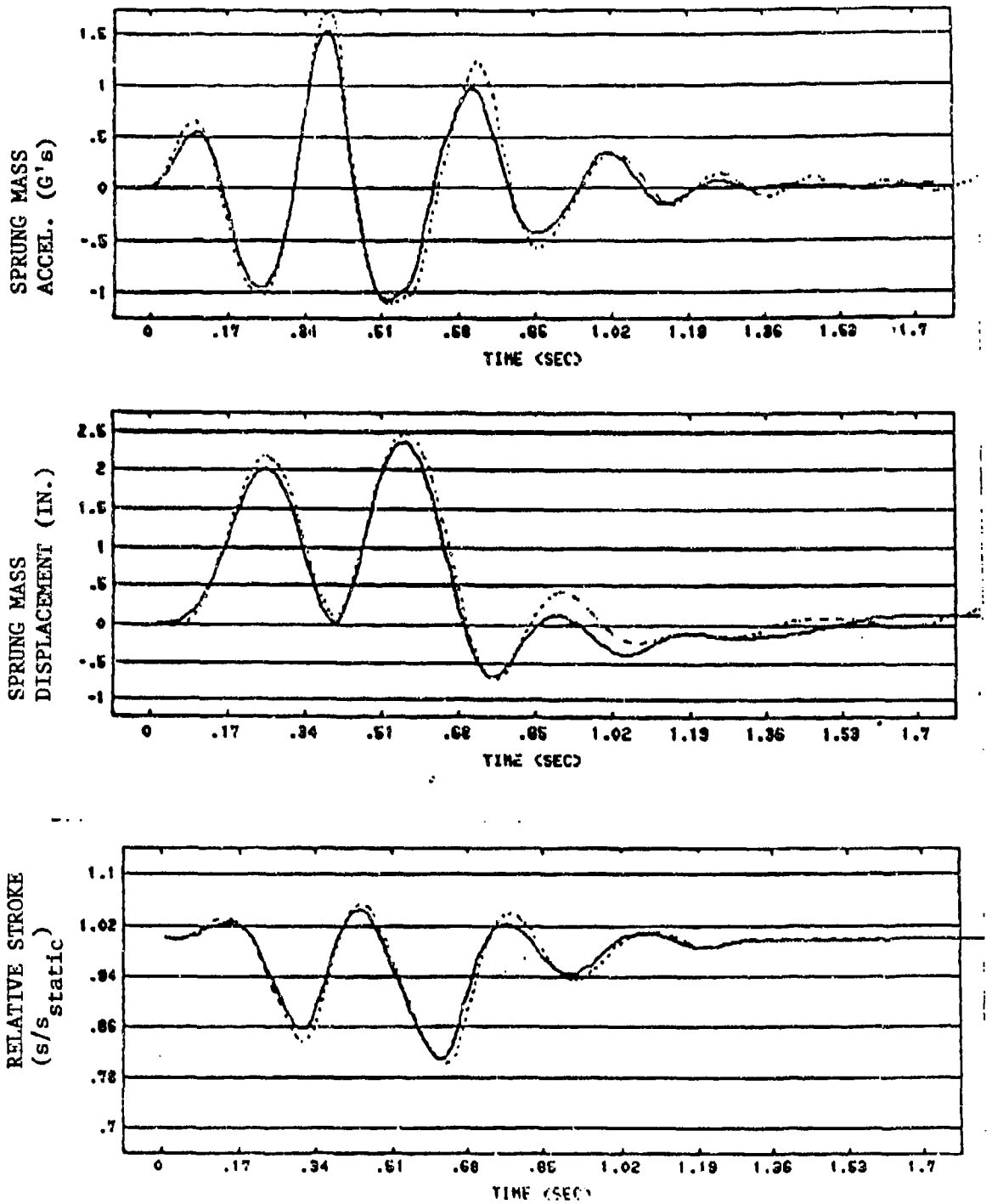

	TAXI SPEED	LEGEND
FIGURE 64. Model Gear (Phase IIa)	5.7 Ft/s	———
vs.		
Model Gear (Phase IIb)	5.7 Ft/s	.....

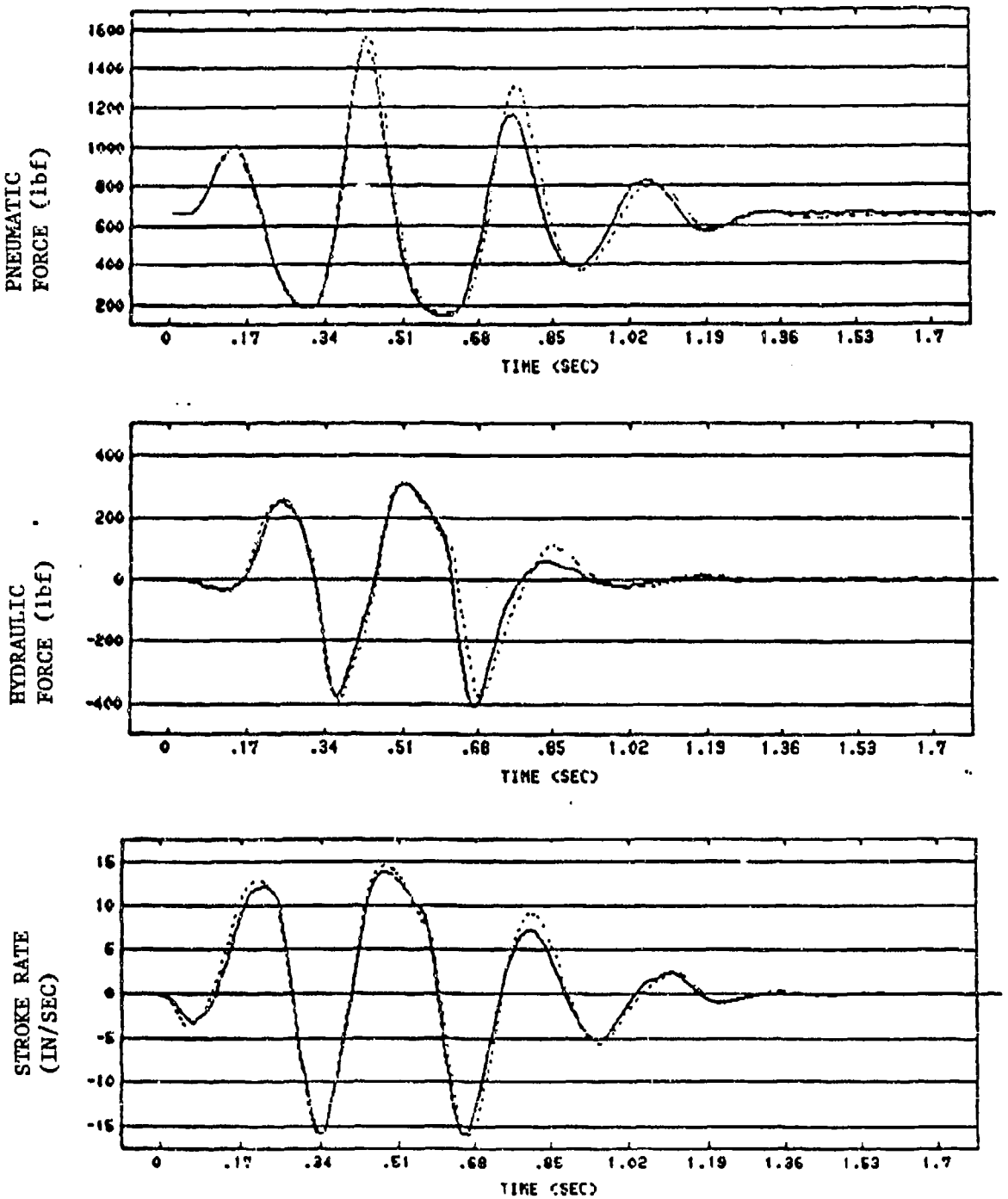

	TAXI SPEED	LEGEND
Model Gear (Phase IIa)	5.7 Ft/s	.....
vs.		
Model Gear (Phase IIb)	5.7 Ft/s	_____

FIGURE 65.

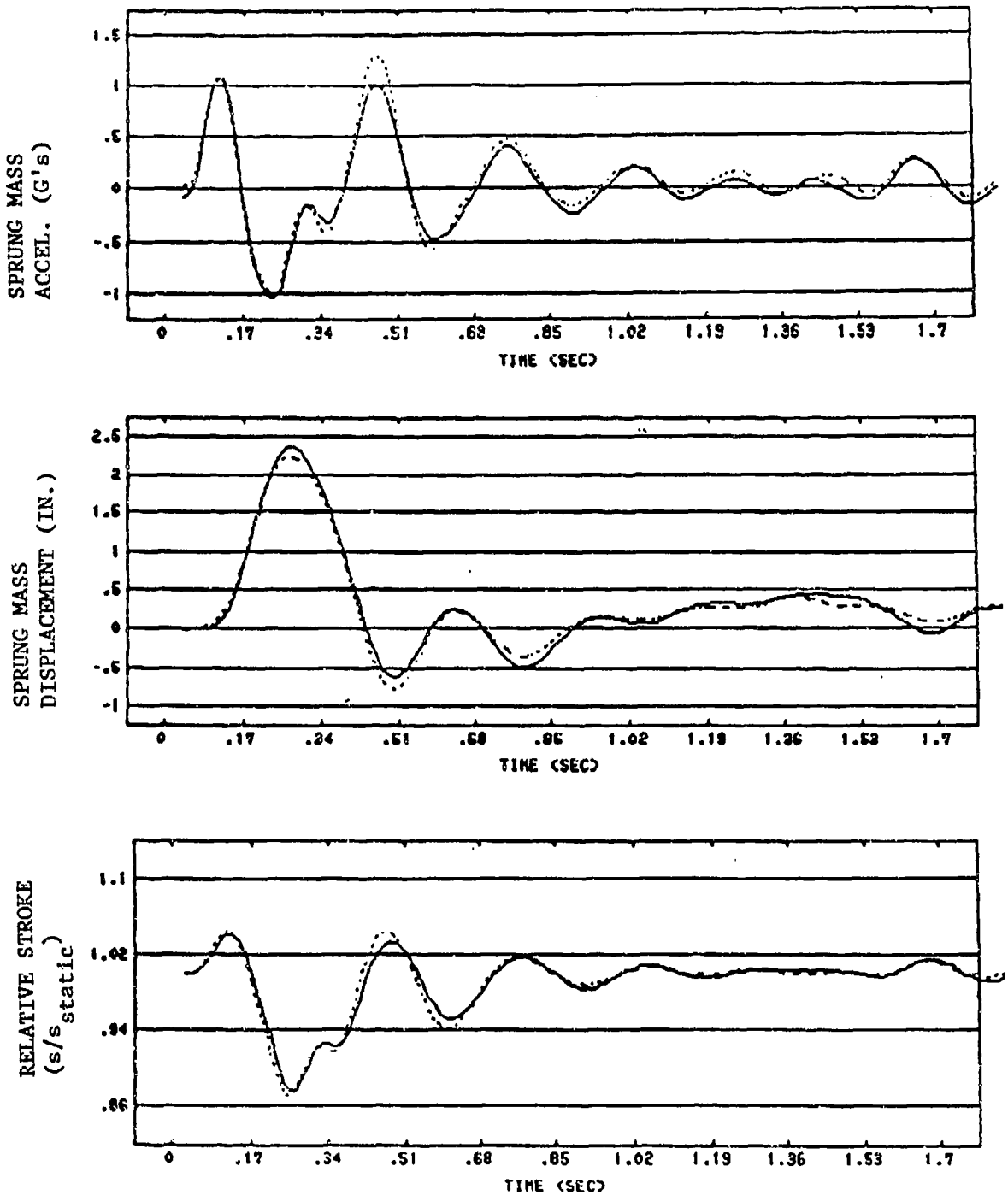

	TAXI SPEED	LEGEND
FIGURE 66. Model Gear (Phase IIa)	11.5 Ft/s	.....
vs.		
Model Gear (Phase IIb)	11.5 Ft/s	_____

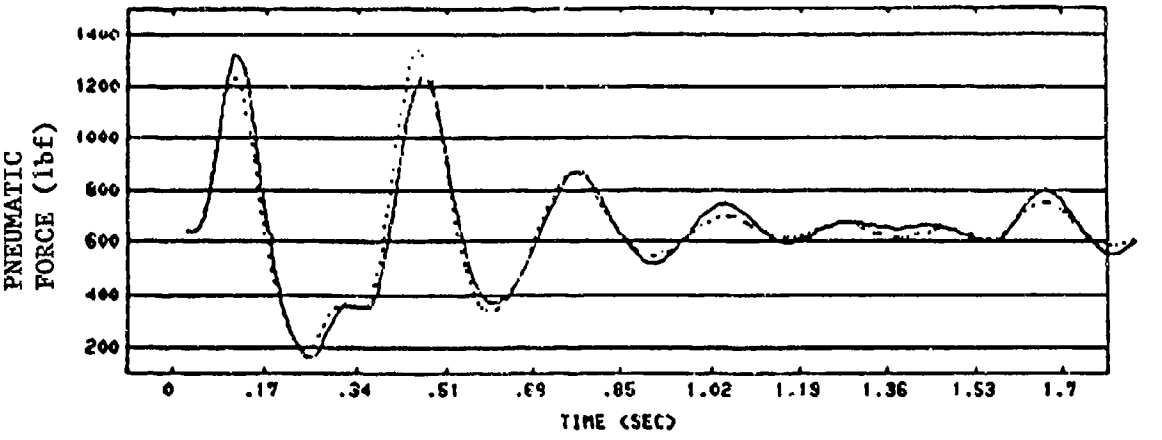

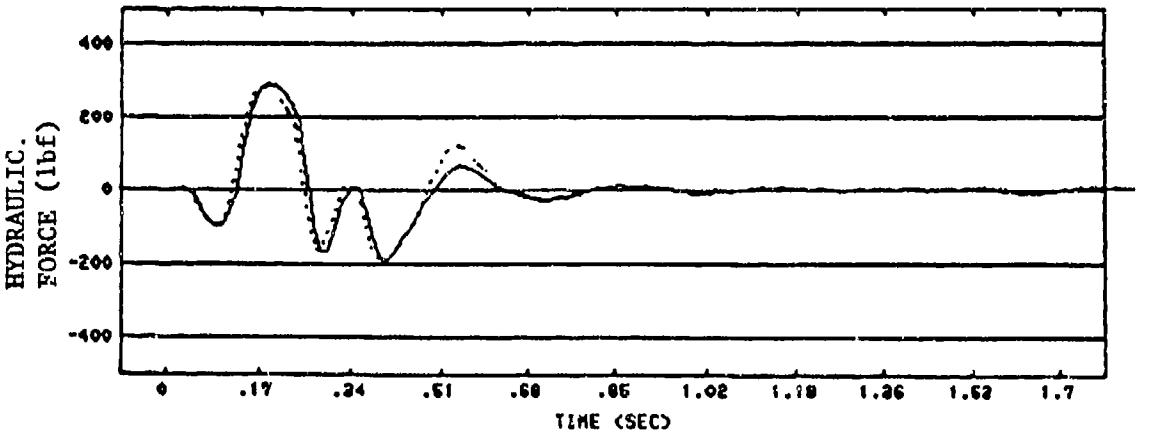

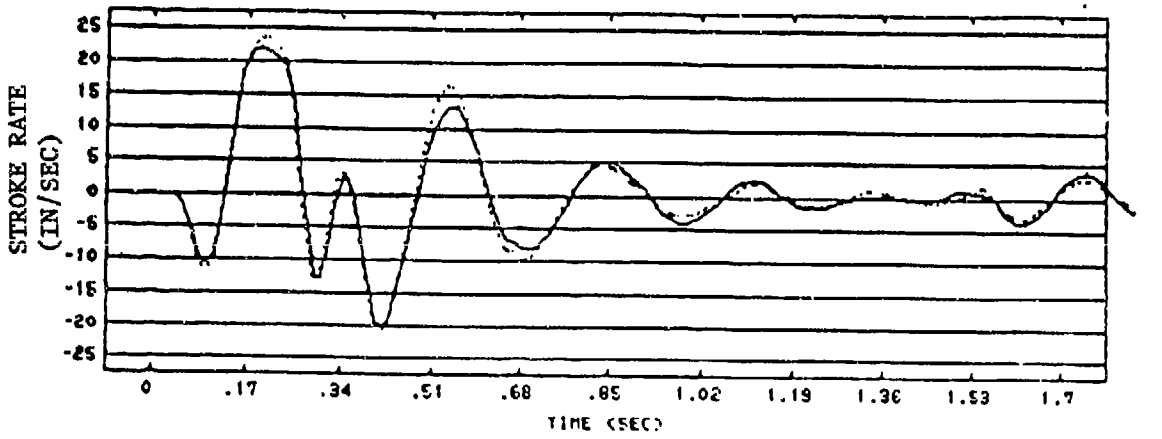

	TAXI SPEED	LEGEND
FIGURE 67. Model Gear (Phase IIa)	11.5 Ft/s	.....
vs.		
Model Gear (Phase IIb)	11.5 Ft/s	_____

SECTION IX

CONCLUSIONS

1. The primary objective of this program was to assess the feasibility and practicality of using dynamic scaling techniques to design, fabricate, and test a model of a simple oleo-pneumatic landing gear strut and tire. The data presented in the preceeding section demonstrated that good results were obtained from tests of a small, dynamically scaled model of an A-37 NLG strut and tire, although some nonsimilarities were present. However, despite these nonsimilarities, the dynamic response of the model gear was considered as fully representative of the dynamic response of the full-scale A-37 NLG, at the two highest test speeds. The scaling techniques developed for each of the subsystems of the strut were considered as generally adequate for application to other landing gear struts, although some refinement in the techniques of scaling the air spring and hydraulic damping orifice may be required to improve quantitative correlation.

2. The time history data presented in the preceeding section showed a distinct improvement in correlation of data at increased test speeds. Correlation at the lowest test speed (7.0 ft/sec for the A-37 NLG and 4.0 ft/sec for the model gear) was not good, whereas correlation at the two highest speeds was better. The poor correlation at the slow test speed was caused primarily by nonsimilar seal friction, which was more dominant in the model gear strut than in the A-37 NLG at this test condition. A simple analysis of seal friction effects on the dynamic response of the A-37 NLG strut (see Appendix B) demonstrated that friction is more dominant at slower taxi speeds during obstacle

traversal, and becomes less of a factor at higher speeds. This explains the general improvement in the correlation of test data at the higher test speeds, for this case. Thus, it was possible to obtain good results, despite nonsimilar frictional characteristics in the model gear strut.

3. There were some disparities that existed in the data at the higher test speeds, which were primarily caused by nonsimilarities in the polytropic characteristics. These nonsimilarities are clearly evident in the plots of dynamic pneumatic force vs. stroke data for each strut, presented in Section VIII.This data indicates that the model gear was apparently operating over a broader range of polytropic exponents than the A-37 NLG. The polytropic characteristics of both struts showed a tendency to become softer (more isothermal) at the highest test speed (20.0 ft/sec for the A-37 NLG, and 11.5 ft/sec for the model gear) and stiffer (more adiabatic) at the slower test speed (10.0 ft/sec for the A-37 NLG and 5.7 ft/sec for the model gear). Also evident was a stiffening of the air spring during compression, and softening during extension. These effects were more pronounced in the model gear strut (Ref. Fig. 57). The reasons for this behavior were not readily determined from the available test data, but it may be because of some interaction of the air spring and the hydraulic oil, during strut actuation.

4. Plots of the effective discharge coefficient calculated for each strut indicated that there were some differences in the orifice flow characteristics, especially at the highest test speed (20.0 ft/sec for the A-37 NLG, and 11.5 ft/sec for the model gear). Fig. 62b and 63b, presented in the preceeding section, show that the A-37 NLG orifice was apparently operating at an extremely high effective C_d, at this test speed, whereas the model gear results

remained consistent with the results obtained at 5.7 ft/sec. The reasons for the high C_d in the A-37 NLG could not be determined from the test data, however, indications suggest that pressures measured in the hydraulic chamber were considerably less than expected, for the stroke rates produced. This result could possibly be due to compressibility effects caused by air entrainment below the orifice, or dissolved air which momentarily comes out of solution. It was noted that the C_d returned to the values obtained at a test speed of 10.0 ft/sec after the A-37 NLG tire cleared the second cosine bump (Ref. Fig. 62b and 63b), i.e., the very high values of C_d were present only during obstacle traversal, under highly transient orifice flow conditions. This would tend to support the conclusion that the effect was a temporary one, possibly linked to dissolved air quickly coming in and out of solution under rapidly changing conditions, which occurred during the forced response of the strut. These effects did not show up in the model gear, possibly because of the small volume of oil inside this strut. Also, actual operating pressures were smaller, which would cause less compressibility effects than in the A-37 NLG strut.

Results obtained from Phase IIb tests, indicated that the effect of better flow similarity on overall orifice performance was minimal for this case. Complete flow similarity was not an important factor in obtaining dynamically similar response in the model gear strut. However, this result does not imply that orifice flow similarity considerations should be omitted from a future model gear design. Flow similarity may be more important, if the chosen model scale is smaller than 1/3 i.e., 1/10, 1/100, etc. Such an extreme

scaling factor (which would be required for a larger class landing gear strut) could possibly cause more flow similarity related affects on orifice damping characteristics.

SECTION X

RECOMMENDATIONS

The scaling techniques developed during this program were proven as suitable for design, fabrication, and testing of dynamically scaled model landing gear struts and tires. However, it is emphasized that this program was an initial attempt at scaling a relatively simple oleo-pneumatic shock strut and tire. Several areas were identified during the course of the program as requiring further analysis and development, to improve and solidify the scaling techniques for application to any landing gear strut. Thus, the following recommendations are made:

1. A comprehensive approach for predicting the frictional characteristics of a landing gear strut should be developed. It should be based on the aspects of seal and bearing design, which includes such factors as seal type, seal and bearing material, mating part surface finishes, lubrication, and expected loading conditions. Such an approach is required, since measurement of actual friction from full-scale strut testing would be impractical, especially for a large gear.

Proper seal/bearing design for a model gear strut would, in general, be required to accurately simulate the dynamic response of a full-scale strut. The low-speed tests of the A-37 NLG and the model gear struts demonstrated the nonsimilarity that can result if frictional effects are not properly represented. Fortunately, frictional effects were small during forced response of each strut at the two highest test speeds, and good results were obtained. However, this may not necessarily have been the case for a different strut. A

method to estimate frictional contributions to overall strut response would be valuable in establishing an acceptable range of variation for frictional characteristics, for a model gear strut design. A suitable seal/bearing design for a model gear could then be chosen without a necessity for measuring friction in a full-scale strut.

2. More analytical and experimental work in the areas of orifice flow and polytropic compression is required to better understand and quantify the interaction of these two subsystems in a single chamber oleo-pneumatic strut. The polytropic compression/rarefaction process should be investigated for a broad range of stroke rates of both short and long duration. Tests should be conducted with and without the presence of hydraulic damping effects. Also, the effect of entrained and dissolved gas on orifice flows should be investigated for MIL-H-5606, and other hydraulic fluids in service. Experimental work should include measurement of the temperature and pressure profile along the orifice entrance and throat. This data would be valuable in determining the variation of fluid properties through the orifice. As a minimum, the temperature history of the hydraulic fluid and the gas charge should be recorded during future landing gear dynamic tests. Better understanding of these phenomena will result in more accurately scaled model landing gear struts, and better designed operational hardware.

3. The scale (physical size) of a model gear should be selected based on considerations of the capacity of the test rig to be used, and the feasibility of obtaining a proper scale model tire of the required size. The size and weight of the model should fall in the mid to upper range of the test rig capacity, if possible. This recommendation is based on some of the difficul-

ties encountered in working with a very small model gear. The model was particularly sensitive to slight errors in setting the pneumatic volume and charge pressure, which affected the stiffness of the air spring. A larger scale model would not have been as sensitive in that respect, and better correlation could have been obtained. Also, the small scale chosen for the model caused difficult limitations on the unsprung weight. The weight required to ensure structural integrity of the model gear components, was greater than the dynamically similar value calculated from the scaling laws. This limitation was relaxed by adding an appropriate amount of dead weight to the A-37 NLG axle. However, the necessity of the weights may have been avoided if the model scale had been larger.

4. The scaling methods developed during this program should be applied to a strut with a metered orifice. This added degree of complexity seems to be the next logical step in validating and refining the scaling techniques. The A-37 NLG is probably the best candidate for baseline full-scale tests with a metered orifice, since procedures and test hardware are already available. The one-third scale model, however, is not appropriate for metered orifice testing because of difficulties associated with fabricating such a small metering pin. A half-scale, or two-thirds scale model of the A-37 NLG would present less of a problem.

5. The developed scaling techniques should also be applied to a larger class of landing gear struts than the A-37 NLG, which is a small capacity strut of fairly simple design. Two potential candidates for a follow-on program are

the F-15 main gear and the C-130 NLG strut, both of which have been tested at the Landing Gear Development Facility (LGDF), Wright-Patterson AFB Ohio.

6. The feasibility of fabricating a scale model tire with the required vertical load-deflection characteristics was demonstrated. These techniques should be extended to other tire properties including lateral, fore-aft, and torsional stiffness. Proper representation of these properties would allow further extension of model gear testing, to include acceleration/deceleration, and side force effects.

REFERENCES

1. Clark, S.K., Dodge, R.N., and others, "Structural Modeling of Aircraft Tires," Journal of Aircraft, 9 (1971), pp. 162-167.

2. Deutschman, A.D., Michels, W.S., Wilson, C.E., Machine Design Theory and Practice. Macmillan Publishing Co. Inc., 1975, pp. 745-746.

3. Dodge, R.N., Clark, S.K., "A Comparison of Some Static and Dynamic Mechanical Properties of 18 x 5.5 and 49 x 17 Type VII Aircraft Tires as Measured by Three Test Facilities," NASA Contractor Report #165720, July, 1981.

4. Fox, R.W., McDonald, A.T., Introduction to Fluid Mechanics. John Wiley and Sons, Inc., 1973, p. 430.

5. Hokanson, L.D., Rollings, R.S., "Field Test of Standard Bomb Damage Repair Techniques for Pavements," AFWAL-TR-75-148, October, 1975.

6. Martini, L.J., Practical Seal Design. Marcel Dekker, Inc., 1984, New York NY, First Printing.

7. Schuring, D.J., Scale Models in Engineering. Pergammon Press, 1977.

8. Shepler, P.R., Noren, O., "Split Ring Seals," The Seals Book, Machine Design, 1961, pp. 24-31.

9. Wahi, M.K., "Oil Compressibility and Polytropic Air Compression Analysis for Oleopneumatic Shock Struts," Journal of Aircraft, 13 (July, 1976), pp. 527-530.

10. Walls, J.H., "An Experimental Study of Orifice Coefficients, Internal Strut Pressures and Loads on a Small Oleopneumatic Shock Strut," NACA-TN-3426, April, 1955.

11. Warring, R.H., Seals and Sealing Handbook. First Edition, Gulf Publishing Co, Houston TX, 1981.

12. Research Committee on Fluid Meters, Fluid Meters: Their Theory and Application, Sixth Edition, The American Society of Mechanical Engineers, 1971.

APPENDIX A

SPLIT RING SEAL DESIGN

Good cylindrical conformity of a split-ring seal depends on proper design of its free (uninstalled) shape. Improper design of the uninstalled shape of this type of seal will result in the seal taking on an oval shape when it is installed. This can cause excessive binding friction and loss of sealing integrity, as discussed in Section VIII.

Proper split-ring design is based on a specific mathematical relation (Ref. Fig. A1) which was obtained from Ref. 8:

$$u = \frac{G}{3\pi}\left(1 + \frac{\theta}{2}\sin\theta\right) \qquad \text{(A-1)}$$

where u: Increase in the radius of the uninstalled ring over the radius of the installed (perfect circle) ring,

G: Uninstalled gap dimension,

θ: Angle as indicated in Fig. A1 (radians).

A split-ring seal accurately designed and fabricated according to this relation will attain the desired "perfect circle" shape when it is installed. Proper split-ring design is especially critical for smaller seals, which are particularly sensitive to small deviations from a perfectly cylindrical shape, and imperfections in the sealing surface.

Initial normal force associated with the compression required to install a split-ring seal can be calculated from the following equation:

$$F_n = \frac{\pi D_o w E G}{7.07 D_o \left(\frac{D_o}{t} - 1\right)} \text{ lbf} \qquad \text{(A-2)}$$

where E: Seal material modulus of elasticity (psi),

G: Uninstalled gap width (in),

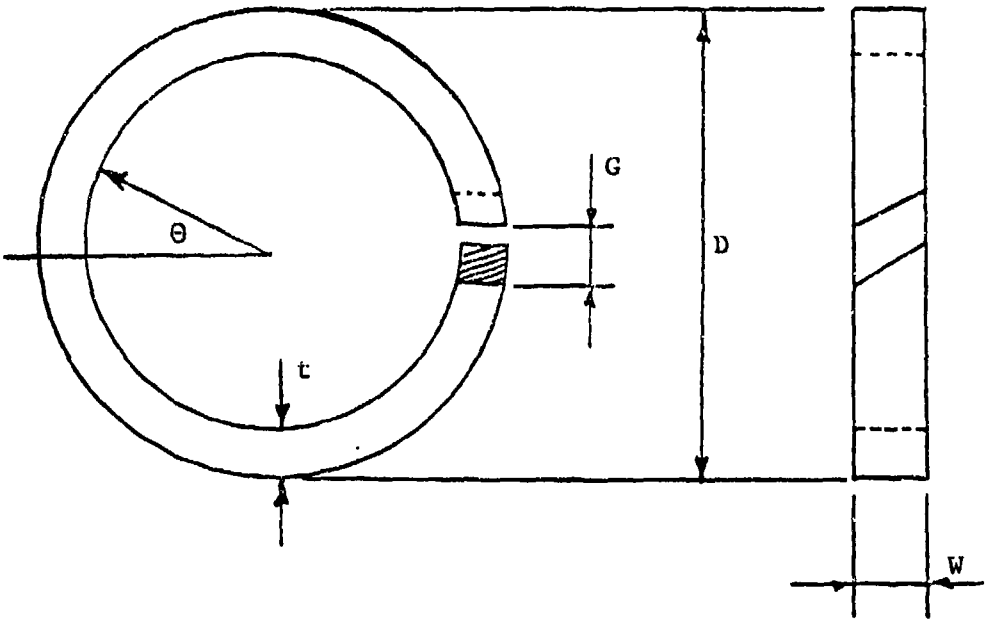

Θ : Angle (Radians)

W : Ring Width

G : Uninstalled Gap Width

D : Installed Diameter

FIGURE A-1. Split Ring Seal Design Parameters

D_o: Fitted (installed) seal outer diameter (in),

t: Minimum radial thickness (in).

This equation was obtained from Ref. 11.

APPENDIX B

ANALYTICAL FRICTION MODEL

Analytical simulations were conducted using the computer program LANSIM, to assess the effect of friction on the dynamic response of the A-37 NLG strut. An additional subroutine was incorporated into the computer program to compute the stroking friction per integration time step. The friction model included bearing contributions caused by horizontal loads at the axle, with an additional component at the bottom bearing caused by o-ring seal compression. Orifice seal friction effects were also included. Specifics of the friction model are as follows:

1. BEARING FRICTION:

Equation (39) was used to calculate bearing friction. It is repeated here for easy reference:

$$F_f = \left[\nu_T \left(\frac{L_a}{L_s + s} - 1 \right) + \nu_\beta \left(\frac{L_a}{L_s + s} \right) \right] F_d \qquad (39)$$

The drag force F_d, was obtained from the radial spring tire model. The friction coefficients ν_T and ν_B were assumed as constant, and were estimated based on bearing/seal materials, surface finishes, and boundary lubrication conditions.

2. O-RING FRICTION:

The o-ring seal exerts additional radial force against the outer piston surface, as a result of the cross-sectional squeeze required to assemble

the mating parts. This force is calculated according to the following equation:

$$F_n = \pi D_m K_1 e^{CS_a} \qquad \text{(B-1)}$$

where D_m: Mean diameter of o-ring, (I.D. + O.D.)/2.0

K_1 & C: Empirical constants determined according to o-ring section width and Shore hardness.

S_a: Percent cross-sectional squeeze of the installed o-ring.

This equation, and values of K_1 and C were obtained from Ref. (6).

There is also a dependence of seal normal force on the pressure differential across the seal. In general, this component can be calculated from (Ref. 11):

$$F_{n_P} = K_2 \pi \Delta P D_m w \qquad \text{(B-2)}$$

where K_2 is an empirical constant which depends on the type of seal being used. Also, ΔP is the pressure drop across the seal (the difference between internal pneumatic pressure and outside ambient pressure). The value of K_2 for the simulations conducted was $K_2 = 1$. Thus, total o-ring seal friction was calculated according to

$$F_{f_{os}} = \nu_B \pi D_m (K_1 e^{CS_a} + \Delta P w) \qquad \text{(B-3)}$$

This equation is plotted in Fig. B1 and B2 for different values of the friction coefficient, ν_B. Fig. B1 was based on the model gear o-ring design and all force and pressures were scaled up with the model law. Fig. B2 was based on the A-37 NLG strut o-ring seal. Fig. B3 shows how cross sectional squeeze affects the friction curve.

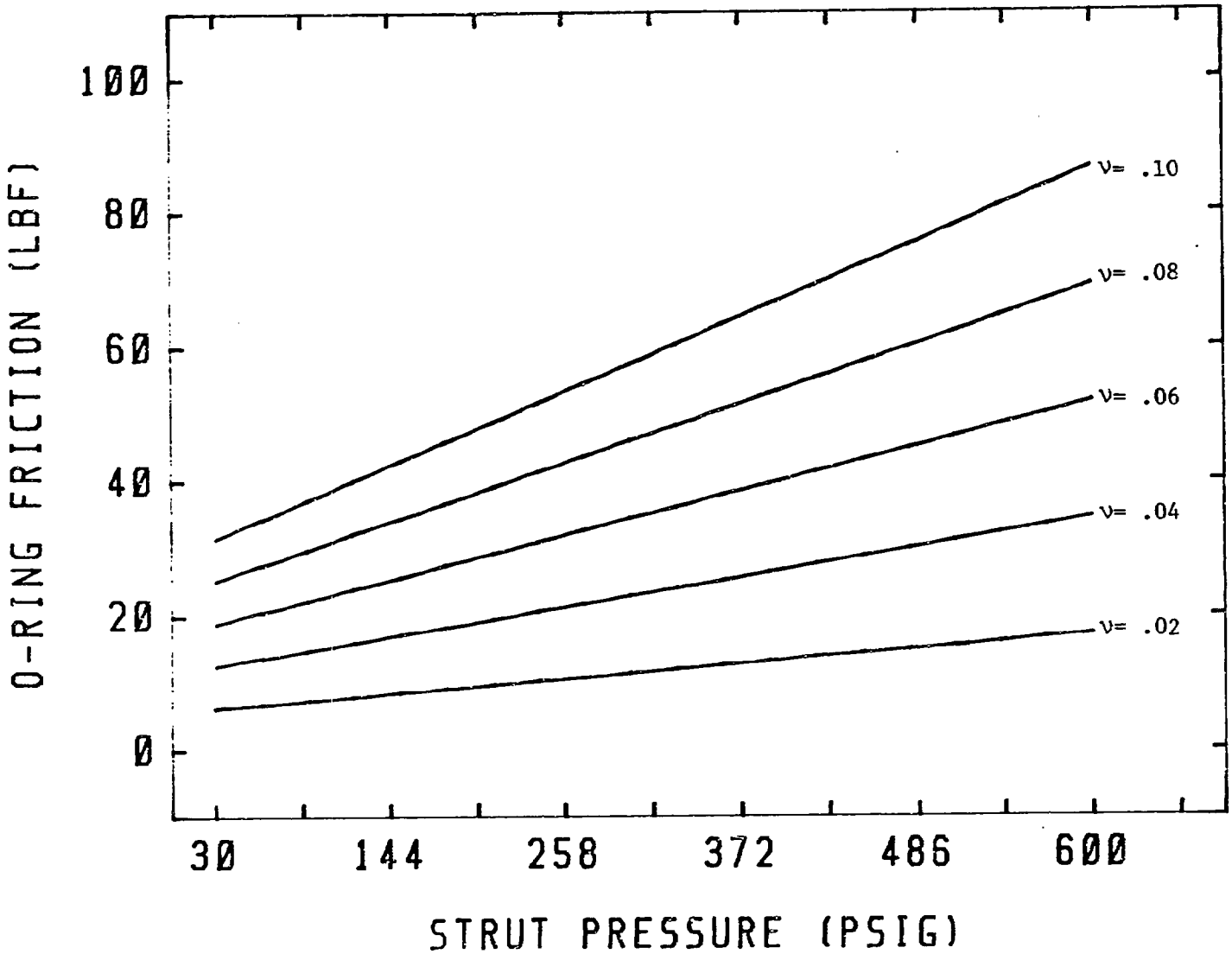

FIGURE B-1. Variation of O-Ring Friction With Pneumatic Pressure For Different Friction Coefficients (Model Gear)

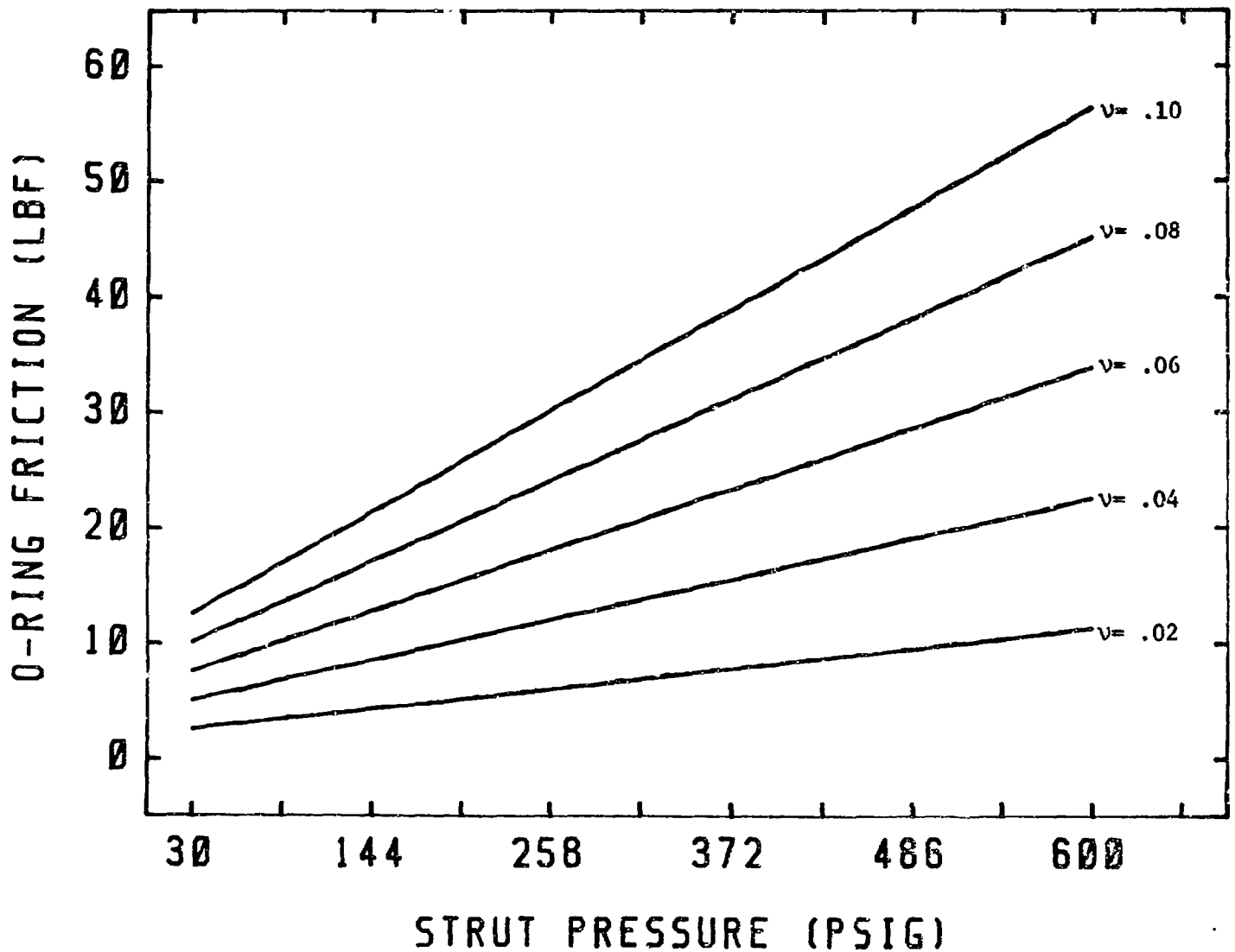

FIGURE B-2. Variation of O-Ring Friction With Pneumatic Pressure For Different Friction Coefficients (A-37 NLG Seal)

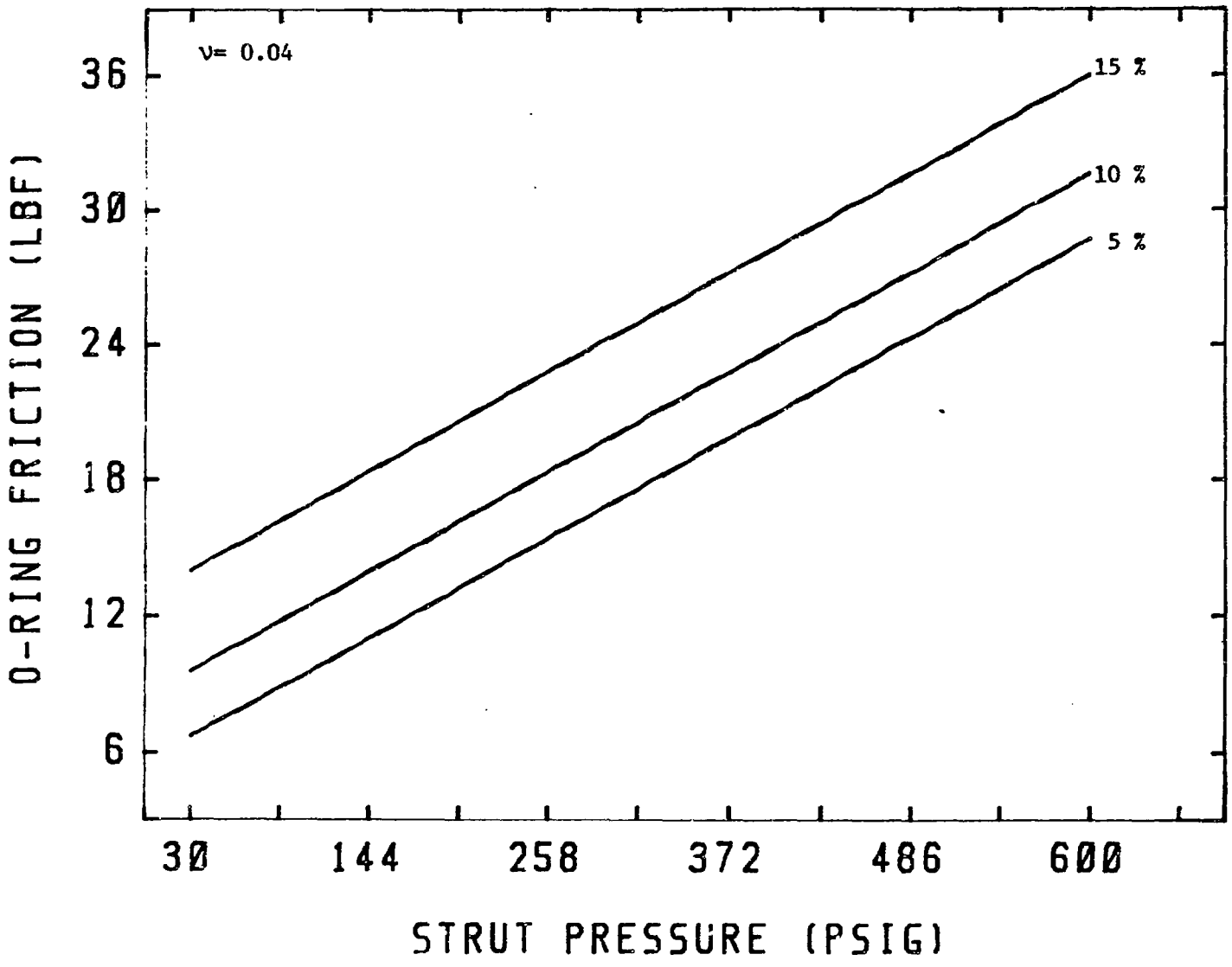

FIGURE B-3. Variation of O-Ring Friction With Pneumatic Pressure For Different Cross-Sectional Sqeeze (Model Gear Seal)

3. ORIFICE SEAL FRICTION:

Friction caused by the orifice seal was calculated according to

$$F_{f_o} = \pi D_o w_o \nu_o \Delta P_o$$

where D_o: Outer diameter of seal (installed)

w_o: Width of seal

ΔP_o: Pressure drop across the seal

ν_o: Friction coefficient

The pressure drop across the seal, ΔP_o, was the difference between hydraulic and pneumatic pressure.

Input parameters for the simulations are listed in Table B1. Tire parameters were identical to those listed in Table 3. Results obtained from the simulations with friction were plotted against results obtained from simulations of a frictionless strut. Typical time history plots of sprung mass parameters are presented in Fig. B4 through B6. This data clearly shows how friction affects the dynamic response during obstacle traversal, and during free response after the strut clears the second bump. During forced response, friction has considerably less of an affect at higher taxi speeds, and more of an affect at the lower taxi speed i.e., the strut behaves like a frictionless strut during forced response at higher speeds. The free response is obviously quite different with the additional friction damping. This was the case for each of the simulated taxi speeds.

Similar runs of the model gear, with friction, were not conducted, however, a conclusion concerning model gear behavior was drawn from the simulations of the A-37 NLG, with friction. The simulation results demonstrated that, during obstacle traversal, an improvement in correlation of test data, at

the higher test speeds, could be expected despite nonsimilar friction in the model gear strut.

INPUT PARAMETERS		NO FRICTION	WITH FRICTION
m_{sp} (lb)	:	660.00	660.00
m_u (lb)	:	44.00	44.00
V_0 (in)	:	18.45	18.45
A_p (in)	:	2.71	2.71
N	:	1.25	1.25
P_0 (psig)	:	11.30	11.30
P_a (psia)	:	14.70	14.70
A_h (in)	:	2.09	2.09
A_o (in)	:	0.02	0.02
C_d	:	0.90	0.90
C_d	:	1.10	1.10
ν_T	:	0.00	0.00
ν_B	:	0.00	0.10
ν_o	:	0.00	0.00
v (FPS)	:	7.00	7.00
		10.00	10.00
		20.00	20.00

TABLE B-1. LANSIM Inputs (Strut Model)

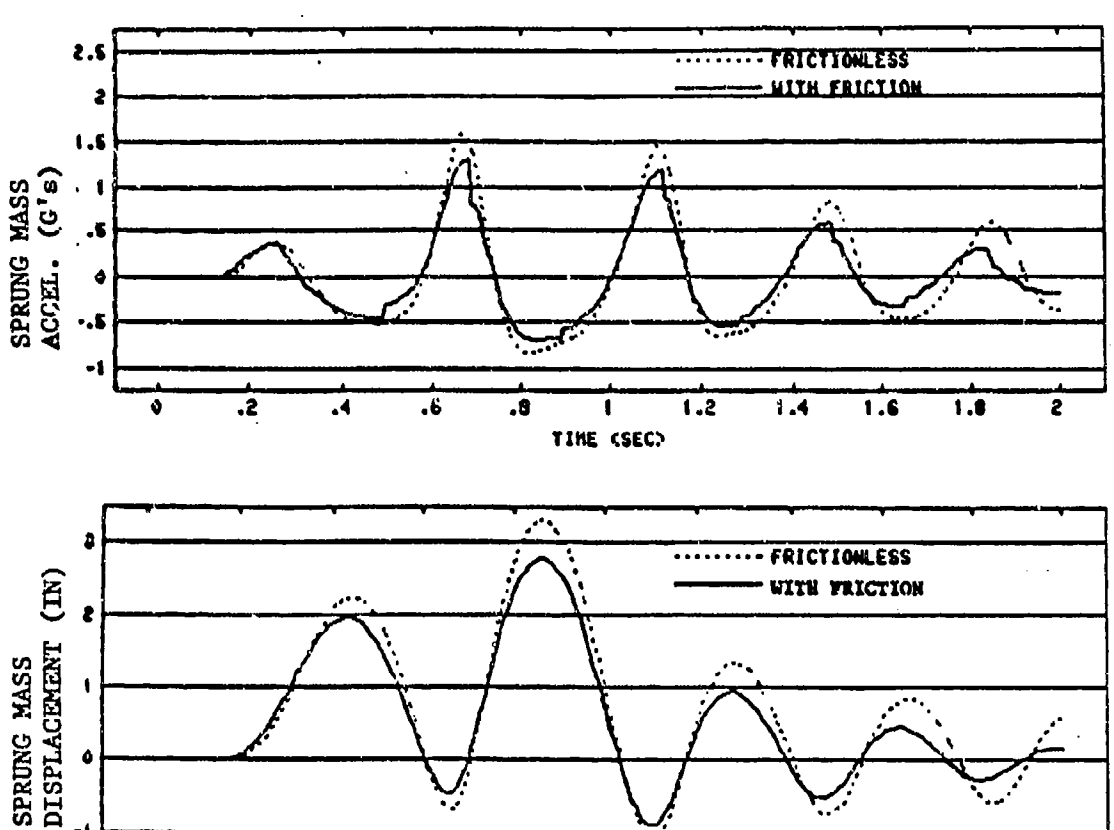

FIGURE B-4. A-37 NLG Strut (Frictionless)

vs.

A-37 NLG Strut (With Friction)
(Taxi Speed = 7.0 Ft/Sec)

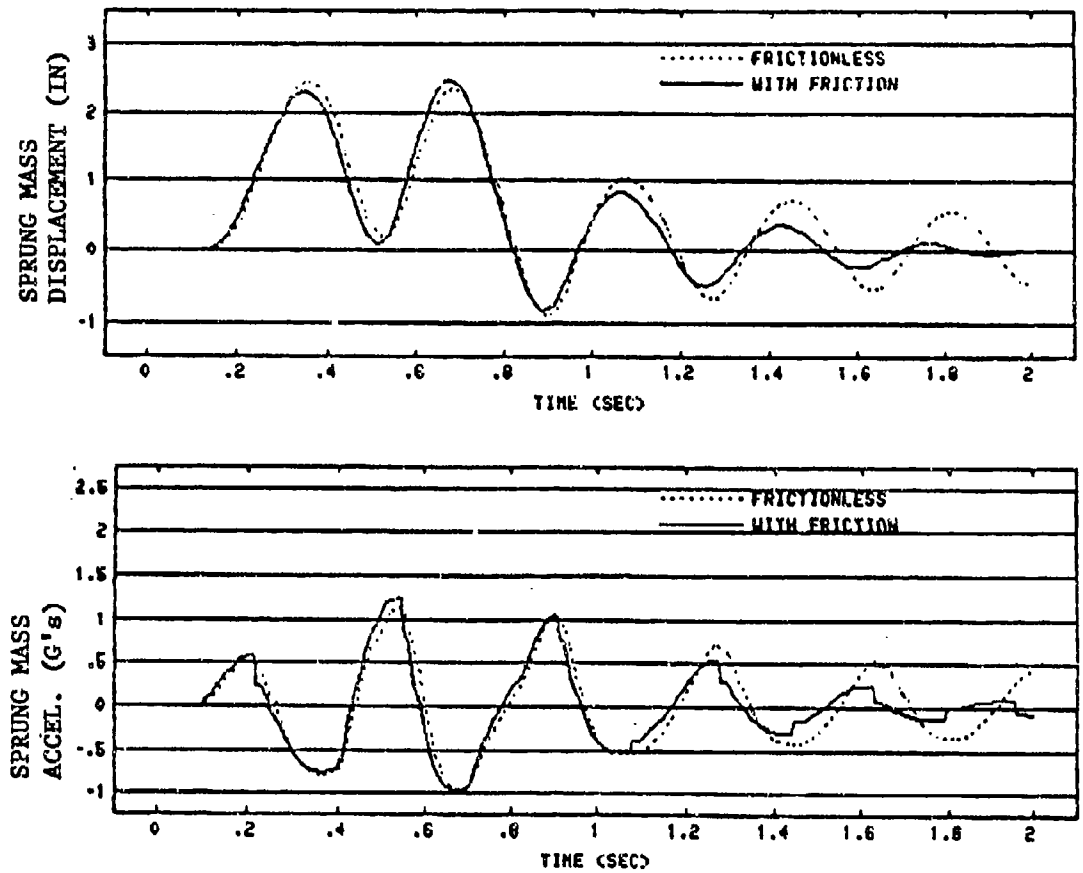

FIGURE B-5. A-37 NLG Strut (Frictionless)

vs.

A-37 NLG Strut (With Friction)
(Taxi Speed = 10.0 Ft/Sec)

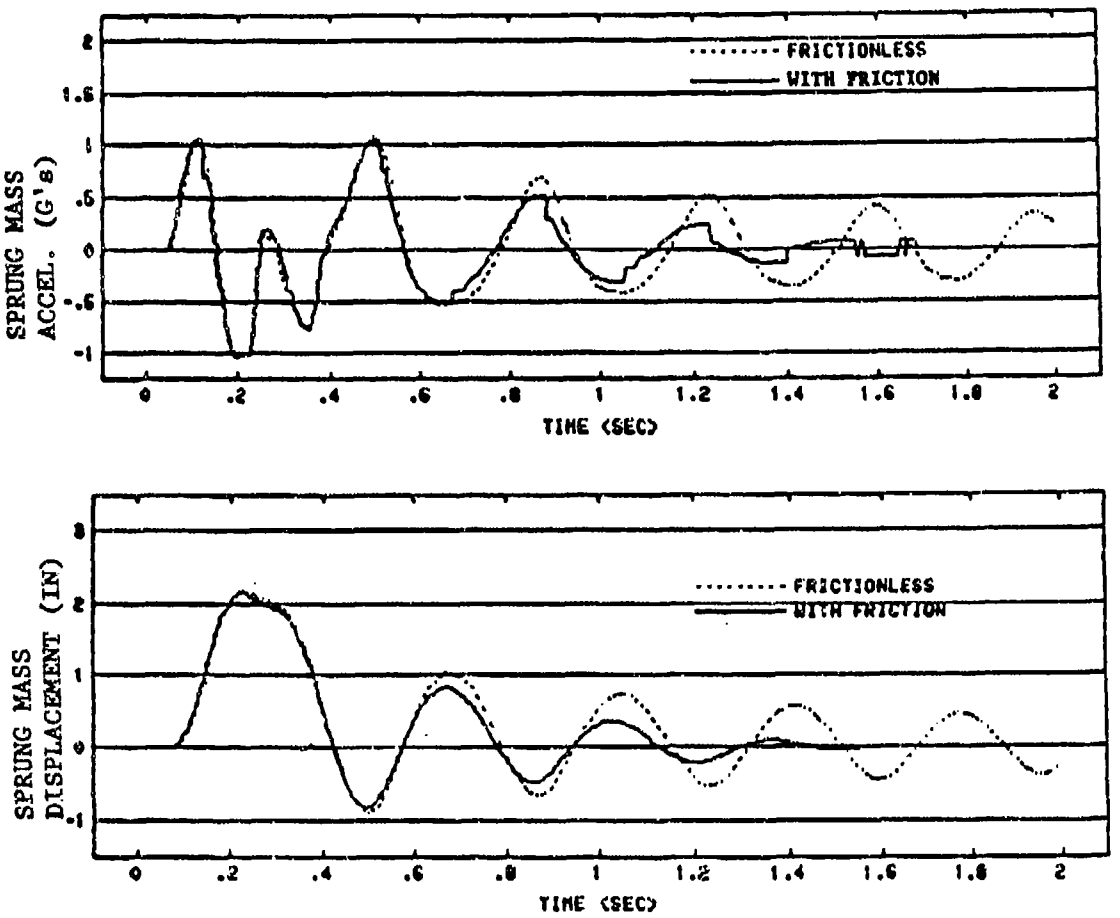

FIGURE B-6. A-37 NLG Strut (Frictionless)

vs.

A-37 NLG Strut (With Friction)
(Taxi Speed = 20.0 Ft/Sec)

*U.S.Government Printing Office: 1987 -- 548-054/80507